THE FRACTOGRAPHY OF INORGANIC GLASS

by

THOMAS ALAN SCHWARTZ

B.S.C.E., Tufts University
1973

Submitted in partial fulfillment of the requirements
for the degree of

MASTER OF SCIENCE

at the

Massachusetts Institute of Technology

February, 1977

Signature of Author .....Thomas A. Schwartz.....
Department of Materials Science and Engineering
January 21, 1977

Certified by .....
Thesis Supervisor

Accepted by .....
Chairman, Departmental Committee on Graduate Students

ABSTRACT

THE FRACTOGRAPHY OF INORGANIC GLASS

by

THOMAS ALAN SCHWARTZ

Submitted to the Department of Materials Science and Engineering on January 21, 1977 in partial fulfillment of the requirements for the degree of Master of Science.

The purpose of this research was to correlate the physical circumstances of inorganic glass at the onset of fracture, with the resultant fracture surface characteristics. Mechanical, thermal and impact modes of fracture were investigated. Annealed, tempered and heat strengthened soda-lime-silicate glass was tested in various flawed and unflawed conditions. Characteristic strengths under the various conditions formed an essential part of this study. Typical fracture surface markings such as mirror, mist, hackle, rib-marks, Wallner lines and striations were used to determine fracture stress, crack front orientation, crack speed, crack branching, elastic energy release rate, and the form of applied and residual stress gradients. The relationship between fracture stress and fracture mirror radius was confirmed for annealed glass. A correlation between fracture stress and the angle of crack branching was shown for mechanical fracture of annealed plates. The average strength of annealed specimens "as-received" from the manufacturer was approximately 10,000 psi. The strength initially dropped 20% when environmental stress corrosion was first introduced. The strength increased approximately 15% for each decade increment in the rate of stress application in the range of testing (250 psi/min. to 25000 psi/min.). Fractures at stress levels as low as 1000 psi were produced under conditions of severe environmental stress corrosion and static fatigue. The weakening effect of various edge conditions was investigated. The presence of a certain edge characteristic (shark teeth which penetrate 1/2 the edge thickness) which is considered "acceptable" by glass manufacturers was shown to constitute a weakening defect at least as serious as severe mechanical damage. The strengths of tempered and heat-strengthened glass, in "as-received" condition, were approximately 32000 psi and 18000 psi respectively. The fracture surface characteristics of heat strengthened glass were found to be similar to both annealed and tempered glass fracture surfaces, depending on the size and location of critical flaws.

The recessed edge configuration typical of most glazing construction details was shown to be dangerous with respect to thermal stresses.

A thermal gradient as low as 42°F across a 1/2 inch "cold edge" initiated fracture in annealed plates. The fracture surface markings for annealed glass fractured thermally were correlated with the stress gradient and the onset of crack branching. The initiation of hackle and crack branching were shown to be simultaneous occurrences.

The fracture surface markings and the general fracture patterns associated with high mass/low velocity and low mass/high velocity impacts were discussed. The sequence of crack pattern development was analyzed as an indicator of the type of stress that governed a particular impact fracture mode.

Thesis Supervisor: Donald R. Uhlmann

Title: Professor of Ceramics and Polymers

TABLE OF CONTENTS

TABLE OF CONTENTS (Cont'd.)

TABLE OF CONTENTS (Cont'd)

LIST OF FIGURES

LIST OF FIGURES (Cont'd.)

LIST OF TABLES

LIST OF PHOTOGRAPHS

ACKNOWLEDGEMENTS

I wish to express my gratitude to Professor Uhlmann for his guidance and supervision in the pursuit of my research interests. Our association has been most rewarding.

I would like to thank the personnel of Simpson, Gumpertz and Heger, Inc. for their inspirational and technical assistance. Specifically I am grateful to Werner H. Gumpertz, whose guidance is always memorable, and to Richard E. Chambers, for his many helpful suggestions.

Financial support for this research was paid for in part by the National Science Foundation.

I. INTRODUCTION

Few substances in the vast field of building materials can compare with glass in terms of service quality and durability. Many colonial homes have survived numerous renovations and restorations and still retain their original glass units. But in recent years it has become painfully apparent to those of us involved in building technology that our level of understanding of glass in a semi-structural capacity has not kept pace with the demands placed on this material by the modern construction market. The high incidence of glass failure in large curtain wall systems has indicated that a reassessment of our traditional methods of design, manufacture and installation are appropriate.

In order to achieve a lower probability of service failure it is first desirable to establish the exact nature of the relationship between physical stress and fracture. One of the most effective means to date for the investigation of the nature of glass failure is the "post-mortum" optical analysis of the fracture origin and the subsequent crack propagation paths.

The general physical characteristics of glass fracture surfaces have been established and confirmed, but the correlation between these well known markings and such factors as stress concentrations, crack path characteristics, and environmental and mechanical stress states during initiation and propagation of fissures is not complete. It is the purpose of this research to shed some light on the relationship between the physical characteristics of fracture surfaces and the factors surrounding the onset and propagation of fracture. Effective

correlation between these parameters will allow engineers to retrace and reconstruct the critical conditions that culminate in glass failure and thereby contribute to the development of greater service reliability in modern glass applications.

II. GENERAL COMMENTS ON BRITTLE FRACTURE

Brittle fracture is a process which involves the extension of cracks with little or no inelastic deformation. Generally, the cracks in a homogeneous isotropic solid, will extend in a path that is normal to the direction of the principal tensile stress ahead of the crack tip. The conditions that govern the onset of brittle fracture have been discussed by a number of researchers who have developed the following concepts of fracture.

A. Energy Approach

Griffith[1] approached the fracture problem in terms of the energy of the system under stress. His essential concept is that fracture will occur in a perfectly elastic solid when the elastic energy that is released from the stressed body as the crack extends is greater than the surface energy required for the formation of new surfaces ahead of the crack tip. Stated in another way, Griffith's criterion holds that elastic crack propagation will proceed only if the system can pass into the fractured state by a process that involves a continuous decrease in potential energy. The source of energy for crack propagation is the elastic energy stored in the material ahead of the crack tip. The energy associated with the new surfaces is equivalent to the surface tension (or γ, referred to as the fracture energy). In reality the fracture energy is greater than the surface energy created due to other energy releasing effects such as microplastic deformations at the crack tip and heat dissipation. Nonetheless the basic concept is

valid and useful in determining limits for the stresses that can safely develop in brittle materials in the presence of flaws.

Griffith derived the following equations for an elliptical crack in a linear elastic continuum under stress. For plane strain (i.e., zero strain in the y direction in Fig. 1):

$$\sigma_a^2 \, c \geq \frac{2E\gamma}{\pi(1-\nu^2)} \tag{1}$$

and for plane stress (i.e., zero stress in the y direction in Fig. 1):

$$\sigma_a^2 c \geq \frac{2E\gamma}{\pi} \tag{2}$$

where E is Young's modulus, ν is Poisson's ratio, σ_a is the applied tensile stress, and c is one half the crack length. Fracture will occur when $\sigma_a^2 c$ exceeds the given critical value.

B. Stress Approach

An alterate approach to brittle fracture was proposed by Inglis[2]. He calculated the stress raising effect of flaws in an elastic material. For a stress applied perpendicular to a crack of elliptical cross section as shown in Figure 2, Inglis found that,

$$\sigma_t = 2\sigma a \sqrt{c/\rho} \tag{3}$$

where σ_t is the concentrated stress level and ρ is the radius of curvature of the crack tip. This concept postulates that fracture proceeds when the stress at the tip of an existing flaw reaches the theoretical cohesive strength of the material, approximately E/10, and atomic bonds ahead of the crack tip are broken, thereby creating new

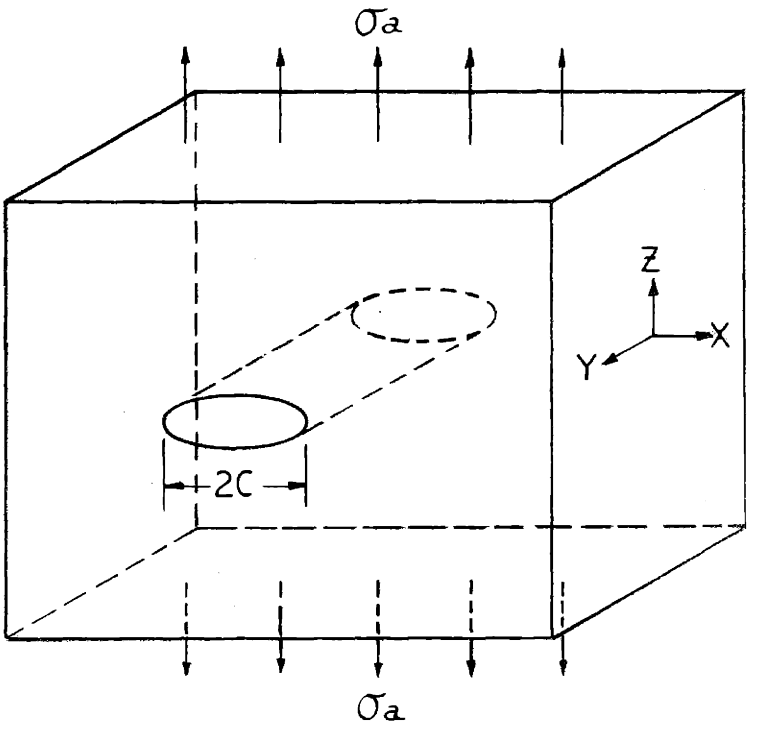

FIGURE 1: IDEALIZED ELLIPTICAL CRACK IN AN ELASTIC CONTINUUM

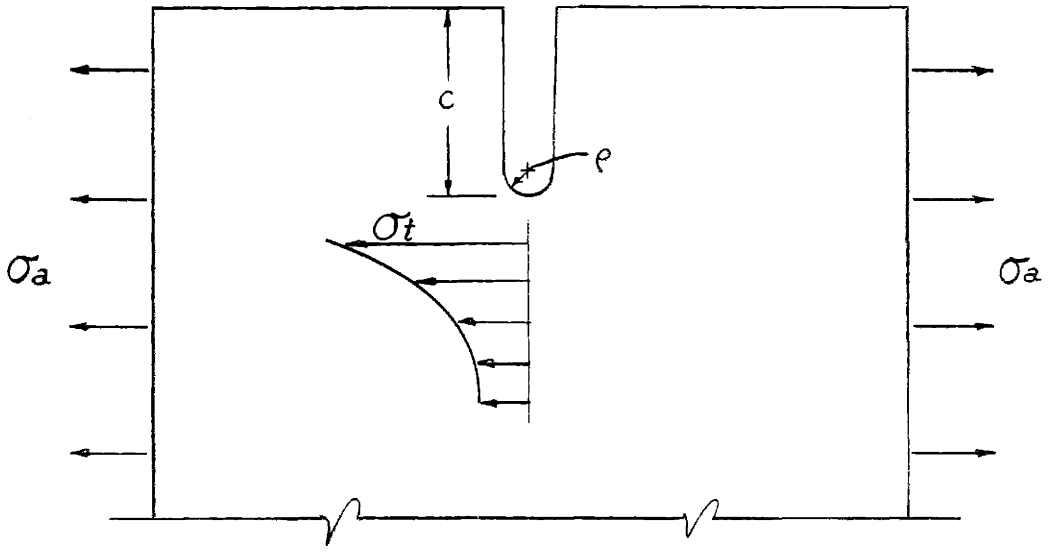

FIGURE 2: STRESS CONCENTRATION AT TIP OF AN ELLIPTICAL CRACK

surfaces with surface energy, γ. The stress concentration factor is seen to be proportional to $\sqrt{c}$. The nominal fracture stress is proportional to $\sqrt{\gamma/c}$ as predicted by the Griffith equation.

The Inglis presentation of fracture analysis shows that the nominal stress σ is a function of the square root of the crack length, or flaw depth c. Expanding on this relationship, Irwin[3] introduced a parameter known as the stress intensity factor, K. For an atomically sharp elastic crack, in an infinite plate, the stress intensity factor is defined as:

$$K = \sigma \sqrt{\pi c} \tag{4}$$

Physically, K represents a material property which characterizes the material's susceptibility to brittle fracture. Irwin proposed that fracture occurs at $\sigma = \sigma_F$ when a parameter called the crack extension force, G, defined as:

$$G = \frac{K^2}{E} \quad \text{(for plane stress)} \tag{5}$$

equals some critical value called G_c, the critical strain energy release rate. When $G = G_c$, then $K = K_c$ where K_c is called the fracture toughness. Combining equations (4) and (5) we find,

$$\sigma_F = \sqrt{\frac{EG_c}{\pi c}} \tag{6}$$

When compared with the Griffith criterion for fracture it is apparent that $G_c = 2\gamma$. The terminology varies but the Griffith, Inglis, and Irwin concepts reach the same general conclusion as to the mechanisms

of crack initiation and propagation in an elastic medium, namely that the stress at which a given material will fracture is related to a defined material property and is a function of the depth or length of stress concentrating flaws.

III. NATURE OF INORGANIC GLASS AND ITS FRACTURE CHARACTERISTICS

A. Structure

Inorganic glass is composed of fused mixtures of oxides. The vast bulk of commercial glasses produced are soda-lime-silicates which are mixtures of silica (SiO_2), sodium oxide (Na_2O) and calcium oxide (CaO). Most window glass is of this type, and for this reason the glass investigated in this research was exclusively soda-lime-silicate.

The term "annealed", refers to glass that has been solidified from the liquid phase by a carefully controlled temperature reduction process so as to minimize differential cooling within the glass body, thereby eliminating residual stress. In some cases specific residual stress is desirable; the introduction of compressive stress in the surface layers of glass is one such case. Glass treated in this manner is referred to as "tempered". A compressive surface layer strengthens the glass considerably since almost all fractures originate at the surface due to tensile stresses. The residual compressive stress is also important in protecting the glass from static fatigue and environmental attack as will be discussed later in this paper.

There are numerous methods for producing compressive surface layers in glass, but the primary commercial process is known as chill tempering. This process involves the rapid cooling of the glass from a high temperature state at which time the glass is an unstressed, highly viscous liquid. The glass is then rapidly cooled by a blast of air. As its temperature drops below the glass transition temperature (T_g), the surface structure of the glass becomes rigid, while the interior

body is still above T_g, and hence fluid. In this state, stresses can relax out in the liquid interior. When the central region eventually cools and becomes rigid its molecular structure densifies producing compressive stresses in the surface and tensile stresses in the interior. The stress distribution is as shown in Figure 3a. Compressive stresses as high as 10,000 to 15,000 psi can easily be achieved by this method. In use, no tensile stress will be produced in the glass surface until the residual compressive stress is overcome, as shown in Figure 3c where the bending stress shown in Fibure 3b is superimposed on the residual stress of 3a.

B. Strength and Defects

Many researchers have shown that the theoretical strength of any given material is of the order of E/5 to E/10 where E is Young's modulus. This prediction is based on the simultaneous separation of atoms across a single cross section. The actual strength of soda-lime-silicate glass seldom exceeds 10,000 psi which corresponds to approximately E/1000. The discrepancy may be explained on the basis of either the energy or stress concentration fracture criteria, as proposed by Griffith and Inglis respectively. (The concepts were discussed in the preceding section.) In general, both approaches consider the discrepancy a result of stress concentrations at the tips of flaws, which lead to the sequential rather than simultaneous separation of the atomic bonds across the specimen. The reduction in actual strength from the theoretical prediction may be seen in quantitative terms by calculation of the fracture surface energy, γ, from stable crack propagation experiments.

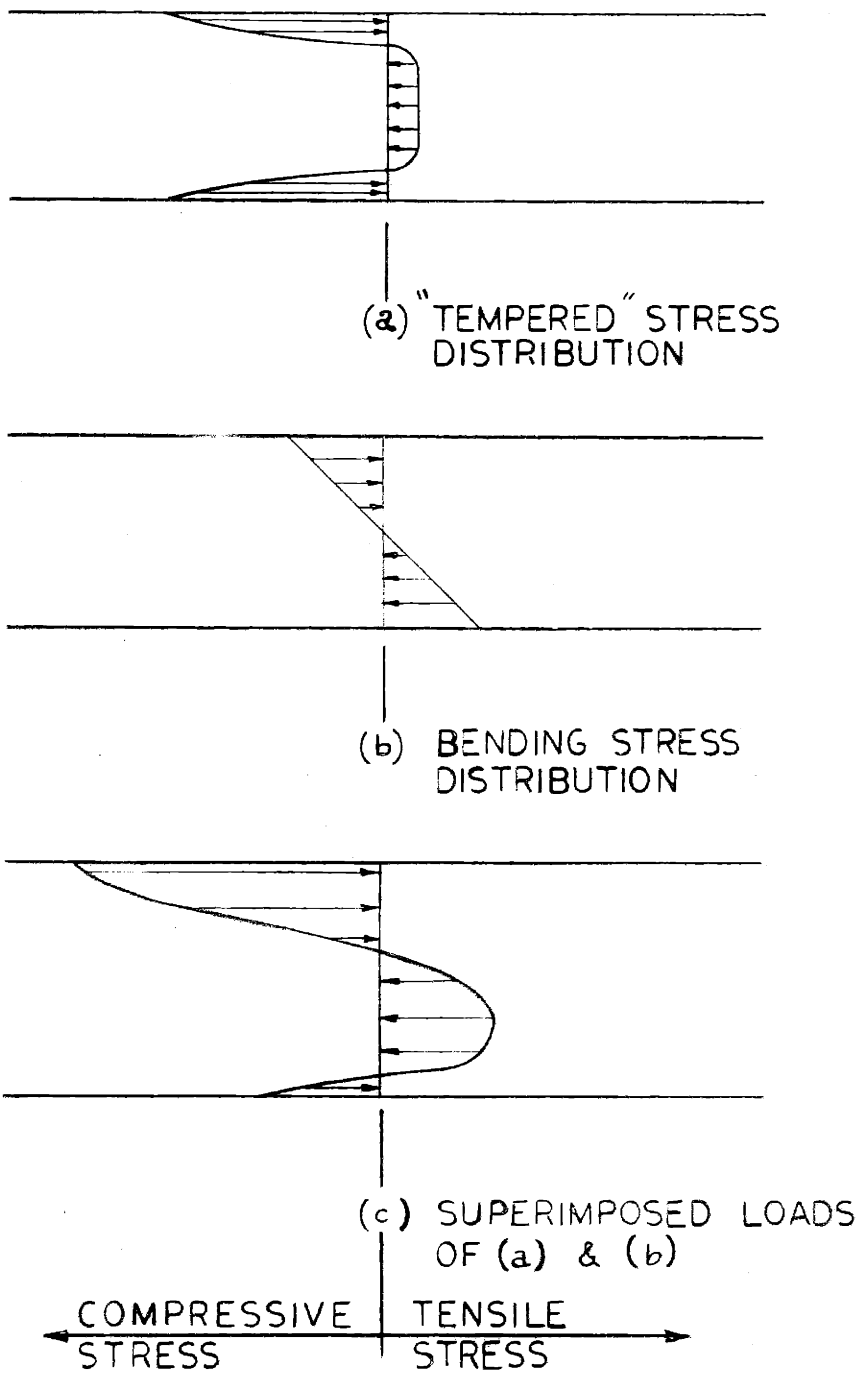

FIGURE 3: MECHANICAL & RESIDUAL STRESS DISTRIBUTIONS

is of little consequence.[5] (Hard second phase particle inclusions are an exception.) Furthermore, chemical etching to remove the surface layers and their inherent flaws effectively increases the glass strength regardless of sample size.[4] Table 1 shows the marked dependence of strength on surface condition. Merely touching the surface of "clean" glass with one's finger can lower its strength by an order of magnitude[3].

Defects arise in commercial glasses from incomplete melting of the glass feedstock, from foreign particles introduced during processing, surface roughness from forming machinery, and from mechanical damage during transportation and handling.

Melt related defects include voids, inhomogeneities, second phase particles and crystalline inclusions. These discontinuities serve as stress concentrators due to changes in elastic modulus and coefficients of expansion across their boundaries. They are particularly dangerous at free surfaces where the highest tensile stresses usually arise during loading, and where the defect is exposed to possible chemical attack from the environment. The effect of these defects can be disastrous when they are located in the tension zones of highly tempered glass.[7]

Defects arising from fabrication include excessive roughness and foreign particles which may be imparted to the glass by metal forming equipment. These flaws exist at the surface and therefore constitute serious strength reducers.

The most common major defect is that which results from mechanical damage during handling. Serious flaws may develop from high local

Table 1 [3] - Effect of Surface Condition on Strength

Surface Treatment	Strength (psi)
As Received from Factory	6500
Severely Sandblasted	2000
Acid Etched and Lacquered	250,000

pressures produced by the contact of hard objects. Smooth objects usually produce circular cracks surrounding the point of impact. Sharp objects result in local crushing of the glass at the point of contact together with the penetration of sharp cracks into the glass body.

Silicate glasses with "flaw-free" surfaces have shown strengths up to 75% of their theoretical strength, or approximately 2,000,000 psi.[5] This was accomplished by fire-polishing the surface in a "clean" environment. Actual strengths usually lie between 10000 and 15000 psi. In tests that will be described later in this paper, strengths of 1000 psi were common in samples that were severely flawed and then statistically loaded in the presence of a corrosive environment.

C. Fatigue and Environmental Stress Corrosion

When inorganic glass is subjected to long-term static loading it will fracture at a stress well below the fracture stress associated with loads of short duration. This phenomena is known as static fatigue. Static fatigue in glass is a serious strength-reducing mechanism which is capable of reducing the load bearing capacity by as much as 80%.

Two mechanisms appear to control the static fatigue process. First, a lowering of the surface energy (γ) by adsorption of elements from the atmosphere is possible with a simultaneous reduction in the fracture stress (σ_f) (see equation 7). A sizable reduction in the surface energy due to this process could account for the large decrease

in measured strength.[3] A more widely accepted mechanism is termed the stress corrosion process. Glathart and Preston[8] first demonstrated that static fatigue was the result of environmental interaction with material at the tip of sharp flaws or cracks. Furthermore, large stresses which are usually present at the tips of these stress concentrations accelerate the rate of corrosion of material at the crack tip, leading to sharpening and/or extension of the crack until its length or length-to-crack tip radius ratio is sufficient to cause fracture. R. J. Charles[9] postulated that the preferential attack at the crack tip which is necessary for a continuous increase in the stress concentration is the result of high tensile stresses at the crack tip which expand the glass network and allow increased diffusion and higher rates of corrosion. According to this theory the denser the glass structure the less its susceptibility to static fatigue. This is confirmed by the fact that quenched glasses with their open molecular network show higher rates of corrosion.[3] The validity of the stress corrosion theory is further confirmed by the dependence of static fatigue on temperature and humidity.

Static fatigue does not operate at the temperature of liquid nitrogen. The susceptibility of soda-lime-silicate glass to static fatigue increases with increasing temperature to a peak at approximately 200°C. At temperatures above 200°C there is increased resistance to static fatigue which may be due to decreased adsorption of atmosphere water or to inelastic deformation at the crack tip. This leads to the blunting of the crack and reduction of the stress concentration.[4]

Wiederhorn[10] investigated the crack propagation velocity in soda-lime-silicate glass as a function of environment and stress intensity. Temperature was held constant in these experiments. His results show that the relation of crack velocity to these parameters falls into three distinct regions. At low stress levels the velocity is exponentially dependent on stress, and increases with increasing humidity in the environment. The velocity is evidently a function of the rate of chemical reaction at the crack tip. In region II, at higher stresses, the dependence on stress diminishes until the velocity is independent of stress. The velocity is strongly dependent on humidity in this region. Wiederhorn has suggested that the rate of transport of water vapor to the crack tip limits the crack velocity in region II. At still higher stresses, region III, the velocity again increases exponentially with stress and no longer shows any dependence on environmental conditions. At this point the crack velocity exceeds the rate at which water vapor can be transported to the advancing crack tip.

Varner and Frechetti[11] have attributed certain ripple marks on the fracture surface of soda-lime-silicate glass to crack front hesitations in region II where crack velocity is dependent on humidity alone. They postulate that the crack stops in this region because water vapor cannot be transported fast enough to the crack tip to maintain continuous corrosion and constant propagation. The crack halts if the stress is not large enough to cause fracture without the aid of stress corrosion. The stoped crack allows moisture to reach the crack tip

whereupon stress corrosion again operates, and the crack advances.

The effect of cyclic fatigue on soda-lime-silicate glass was investigated by Gurney and Pearson.[12] They concluded that the fatigue limit, or the stress below which no long-term failure occurred was essentially the same for both statically and cyclically loaded specimens. When the cyclic stress varies in a step function between $-\sigma$ (compressive stress) and $+\sigma$ (tensile stress) the strength reduction of the specimen can be described by static fatigue processes with the time under load being the sum of the time under $+\sigma$.

D. Fracture Surface Morphology

The critical stage in the fracture of glass is the initiation of the crack. In a uniform stress field the conditions that result in crack initiation will also result in the propagation of that crack to failure.[3] This behavior is typical of brittle materials which show no deformation mechanism capable of absorbing large amounts of energy during the fracture process, such as plastic deformation in metals. Since glass fracture is an initiation dominated process, the examination of the conditions at the origin of fracture is of primary interest. A thorough analysis of the conditions that govern fracture initiation must describe the severity of the most critical flaw, as well as the direction and magnitude of the stress field in the immediate vicinity of that flaw. The most common procedure for determining the nature of these parameters is the visual analysis of the fracture surface.

A detailed study of the morphology of glass fracture surfaces provides a wealth of information concerning critical flaws, stress magnitude, stress direction, strain energy release rate, and crack speed and orientation. The analysis of these factors during unstable crack propagation in a brittle material is a complicated dynamic problem. But the conditions of stress at any point in a continuum at the onset of fracture may be closely approximated by the laws of static analysis. For this reason, the fracture surface characteristics in the vicinity of the origin are of great interest since they can be correlated with a known stress condition.

There are generally three distinct zones adjacent to the point of origin as illustrated in Figure 4 and Photo 1. The region nearest the origin is a smooth area marked by small ripples which are visible in reflected light. This region, known as the mirror, is bounded by a narrow band of hazy surface, known as mist, which in turn gives way to a very coarse hackled region. Higher magnification shows that the surface irregularities in the mist region resemble those in the hackled region, but on a smaller scale, and so are termed micro-hackle. The mist region represents an insipient stage in the progression of surface roughness from mirror to hackle. The coarse hackles are oriented parallel to the direction of crack advance. The sequence of mirror to hackle portrays the crack front's response to an increasing rate in the release of elastic strain energy during the fracture process. As the crack tip enters a region of high elastic energy release rate, it tends to maximize the fracture surface area created in an attempt to

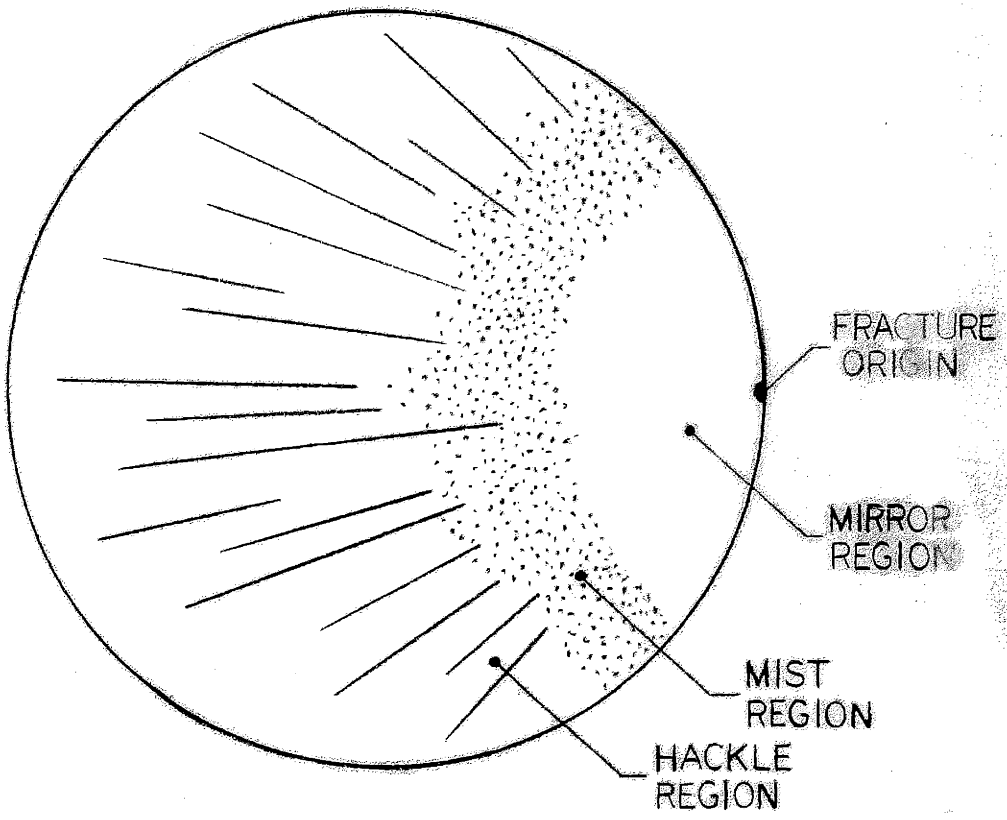

FIGURE 4: TYPICAL FRACTURE SURFACE MORPHOLOGY

Photo 1 - Typical Fracture Surface Morphology for Annealed Glass

convert all the elastic energy into surface energy. The maximization of surface energy, and therefore surface area, might be achieved by the creation of zones of hackle, or by crack branching, or both, as is generally the case.

The release of elastic energy can result in the instantaneous reduction of the stress ahead of the crack tip in which case the crack may reenter a mirror region and the surface roughness build-up begins again. Such a release is often seen when the crack front branches. Specific examples of this phenomena will be noted and discussed later in this paper.

At high levels of stress, branching or forking of the crack front occurs. The onset of branching and the appearance of hackle occur simultaneously. Preston[13] showed that the angle of branching of cracks is an indicator of the stress system in the member prior to fracture. The angle is a function of the ratio of the biaxial stress components in thin walled members under bending, torsion and hydrostatic pressure. Preston's results are illustrated in Figure 5.

An accurate estimate of the magnitude of the fracture stress, rather than the stress system, can be calculated by measurement of the size of the mirror zone surrounding the fracture origin. It has been shown by many researchers,[14-17] that a relationship exists between the size of the mirror zone and the stress required to initiate fracture. The relationship has been described by the empirical equation:[14]

$$\sigma = \frac{C}{r^b} \qquad (8)$$

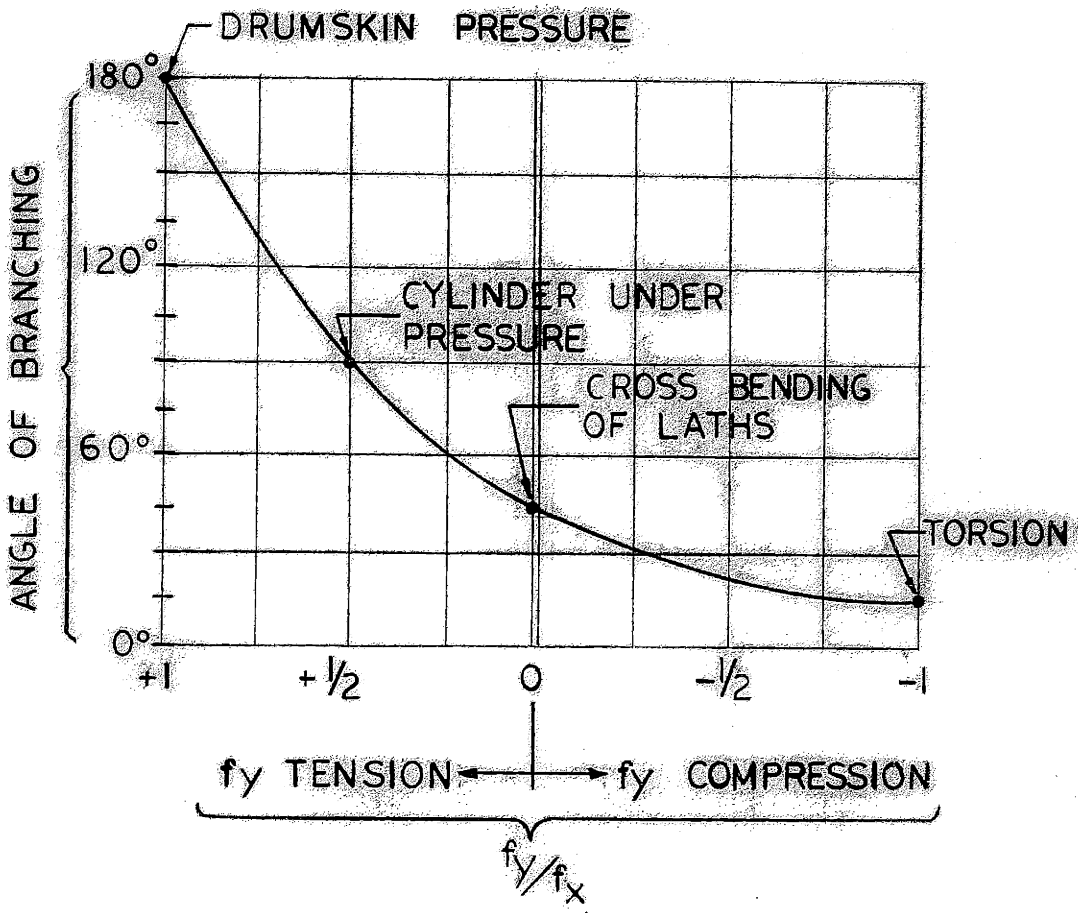

NOTE: f_x denotes principal biaxial stress component

FIGURE 5 [13]: ANGLE OF CRACK BRANCHING VS. STRESS SYSTEM

where σ is the modulus of rupture in psi, C is an experimentally determined constant and r is the radius of the mirror zone in inches, measured from the point of origin to the mirror/mist interface. For soda-lime-silicate glass a value of 0.5 for b and 1950 for C agrees reasonably well with experimental results as shown by Orr.[18] Kerper and Scuderi[14] found that the correlation between mirror size and modulus of rupture was independent of other factors that affect the strength of glass such as surface roughness, test temperature, and loading rate. Furthermore, they found that the value of C varied with glass composition and the value of b decreased slightly for fractures at low stress. Kerper et al., were also able to show that the correlation between fracture stress and mirror radius holds for tempered glass, although the values of the constants change considerably when residual stresses are introduced. For example, typical values for tempered glass were C = 7500, b = .31 for fracture origins at the surface, and C = 15200, b = .17 for edge origins.[15] Kerper and Scuderi attribute the change in the values of b and C to variations in the residual stress distribution at the different locations in the tempered specimen.

The theoretical basis for the empirical equation relating fracture stress and mirror radius can be shown by consideration of Griffith's energy criterion for fracture. Let C in equation (8) equal the product of the terms γ and E in equation (7). If b is taken to equal 0.5, which is generally the case then the term r in equation (8) is seen to equal c, which is the half crack length in equation (7). In other words,

the mirror can be seen as the Griffith flaw in quasi-stable crack growth. This argument can be used to shed some light on the progressive roughening of the fracture surface in the area of the fracture origin. If we treat the mirror as the Griffith flaw, then, as the mirror grows in size during the initial stage of fracture, the material ahead of the crack tip will realize an ever increasing stress intensity as predicted by the Griffith equation. When the stress intensity reaches some critical value, each additional increment of crack propagation will release excessive amounts of elastic energy. At this stage the crack begins to propagate unstably. This occurrence is manifest on the fracture surface as the onset of mist and hackle. Crack bifurcation may also occur at this point. Both the increased surface roughness and the branching of the crack front serve to dissipate the excess elastic energy released by the fracture process in this stage.

Fractures that are initiated at low stress levels due to serious flaws do not show defined mirror, mist, and hackled regions. Under these conditions the level of elastic energy released by the propagating crack is not sufficient to cause roughening of the fracture surface and bifurcation of the crack front. In this instance the only markings that may be apparent on the fracture surface are rib-marks, Wallner lines, and occasionally striations.

Rib-marks represent the imprint of the actual crack front at a single time during the propagation process. They are produced by a momentary hesitation in the crack front, or by the interaction of the entire propagating crack front with a stress pulse.[19] Elastic stress

pulses, which are normally associated with impact loading, are also produced by rapid changes in internal forces due to the redistribution of stress during crack propagation, or by the crack front itself as it passes an irregularity at the surface of the specimen. As these elastic waves propagate through the material they interact and alter the magnitude and/or direction of the principal tensile stress. A change in the direction of the principal tensile stress at the crack tip will cause the crack to deflect so as to remain perpendicular to the direction of the altered tensile stress field. Hence, a rib-mark is formed as shown in Figure 6. If the change in the magnitude of the principal tensile stress due to its interaction with the elastic pulse is significant, then the stress may drop below the level necessary to maintain crack propagation and the crack stops.

Rib-marks, and therefore crack fronts, are always concave toward the origin of fracture. Since rib-marks represent changes in the plane of fracture, they are most easily viewed by reflected light as shown in Photo 2.

The second type of ripple marking is known as the Wallner line. Such lines are often observed within the mirror zone of the fracture. Wallner lines are small undulations in the crack plane. They are concave toward the origin of fracture as are rib-marks, but do not represent crack front hesitation, or fracture plane reorientation. Like rib-marks, the undulations arise due to the interaction of the crack front with elastic waves. But unlike rib-marks, Wallner lines represent a transitory interaction as illustrated in Figure 7.

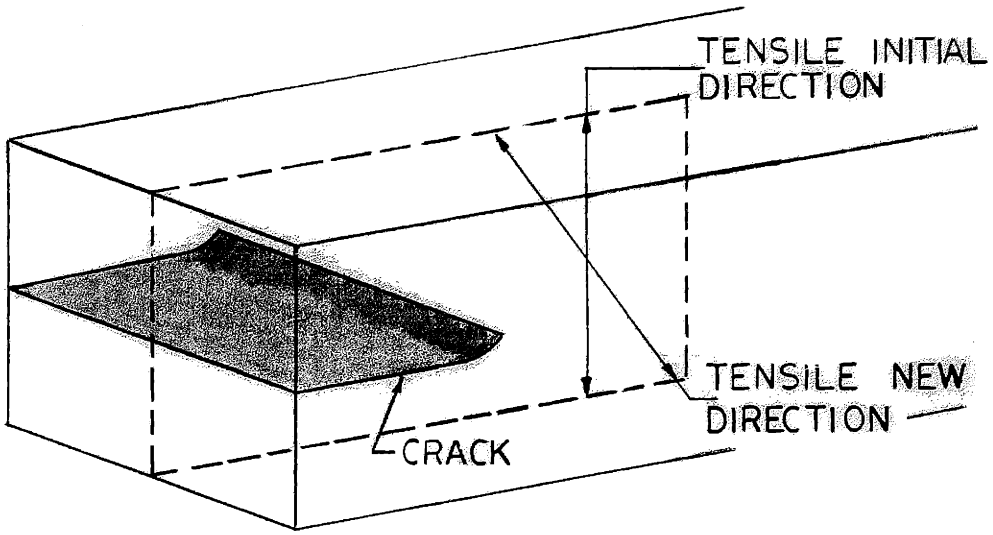

FIGURE 6[19]: FORMATION OF RIBS

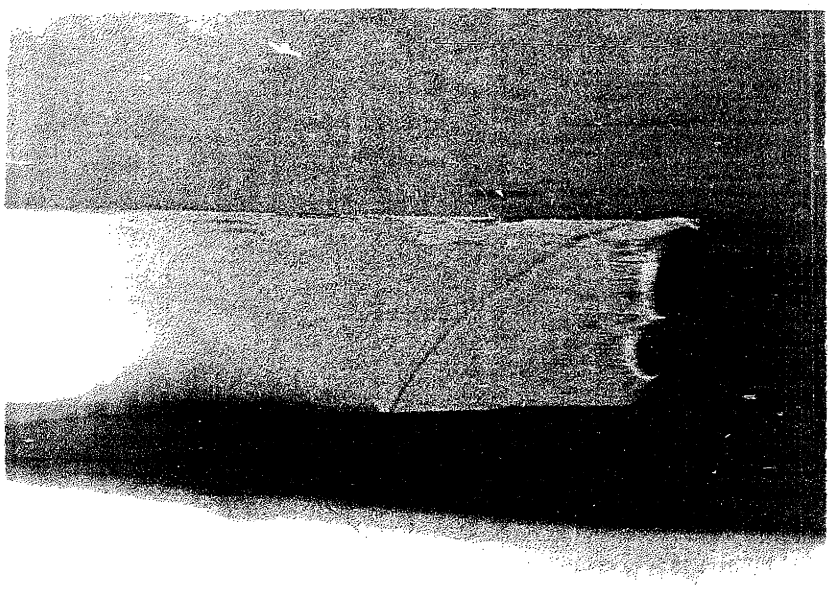

Photo 2 - Typical Rib-Mark

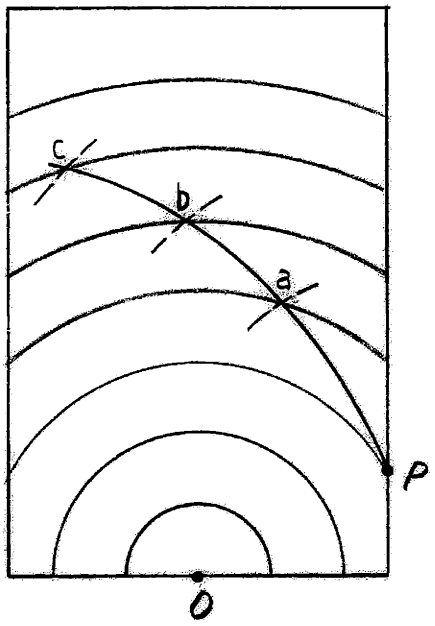

FIGURE 7 [21] : WALLNER LINE FORMATION

The concentric lines about the point O in the Figure represent an idealized crack front at equal increments of time after initiation. If the crack front reacts with some irregularity or surface defect at point P then a stress wave is produced that travels at least twice as fast as the crack front.[20] The dotted lines in the Figure show the locations of the stress wave at equal time increments after its initiation. As the pulse interacts with the crack front at points a, b, and c, the Wallner line Pabc is traced out. Knowing the location of the origin of fracture, the origin of the Wallner line and the speed of the appropriate elastic wave, the crack speed can be calculated. [Note: There are many types of elastic waves that are generated in solids; torsional, compressional and shear waves, to name a few. The effects of these various waves can be major with respect to fracture initiation as well as propagation. A more detailed discussion of these effects is withheld until later in this paper when impact fracture is discussed. For the purpose of the present discussion shear waves are generally considered the appropriate elastic wave.[19]]

It has been shown by many researchers[20, 22] that the speed of a propagating crack in glass reaches a terminal velocity at approximately one half the speed of the shear wave. The speed of this elastic wave is approximately 3000 m/sec, and therefore a terminal crack speed of approximately 1500 m/sec is expected. This value for the terminal velocity has been confirmed by Schardin.[22]

The configuration of Wallner lines within the fracture mirror can be used to determine crack speeds. Figure 8 depicts two

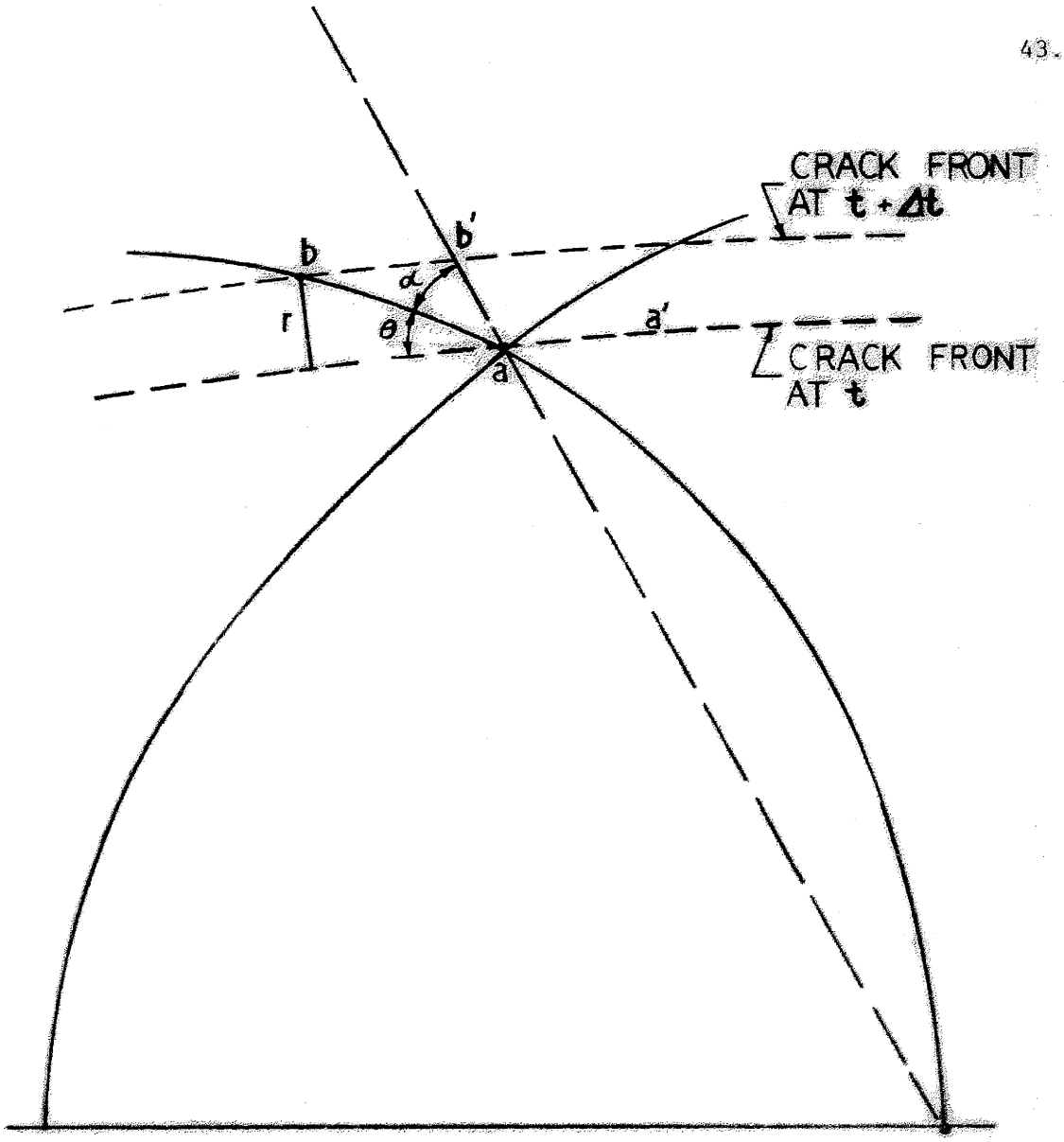

FIGURE 8 [19]: CRACK SPEED DETERMINATION FROM ORIENTATION OF WALLNER LINES

intersecting Wallner lines near the origin of fracture. Curve Oab representsa Wallner line produced by a stress pulse generated at point O; aa' and bb' are the locations of the crack front at times t and t + Δt respectively. The speed of the crack is r/Δt, which equals $\frac{\overline{ba}\ \sin\theta}{\Delta t}$; but the speed of the pulse, V, is $\frac{\overline{b'a}}{t}$; therefore,

$$\text{crack speed} = V\ \frac{\sin\theta}{\cos\alpha} \qquad (9)$$

Another form of surface fracture marking is the striation. Striations form as the crack front attempts to readjust to a change in the orientation of the principal tensile stress as that stress rotates about an axis that is parallel to the direction of crack advance. As the crack front attempts to remain perpendicular to the principal tensile stress, it too rotates about its axis of propagation. This is shown schematically in Figure 9. In order to remain normal to the direction of principal tensile stress it divides as illustrated in the diagram. The striations always develop in the direction of crack propagation.

A propagating crack will tend to orient its plane of fracture perpendicular to the direction of the principal tensile stress. Given this fact, it is difficult to explain why cracks often branch after they have attained terminal velocity. Yoffe[23] explained this seemingly anomalous behavior by showing that the stress field surrounding a running crack differs from that of the static or quasi-static crack in that it shows dual tensile maxima occurring at symmetrical off-axis

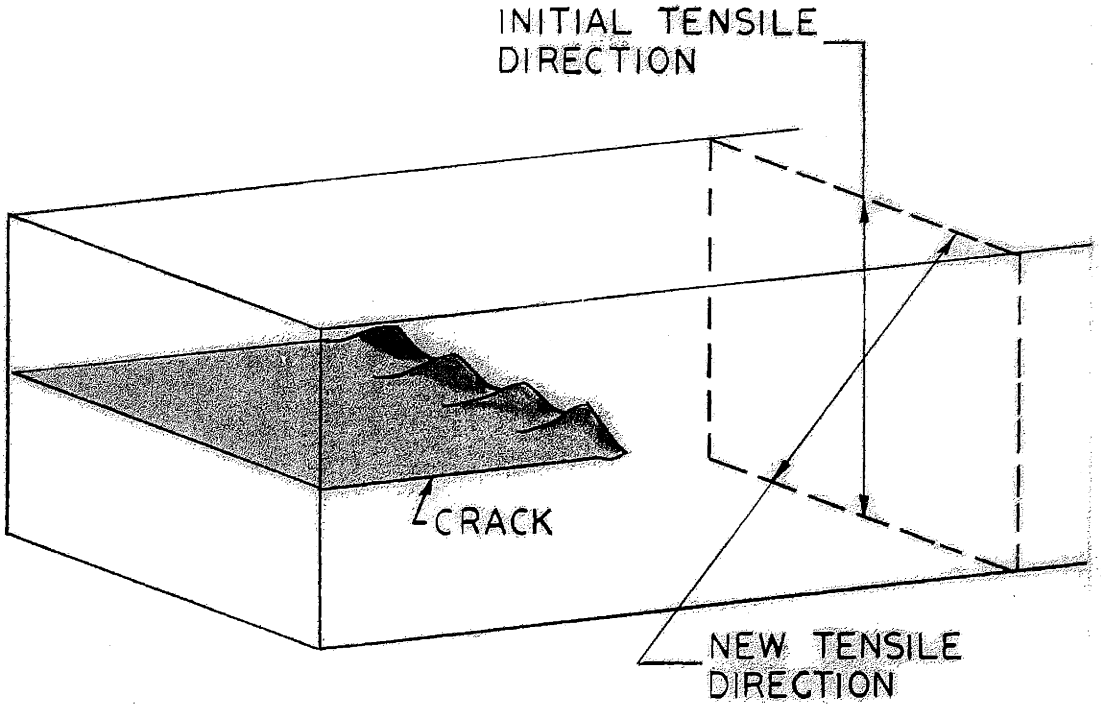

FIGURE 9 [19]: FORMATION OF STRIATIONS

points for a crack travelling at some critical speed. Thus, as the crack reaches this critical speed, which is taken as its terminal velocity, it may propagate directly ahead, deflect to one side, or bifurcate. Hence, the crack is extremely unstable at its terminal velocity with respect to direction as well as fracture surface characteristics.

IV. MECHANICAL FRACTURE

A. Mechanical Stress States

The discussion that follows will be concerned primarily with the tensile stress distribution associated with the bending of thin plates and beams. Tensile stresses are of interest since they initiate fracture.

Figure 10 illustrates the bending stress distributions that are developed in three and four point bending. In three point bending, with the load equidistant from the supports, the maximum tension occurs on the lower surface, directly opposite the applied load. In the case of four point bending, the area between the central, symmetrically placed loading bars, is equally stressed at the maximum tension level.

In the bending of a thin lath, whose width dimension is much larger than its thickness, there is developed a state of biaxial tension on the lower tensile surface. The biaxial state develops due to the effect of transverse bending in thin wide plates. At the edges of the lath the stress is uniaxial, but at the center the transverse component of the biaxial stress is equal to approximately 1/5 the longitudinal stress; according to the formula, $\sigma_y = \mu \sigma_x$, where σ_y is the stress due to transverse bending, σ_x is the stress due to longitudinal bending, and μ is Poisson's ratio, equal to .21 for soda-lime-silicate glass. The stress recorded at fracture is σ_x.

B. Experimental Procedure

Annealed and tempered soda-lime-silicate glass samples were obtained

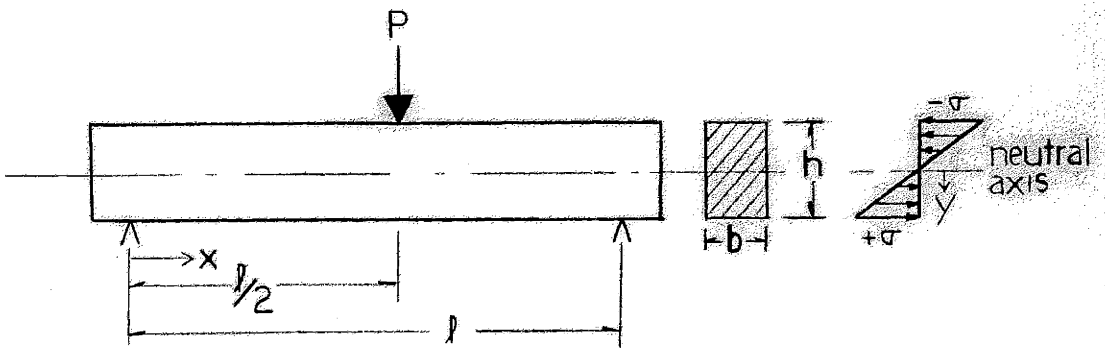

$$+\sigma_{max}\left[\text{at } x=\ell/2,\ y=+h/2\right] = \frac{3}{2}\,\frac{P\ell}{bh^2}$$

(a) 3 POINT BEND

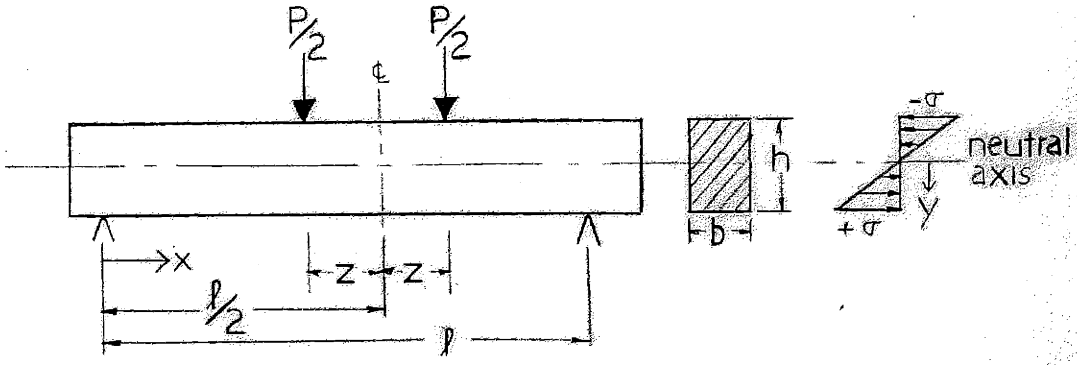

$$+\sigma_{max}\left[\text{at } x=\ell/2-z \text{ to } x=\ell/2+z,\ y=h/2\right] = \frac{3}{2}\,\frac{P\ell-2Pz}{bh^2}$$

(b) 4 POINT BEND

FIGURE 10: BENDING STRESS DISTRIBUTIONS

from local distributors of Pittsburgh Plate Glass. Mechanical stressing to failure was performed by bending at room temperature. The test specimens for three and four point bending measured 10 x 1-1/2 x 3/16 inch in accordance with ASTM C-158. They were tested to fracture on a test jig which consisted of two 1/8 inch mild steel bars spaced 8 inches apart and a center loading block which had one 1/8 inch bar for 3 point loading or two bars at a two inch spacing for four point loading. The test set-ups are illustrated in Figure 11 a, b. In addition a few samples were cut into narrow beams measuring 10 x 3/8 x 3/16 inch for testing in the jig as shown in Figure 11c. Static fatigue tests were conducted on a fixed cantilever beam arrangement as shown in Figure 11d. All samples were loaded in a standard Instron Testing machine. Prior to testing, the test specimens received various surface treatments and various types of flaws.

C. Experimental Results and Discussion

1. Fracture Surface Morphology

The fracture of annealed glass laths by the procedure previously described produces the following typical fracture surface characteristics. A mirror region surrounding the origin of fracture is oriented normal to the direction of the principal tensile stress and is open at the top as shown in Photo 3. The mirror is not enclosed by mist and hackle as a result of the bending stress gradient that develops near the origin. The stress gradient, as shown in Figure 10, includes an initial stress free neutral surface at the mid-plane of the bent lath. There is no

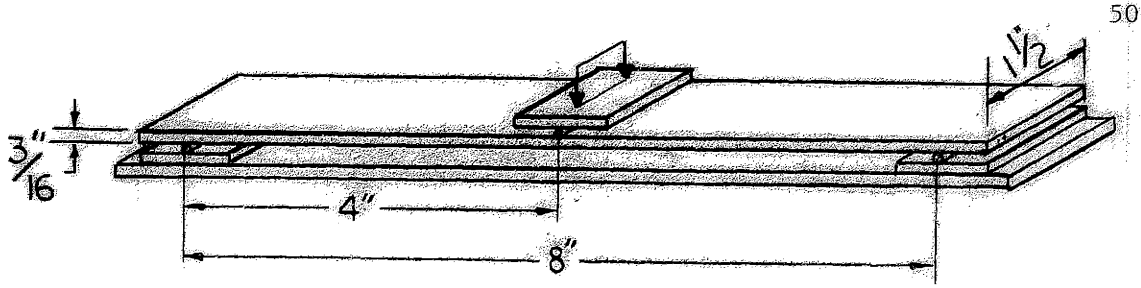

a) 3 POINT BEND - LATHS

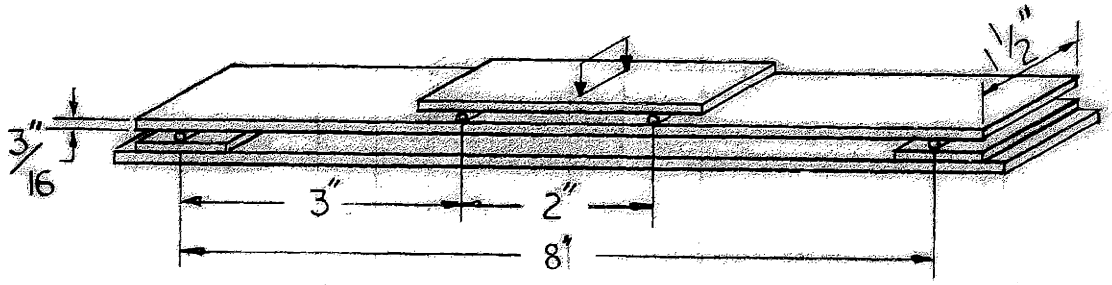

b) 4 POINT BEND - LATHS

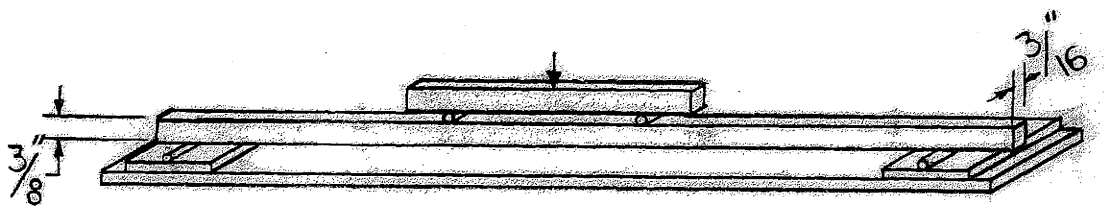

c) 4 POINT BEND - THIN BEAMS

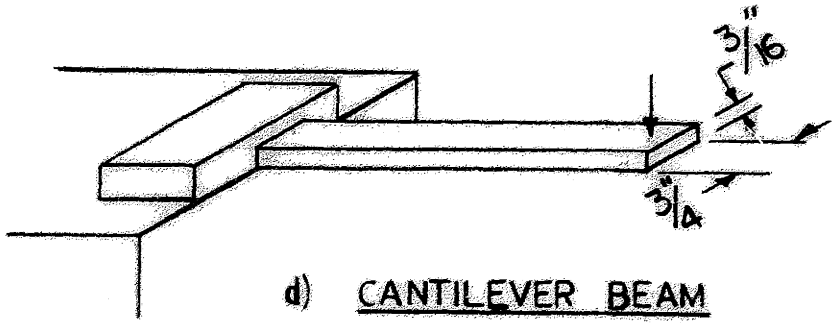

d) CANTILEVER BEAM

FIGURE 11 : BENDING TEST ARRANGEMENTS

large release of elastic energy as the fracture nears the neutral surface since the amount of elastic energy stored in this region is low. Therefore, no mist or hackled regions exist to enclose the mirror. (It should be noted that the assumption of a neutral surface at the mid-plane during crack propagation is an approximation, since the static stress distribution is grossly disturbed during the fracture process.) When the test laths were oriented vertically in the test rig rather than horizontally, the fracture mirror produced was often enclosed completely by the mist and hackled region. The new orientation removed the neutral surface from the vicinity of the fracture origin, thereby creating regions of considerable elastic energy around the entire mirror region and not just near the maximum tensile surface. In thermally induced fractures the stress gradient is not so severe as is generally the case in bending. Therefore, thermal fracture mirrors are usually fully enclosed. This will be discussed in greater detail in Section V below.

In the bending of horizontal laths the mist and hackled regions that bound the mirror take the form of wings that lie along the lower tension surface, as shown in Photo 3. As noted previously, mist and hackle are apparent on regions of the fracture surface that have experienced high elastic energy release. They occasionally appear in a repeating pattern as in Photo 4. This kind of repeating sequence indicates that the release of elastic energy is not necessarily a steady-state process. The pattern shows that an instantaneous reduction of the stress ahead of an advancing crack front is possible.

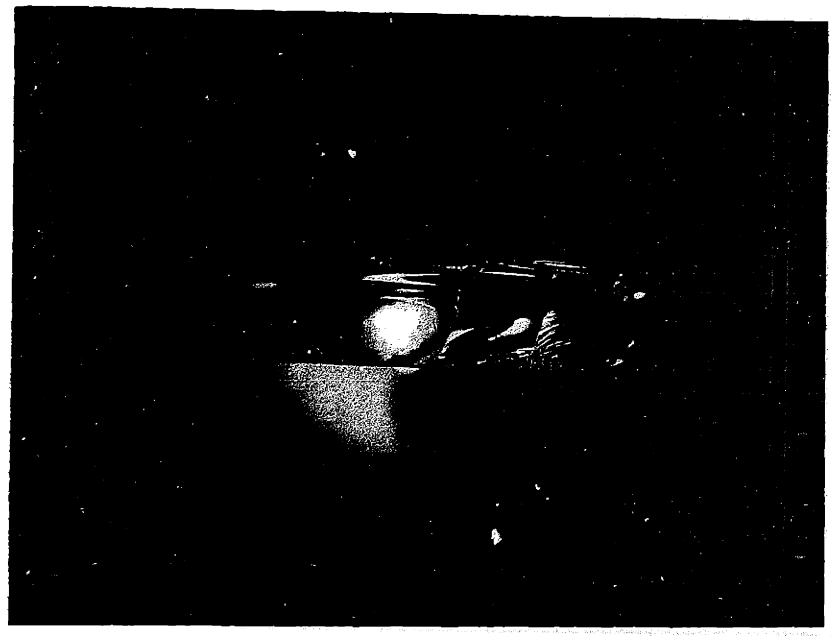

Photo 3 - Orientation of Mist and Hackle on Bending Fracture Surface

Photo 4 - Repeating Fracture Morphology

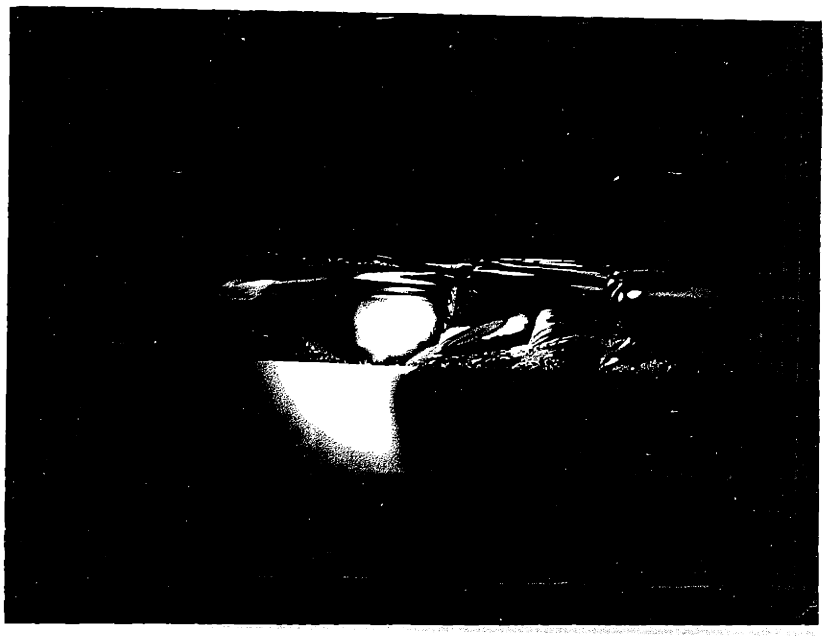

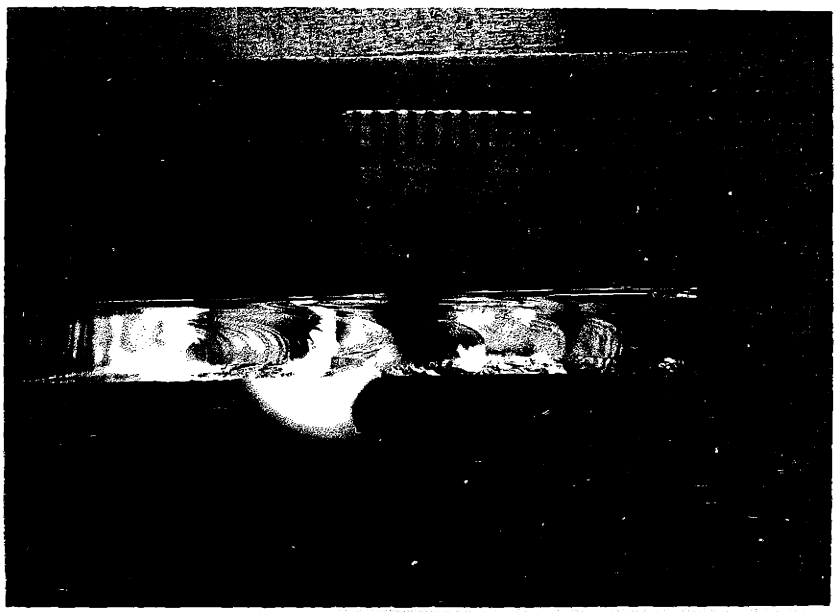

Fractures that were initiated at stresses below approximately 4000 psi created no mist or hackled regions on the fracture surface. Wallner lines and rib-marks were still apparent. In a few of the low-energy fractures,rib-marks and Wallner lines were visible adjacent to each other, and appeared almost coincident. The nearly coincident markings, as shown in Photo 5, indicate a slowly advancing crack front. Striations may occur in low energy fractures if the direction of the principal tensile stress rotates about an axis parallel to the direction of crack propagation, as previously shown in Figure 9.

Flexural tests were also conducted on annealed laths under water to determine the effect of environmental stress corrosion on the stress required to fracture and on the fracture surface morphology. Although samples tested in this manner generally broke at lower stress levels, the typical fracture surface patterns were not significantly altered. The correlation between the size of the fracture mirror and the fracture stress remained unaffected by the increased corrosion rate at the crack tip due to water submersion of the test specimen during testing. The orientation as well as the extent of mist and hackled regions were likewise unaffected.

The fracture stress for all specimens broken in bending was recorded directly from load to fracture measurements and then calculated on the basis of the size of the fracture mirror according to Equation 7. The values of the constants C and b were taken as 1950 and 0.5 respectively, as suggested by Orr[1]. As noted previously, samples that broke at applied stresses below approximately 4000 psi showed no

Photo 5 - Wallner Lines and Rib-Marks of Low Velocity Crack

boundaries to the fracture mirror, and therefore, the fracture stress for these specimens could not be calculated by this procedure. The radius of the fracture mirror was measured with a low power (7X) hand magnifying glass to the nearest .01 inch.

The quantitative and qualitative fracture data recorded for annealed laths tested in three and four point bending are shown in Table 2.

Comparison of the calculated and measured fracture stresses in Table 2 shows that the computation of stress to fracture by measurement of the mirror radius is reasonably accurate. The average deviation of the measured fracture stress from the fracture stress calculated by equation 7 is only 6%. Some error arose from the technique by which the mirror radius was measured, but the basic relationship between the mirror radius and the fracture stress holds despite this inaccuracy. Figure 12 illustrates this correlation graphically. The data also shows that the relationship holds for annealed glass regardless of the location of the fracture origin (i.e., surface or edge origin).

2. Static Fatigue and Environmental Stress Corrosion

The strength reducing effect of environmental stress corrosion is shown clearly by the data in Table 3. These results show that the strength of commercial glass in bending drops by approximately 20% when its surface is contacted by water while the specimen is under stress. The weakening effect of water under long term loading conditions will be discussed later in this section.

Table 2 - Fracture Stress of Annealed Laths Fractured by Bending

Mode of Testing	Test Specimen Surface Condition (1)	Number Tested	Range Measured σ_f (psi)	Average Measured σ_f(psi)	Average Calculated σ_b(psi)(2)	Comments
3 pt. Bending in Air	U	10	8100-10700	9240	9510	
	S	6	7150-9650	8825	9975	Wallner lines were more apparent on the surfaces of sandblasted samples
	N	2	2730-2860	2800	-	No facture surface markings
	P	6	7050-8500	7750	7670	
	C	6	3075-5570	5575	-	Samples with σ_f<4000 psi exhibited - no mirrors
4 pt. Bending in Air	U	7	6000-12400	9850	9450	
	S	6	8600-8900	8850	8530	
	C	6	3200-3800	3650	-	No samples exhibited mirrors
	P	6	4900-5150	5025	4360	
4 pt. Bending in Water	U	6	4950-12400	7550	6380	
	S	5	6200-6850	6750	6500	
	C	6	2550-3900	3225	-	No samples exhibited mirrors
	P	6	4100-7000	5550	-	2 of 3 samples exhibited mirrors

(1) Surface Condition Legend
- U As Received - No Induced Flaw
- S Sandblasted
- N Scored normal to principal tensile stress
- C Corner "Clam Shell" Flaw
- P Surface "Pin" Flaw

(2) $\sigma_b = 1950/\sqrt{r}$ from Reference [18]

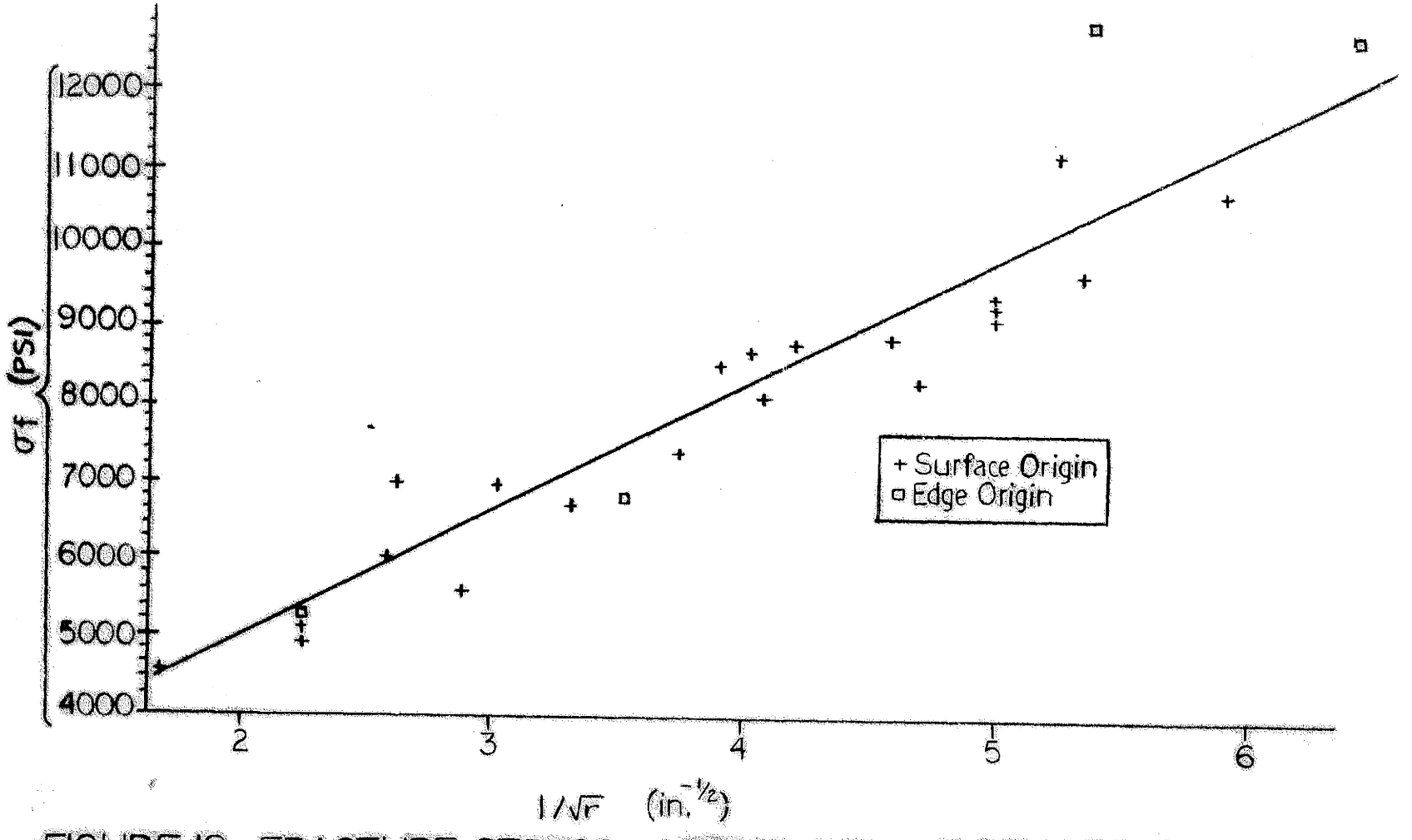

FIGURE 12: FRACTURE STRESS vs. MIRROR SIZE for ANNEALED GLASS

Table 3 - Effect of Accelerated Environmental Stress

Corrosion of Annealed Glass

Sample Condition	Average Measured Fractured Stress - σ_f (psi) In Air	#	In Water	#	% Strength Reduction
As Received (No Induced Flaw)	9460	17	7550	6	20%
Sandblasted	9170	12	6750	5	26%
Corner 'Chip' Flaw	4350	12	3400	6	22%
Surface 'Pin' Flaw	6660	12	5550	6	17%

[Note: The lower initial strength shown by specimens with corner damage was the result of deeper flaws that were produced at the corners, compared to those produced at the surfaces.]

The rate of loading was found to have a slight effect on the breaking stress and no effect on the fracture surface morphology. As the rate of stress application was increased from 250 psi/min. to 25000 psi/min (this corresponds to loading machine cross-head speeds of 0.001 inch/min. to 0.1 inch/min. respectively), the stress level at fracture increased by about 30%. This corresponds to a 15% increase in the strength of the specimen for each decade increment in the rate of load application. This phenomenon is related to the rate of environmental stress corrosion at the crack tip.[2]

The combined effect of static fatigue and accelerated stress corrosion in the presence of serious flaws was investigated by the use of cantilever beam specimens measuring 8 x 3/4 x 3/16 inch, as shown in Fig. 11d. The specimens were scored normal to the principal stress direction at the point of maximum stress. The first set of specimens were loaded to produce a maximum stress of 1000 psi; the second were loaded to a stress of 1500 psi. Water was applied directly into the flaws of some specimens at various time intervals to accelerate the corrosion process. The results are recorded in Table 4. The wide scatter shown by the data is the result of variations in the severity of flaws produced by the scoring technique. It should be added, however, that static fatigue measurements, even under the most controlled test

Table 4. Static Fatigue and Environmental Stress Corrosion

Applied Stress	Sample Designation	Time to Fracture	Time Under Attack by Water Before Fracture
	95	2 min	1 min
	92	2.5	2.5
	96	7	2
	101	13	-
	103	13	-
	91	30	1
1000	99	38	23
(psi)	100	48	18
	102	95	5
	93	*	∿24 hrs.
	94	*	24 "
	97	*	24 "
	98	*	24 "
	104	∿1 sec	∿1 sec
	90	15	-
	105	25	10
	106	30	∿ /sec
	107	45	-
	108	45	-
	110	60	-
1500	111	1.5 min	-
(psi)	112	1.5 min	-
	109	7.5 min	2.5 min
	89	30 min	-
	113	∿2 hr.	∿1 hr
	114	∿4 hr	-
	115	*	∿24 hr

* No fracture after 24 hr.

conditions, often show considerable scatter. Nonetheless, the results shown in Table 4 do show the time dependent nature of glass fracture and the weakening effect of environmental stress corrosion.

In general the static fatigue cracks that developed under these test conditions grew to considerable length before unstable crack propagation occurred. Photos 6 and 7 show static fatigue crack development at 1500 psi maximum bending stress. The cracks grew to a length of approximately 0.1 inch before the specimen fractured. This compares with a critical crack length of .044 inch as calculated by the Griffith criterion for a uniform stress of 1500 psi and fracture surface energy equal to 4700 ergs/cm^2 as suggested by Wiederhorn. The most obvious reason for this critical crack length discrepancy is that the uniform stress distribution assumed by Griffith does not apply to the bending situation where the stress drops rapidly with distance into the specimen. As the crack extends into the cross section, the applied stress ahead of the crack tip diminishes. Correspondingly, the stress concentration at the crack tip drops, and the critical flaw length for unstable fracture increases.

The second possible mechanism allowing deep crack growth is related to the actual geometry of the crack tip under static fatigue and stress corrosion. This argument is open to some controversy.[3] If the radius of the developing crack is relatively blunt under conditions of static fatigue and stress corrosion, then the stress concentration at the crack tip will be reduced according to the Inglis concept and cracks of greater lengths could be accommodated without initiating unstable fracture. This mechanism in

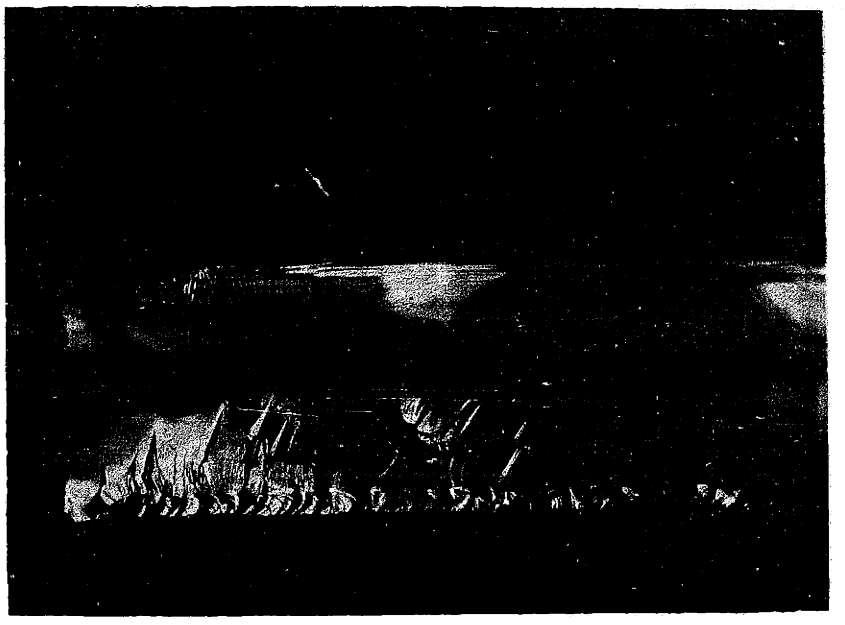

Photos 6 & 7 - Static Fatigue Fracture Surfaces

conjunction with the stress gradient effect might explain the deep cracks observed in these static tests.

Other than the fatigue cracks themselves, the fracture surfaces produced in this test series were essentially featureless due to the extremely low stresses at which the fractures were initiated. Rib-marks and striations where occasionally visible, but markings were not sufficient so as to allow determination of the origin of unstable crack propagation.

3. Edge Condition

Glass units for building construction are typically sized to the required dimensions by scoring the surface with a hard material and then breaking the glass along the scored line by bending across it. The resultant edge that is produced varies from perfectly smooth (except for the scored groove), as shown in Photo 8, to ragged, as shown in Photo 9. The flaws developed in this manner are termed "shark teeth". They are common in glass building panels and are considered acceptable by most commercial distributors if the depth of penetration of the shark teeth is limited to one-half the thickness of the plate.

In order to investigate the effect of shark teeth as critical flaws in fracture initiation, a number of narrow beam specimens measuring approximately 10 x 3/8 x 3/16 inch were cut by scoring in the standard commercial manner. These specimens were then oriented in the 4-point bending apparatus such that the scored edge was on the lower surface, hence in the maximum tension region. This configuration was

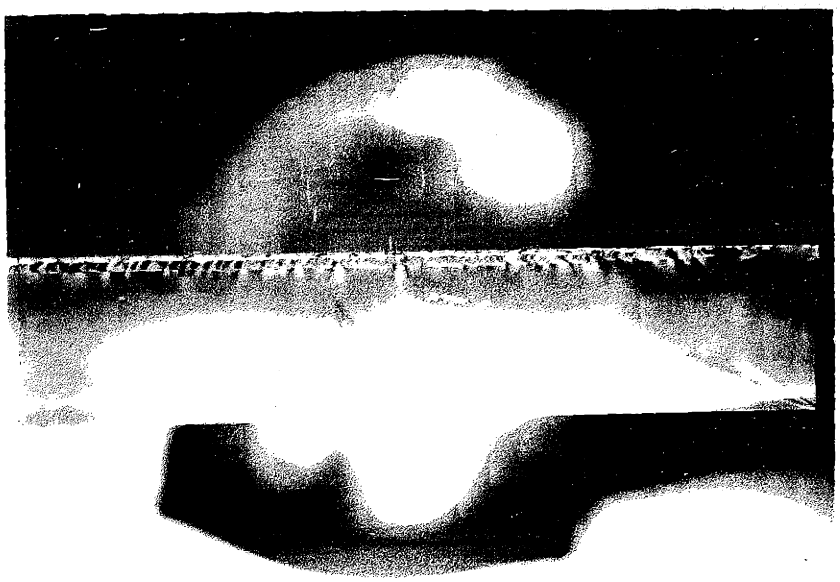

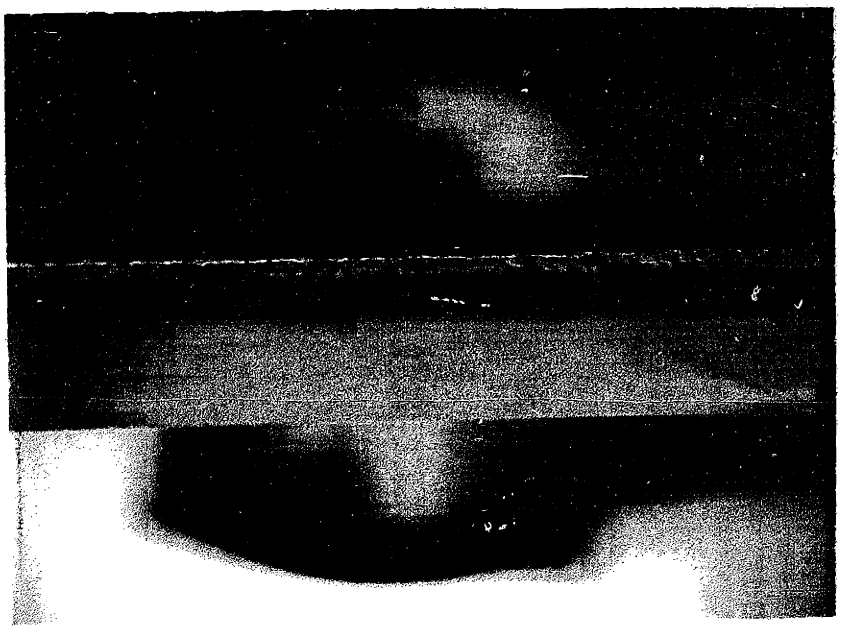

Photo 8 - "Clean" Scored Edge

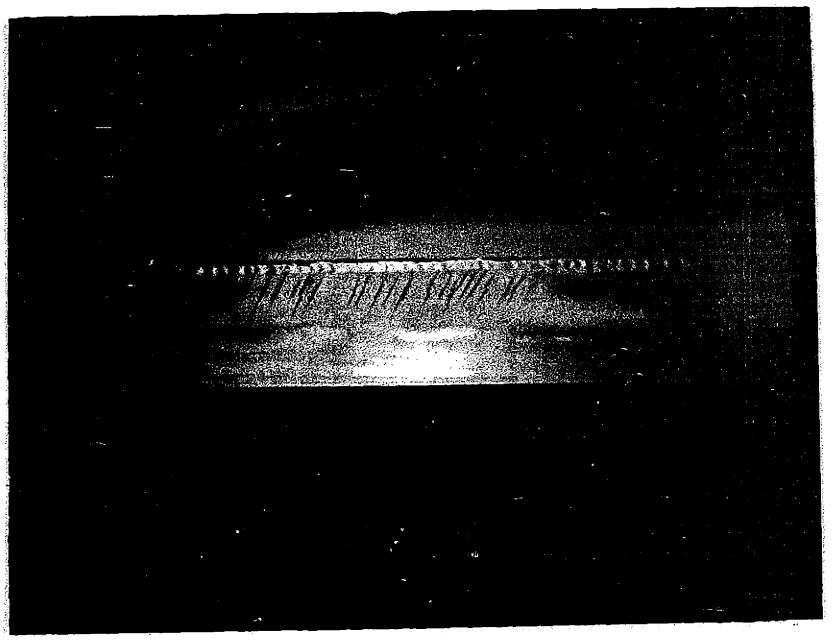

Photo 9 - Scored Edge Showing Shark Teeth

used to roughly approximate the bottom edge condition of glass panels in a building application.

A number of specimens were intentionally damaged by severe corner flaws to provide comparison for the relative weakening effect of shark teeth. Photos 10, 11 and 12 show typical fracture surfaces produced by various edge conditions. The general orientation of the fracture markings differs somewhat from previous tests for the reasons discussed earlier in this section. (That is, the orientation of these test specimens as beams rather than thin plates allows a redistribution of stress gradient over the cross section so that the neutral surface is further removed from the point of fracture origin. The fact that considerable tension exists below the neutral surface allows the mist and hackled regions to penetrate deeper into the body of the specimen than was the case in the bending fracture of laths.) Mirror regions may be completely enclosed as is the case in Photo 10 which represents the fracture surface produced from an edge with no shark teeth. Photo 11 shows the surface resulting from an edge with shark teeth that penetrate approximately one-half the thickness of the plate, and Photo 12 shows the fracture surface of a mechanically damaged specimen. The quantitative results of this test are shown in Table 5. The data show that edges with shark teeth are considerably weakened. The weakening effect is at least as serious as severe mechanical handling damage. All fractures from edges with shark teeth had their origins at the base of the shark teeth, which is the scored edge. This is a significant observation since it implies that the shark teeth themselves may not be the weakening flaw. It is entirely possible

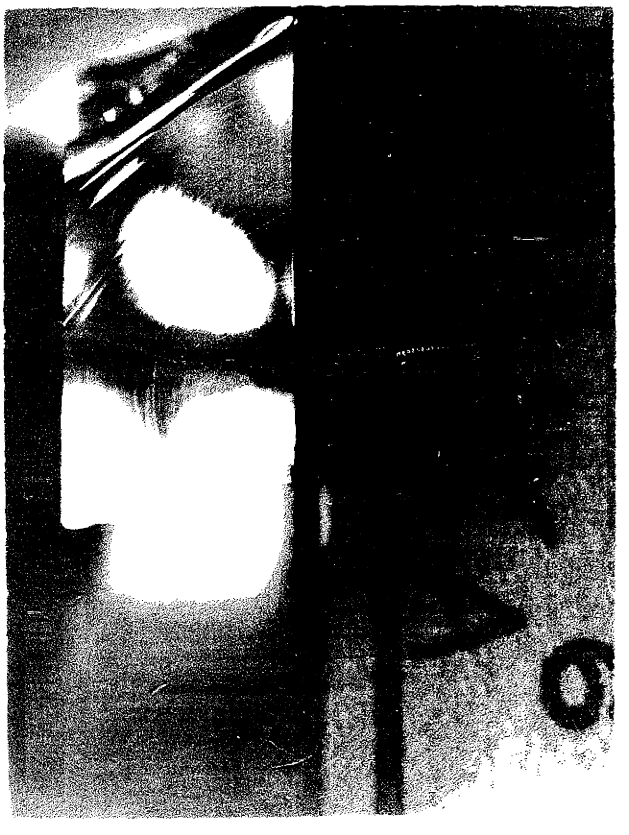

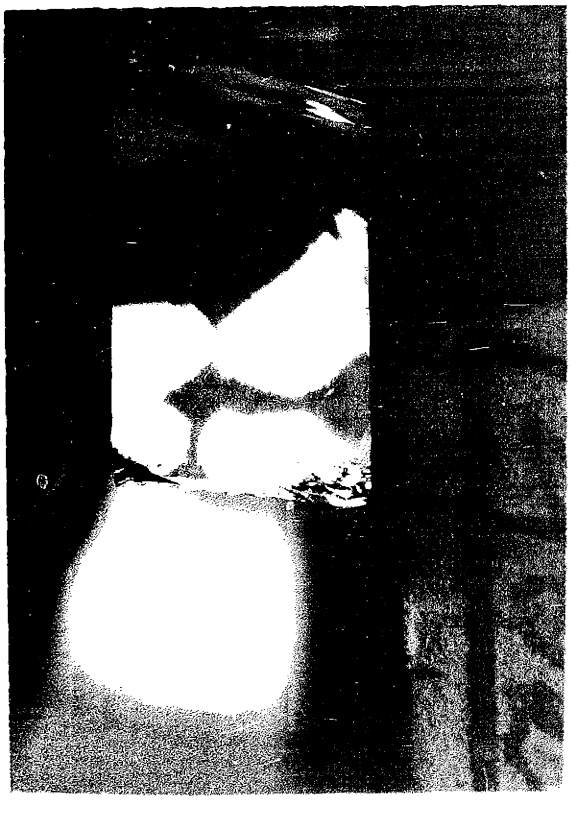

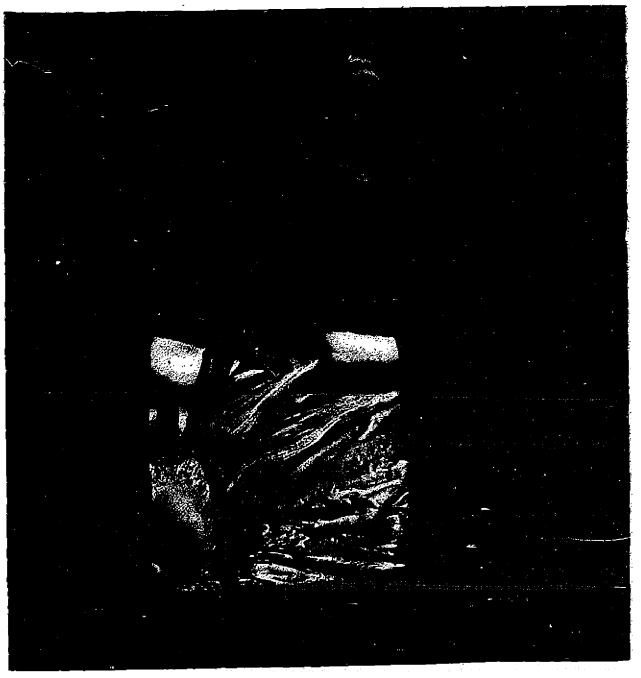

Photo 10 - No Shark Teeth

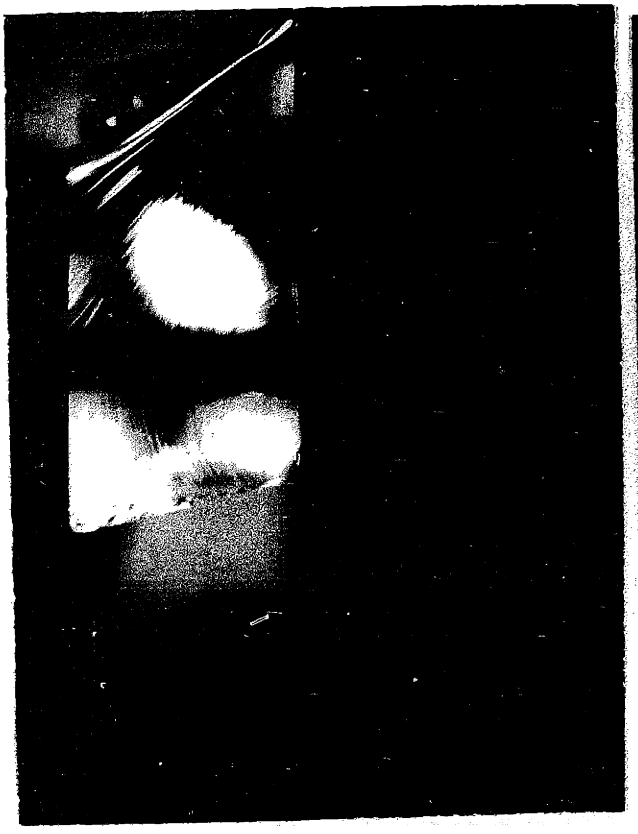

Photo 11 - Shark Teeth that Penetrate 1/2 Plate Thickness

Photo 12 - Severe Mechanical Damage

Table 5 - Effect of Shark Teeth on Strength Of Edge

Tested	Edge Condition	Ultimate Strength of Edge (σ_f)	Range in σ_f
	Good		
5	(No shark teeth) (No corner damage)	10500 psi	9450-11150
	Acceptable		
6	(Shark teeth - penetration ~1/2 width of eged)	4875 psi	3280-6810
	Poor		
6	(Mechanically Damaged by Chipping Corner)	4590 psi	2280-6460

that the shark teeth are important only insofar as they indicate a seriously weak scored edge.

4. Crack Speed

The speed of the crack front at its initial propagation stages (i.e., within the mirror zone of the fracture surface) was investigated by the graphic method described in Section III and illustrated in Figure 8. Four specimens that showed clear Wallner line formation within the mirror were analyzed by this approximate graphic procedure. Each showed that the speed of the crack in the outer extremes of the mirror zone was approximately 1500 m/sec., or terminal velocity. Thus, the fracture was propagating at maximum velocity before it had reached the stage of maximum energy release which is signified by course hackle and crack branching. This fact casts doubt on the assumption made by many glass researchers that crack speed and fracture energy peak simultaneously. These results should, however, be viewed with caution since the method of analysis is approximate.

5. Crack Branching

Preston's research on the angle of crack branching as an indicator of the stress system was discussed in Section III above. He showed that the angle at which the crack front diverges is related to the ratio of the biaxial stress components in thin plates. This research suggests a further correlation between the angle of branching and the magnitude of the breaking stress, as illustrated in Figure 13. The angle of branching for a mechanically fractured lath is shown in Photo 13.

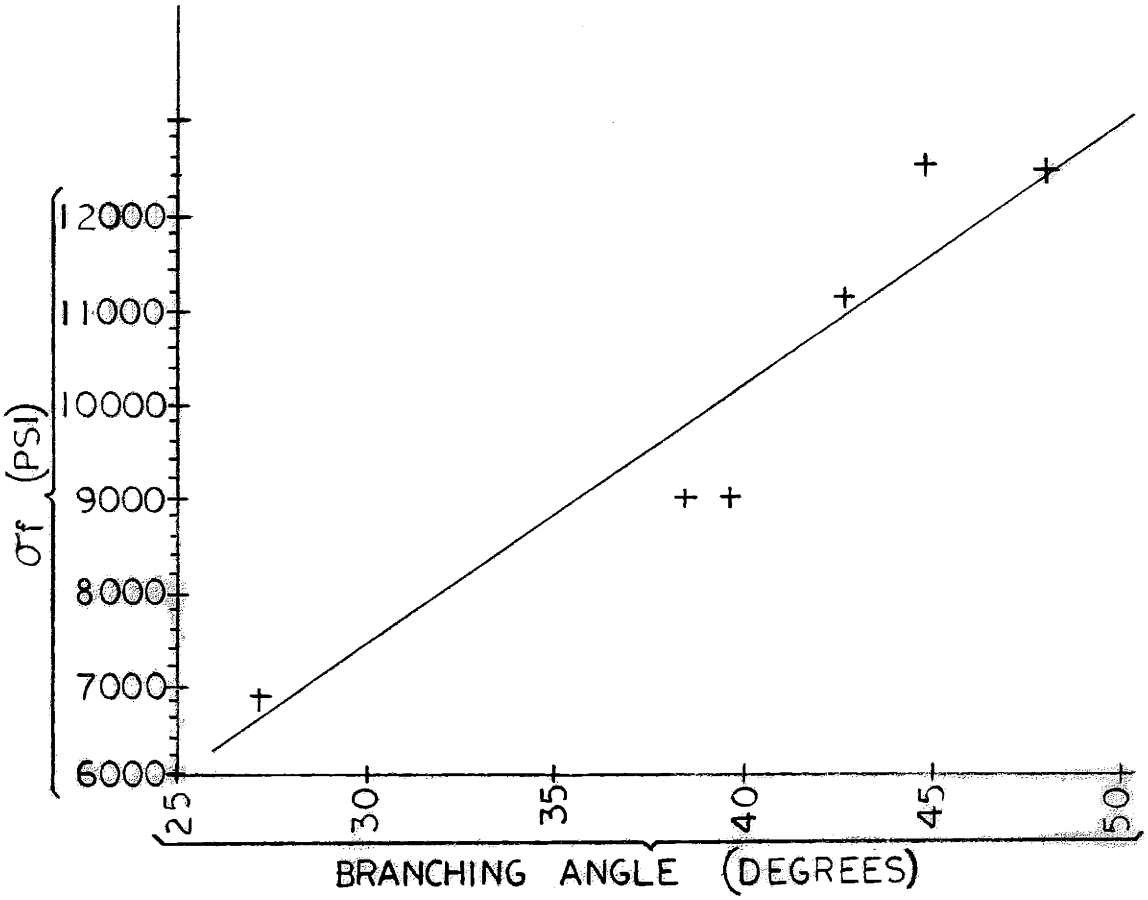

FIGURE 13 : ANGLE OF CRACK BRANCHING VS. FRACTURE STRESS (σ_f) FOR ANNEALED GLASS FRACTURED BY BENDING

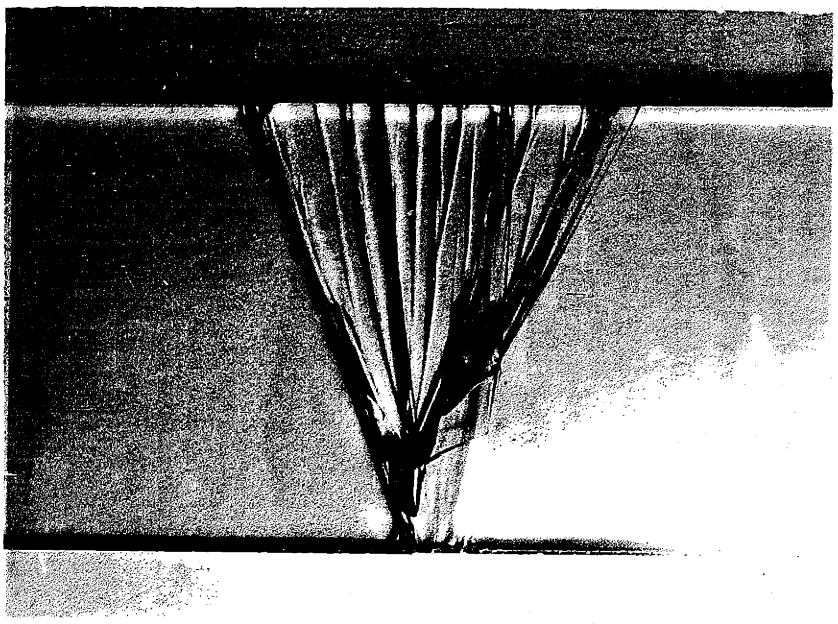

Photo 13 - Angle of Crack Branching

[Note: Specimens that fractured at stresses below 6500 psi generally exhibited no crack branching.]

6. Tempered Glass

The fracture surfaces of fully tempered glass are more complex and somewhat less revealing. Fractures may originate at a surface or edge but once initiated the crack proceeds into the central tension zone and rapidly propagates throughout the body of the glass. The results are that a large amount of new surface is produced, a great deal of energy is released, and the glass fragments are small, rounded, and relatively harmless compared with the fragments produced by the fracture of annealed glass. The elastic energy stored in a tempered glass plate is extremely high. The energy released at fracture is so great that it may obliterate the glass at the origin and reduce it to crushed fragments. Fractures in unflawed (i.e., as-received) samples were initiated at approximately 32,000 psi. The only fracture surfaces that provided a meaningful visual analysis were those that resulted from a somewhat lower fracture energy, or in other words, fractures that originated at serious flaws. The samples tested were therefore first flawed to create the necessary stress concentration. The specimens measured 10 x 1 1/2 x 3/16 inch and were individually tempered by Pittsburgh Plate Glass. The samples were stressed in the 4-point bending apparatus about their weak axes, at a rate of approximately 2500 psi/minute. Both edge and surface flaws were introduced and the resultant fracture surfaces analyzed. The data are recorded in Table 6.

Table 6. Fracture Stress of Fully Tempered Laths

Fractured by Bending

Sample	Location of origin	Measured σ_f (psi)	Calculated* σ_b (psi)
2		20600	15200
3		20600	15200
4		12950	12200
5		13100	11400
10	Surface	16900	12650
12		22800	**
20		29800	32260
21		8400	11800
22		21600	16130
23		23900	22810
6		18750	**
7		23700	**
13	Edge	22800	**
24		18700	12800
25		25200	**

* Edge $\sigma_b = 3841\sqrt{r}$)
Surface $\sigma_b = 3226\sqrt{r}$) from Ref. [4]

** Could not be determined. Origin spalled off or crushed.

Generally, fractures that originated at the edges of fully tempered glass resulted in the crushing and fragmentation of the glass in the vicinity of the origin so that visual analysis of this area was impossible. No fracture mirrors were apparent. Fractures of surface origin did show fracture mirrors and significant markings near the origin as shown in Photo 14. In general the mirrors are closed and have a low profile, extending only 1/4 to 1/3 into the thickness of the plate. The mirror, mist and hackled regions formed are symmetrical about the origin. The hackling extends radially about the mirror. Wallner lines were not visible within the mirror zone but were apparent beyond it. Striations were not produced near the origin but were frequently visible on secondary fracture planes.

Photo 15 shows an edge view of a fractured tempered plate. The photo illustrates the typical progress of the crack into the central tension zone and then laterally outward within this zone. Photos 16 and 17 show some general characteristics of propagating cracks away from the primary fracture plane in tempered plates. The appearance of mist and hackle along the mid-plane signify the elastic energy released from the tensile stresses in that region. Striations are apparent as the crack front approaches the free surfaces. The striations are similar in appearance to those on the fracture surfaces of annealed glass.

Although other researchers[4] have demonstrated a correlation between modulus of rupture and mirror size for tempered glass, only an approximate relationship was apparent on the basis of these very few test specimens.

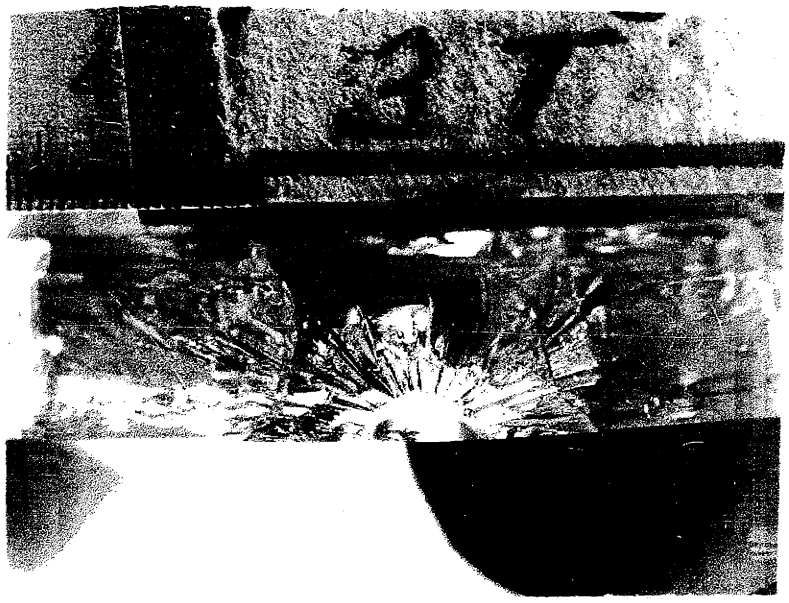

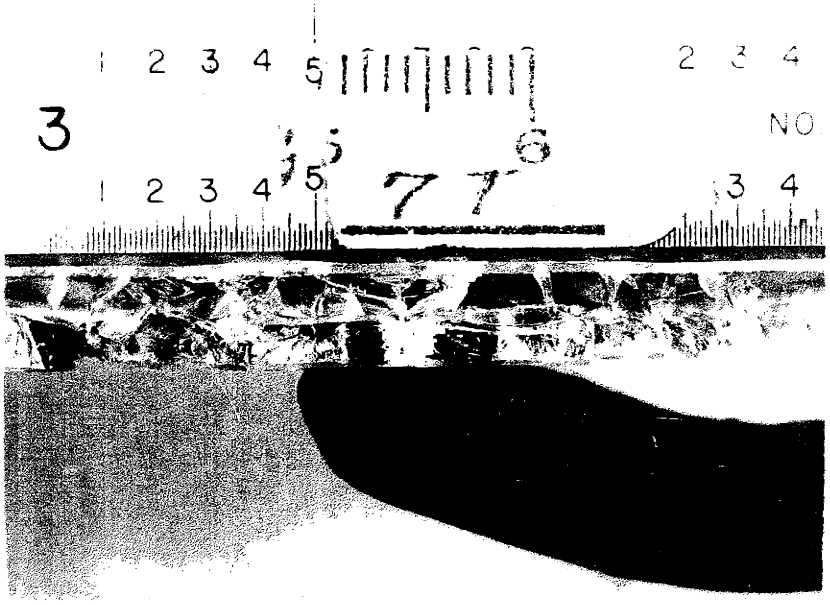

Photo 14 - Typical Fracture Surface Morphology for Tempered Glass

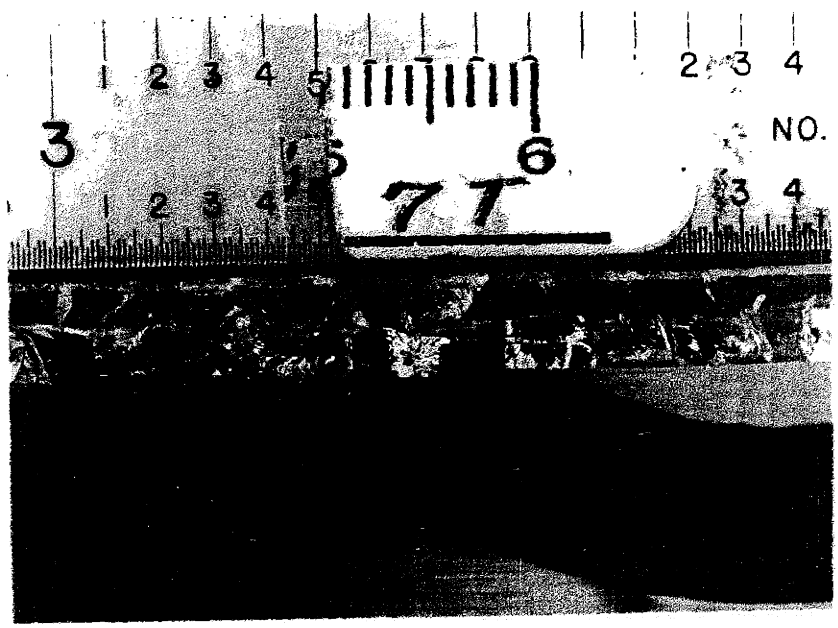

Photo 15 - Crack Divergence as seen from Edge of Tempered Plate

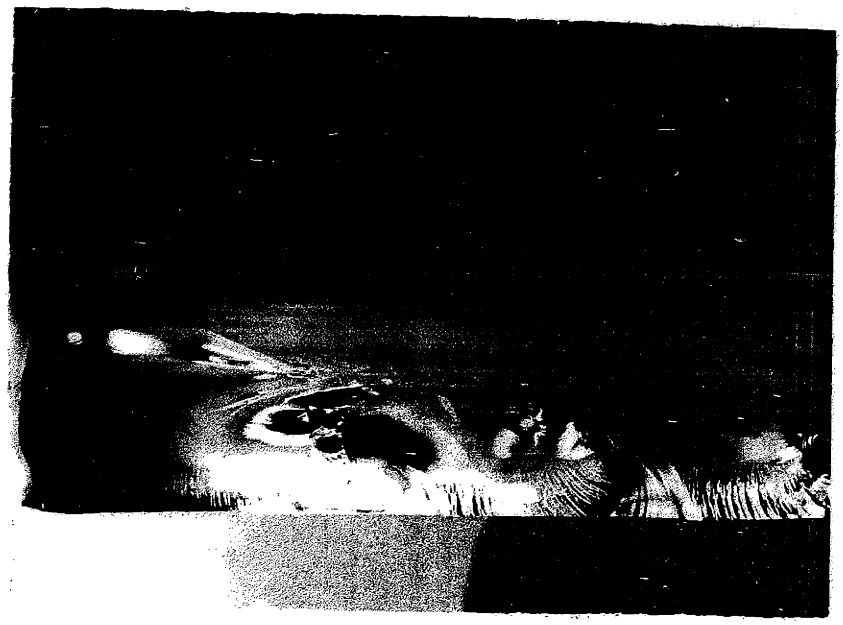

Photos 16 & 17 - Secondary Fracture Surfaces in Tempered Glass

Kerper and Scuderi did find that the relationship does not hold for tempered plates which fracture from the edge. They attribute this to variations in the magnitude of the residual stress acquired by the surface and edge during the tempering process. This variation would also explain the changes seen in fracture surface markings described previously in this section.

7. Heat Strengthened Glass

Heat strengthened glass is tempered in a manner so that the residual stresses produced are lower than those in fully tempered glass. The specimen size and testing procedure was the same as for the fully tempered specimens. The data are recorded in Table 7. The samples tested failed at 15300-20100 psi where no severe flaws were present. Failure occurred in flawed samples at 10200-18100 psi. The fracture surface characteristics of the high energy breaks resemble those of fully tempered glass; i.e., the mirrors have a low profile and are closed; the initial crack plane branches and diverges throughout the body of the glass as the crack front reaches the central tension region, as shown in Photo 18. The lower energy breaks (i.e., 10,000 psi) show characteristics similar to annealed glass fracture. In this case, crack branching occurs but there is no spontaneous divergence of the fracture throughout the interior tension zone of the glass, as is apparent in fully tempered glass. Mirrors surrounding surface-flaws resemble tempered glass mirrors, as seen in Photo 19, but those surrounding corner flaws are similar to annealed glass mirrors as shown in Photo 20. The similarity of the fracture

Table 7. Fracture Stress of Heat Strengthened Laths Fractured by Bending

Sample	Location of origin	Measured σf (psi)	Calculated* σ_b (psi)
1		15300	13700
2		20100	18800
3		16000	16300
5		10200	11500
7	Surface	14900	15100
8		15300	14100
11		13100	11500
12		16500	16400
6	Edge	10200	11050
9		13500	10700
10		14100	9400

* $\sigma_b = 2820\sqrt{r}$, constant experimentally determined

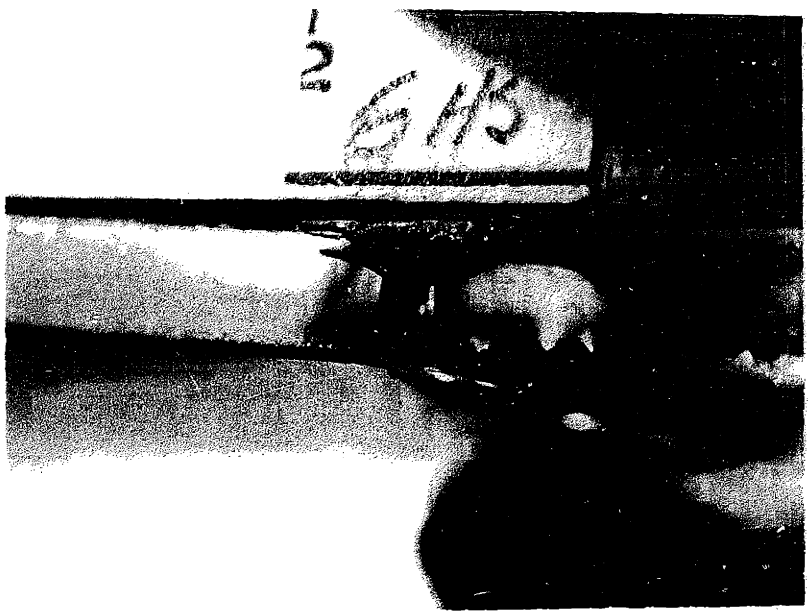

Photo 18 - Crack Divergence as seen from Edge of Heat Strengthened Plate

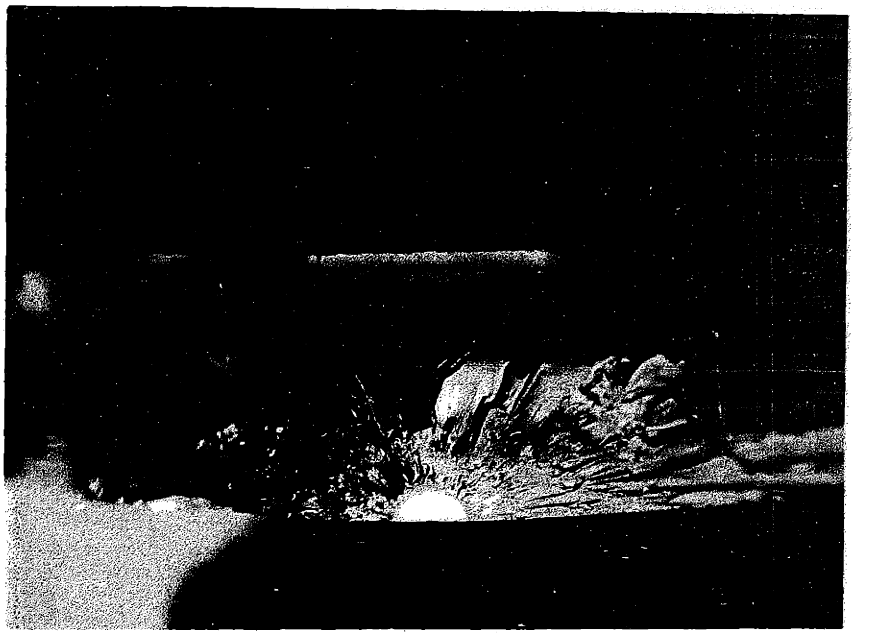

Photo 19 - Fracture Surface of Heat Strengthened Glass with the Fracture Origin at a Surface Flaw

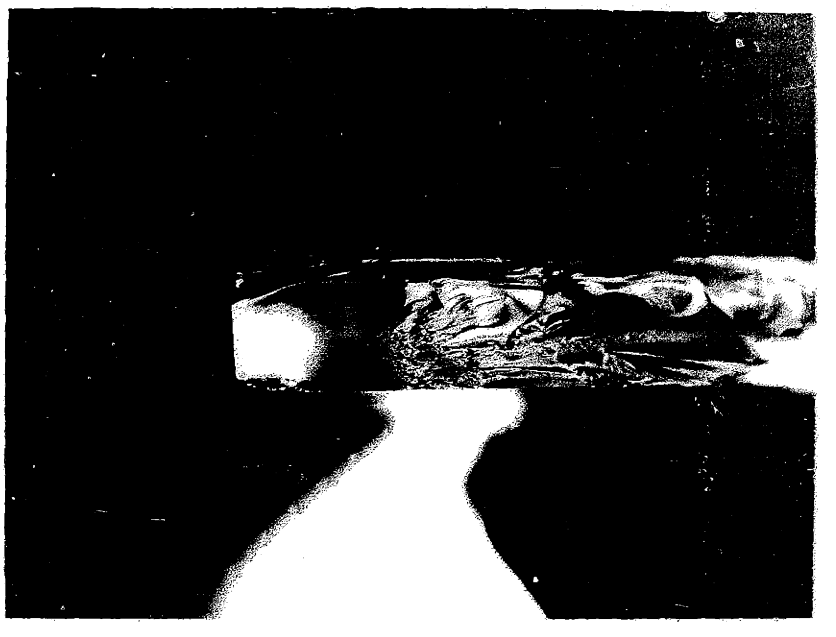

Photo 20 - Fracture Surface of Heat Strengthened Glass with the Fracture Origin at a Corner Flaw

mirrors associated with fractures in annealed glass, and with corner-origin fractures in heat strengthened glass is not so unusual when one considers that the residual compressive stress exists through the plate thickness at the edges of heat strengthened glass. The residual stress gradient associated with interior portions of the plate is eliminated at the edges. The only significant stress gradient at the edges is therefore that due to applied loads, as is the case in annealed glass fracture. Thus the fracture surface morphology resembles the morphology characteristic of the fracture of annealed glass.

The fracture stress vs. mirror size for heat strengthened glass was plotted in Figure 14. A relationship is indicated for surface origin fractures but no relationship is apparent for fractures of edge origin. Any conclusion based on the small number of samples tested is dangerous, since the indicated behavior may be the result of the statistical scatter normally associated with glass fracture.

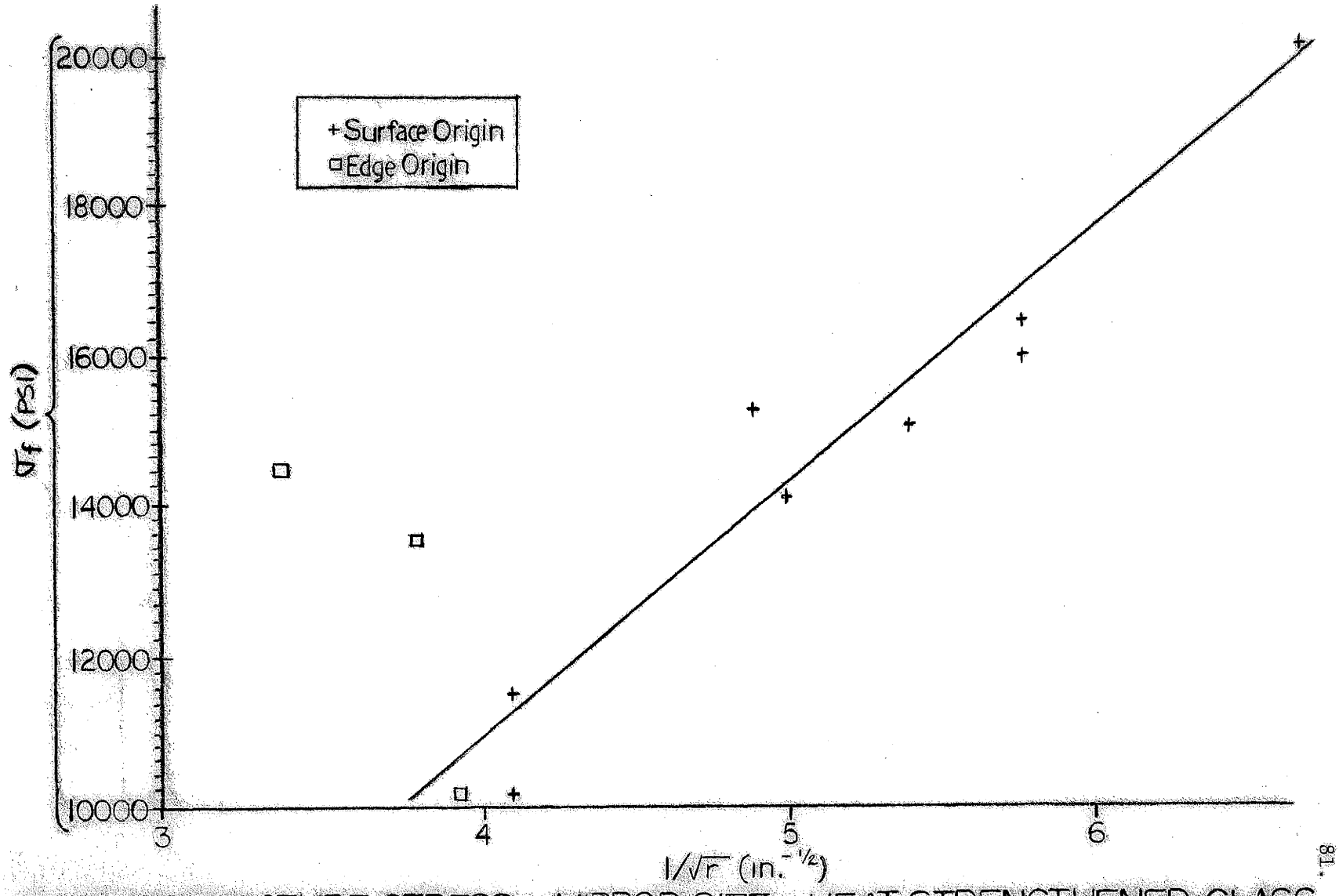

FIGURE 14: FRACTURE STRESS vs. MIRROR SIZE for HEAT STRENGTHENED GLASS

V. THERMAL FRACTURE

A. Thermal Stress States

Variations in temperature within a brittle solid will result in fracture when the thermal stress arising from the temperature difference exceeds the fracture stress. Thermal stresses develop due to restraints on free expansion which may arise from external constraints, internal inhomogeneities, or from temperature gradients within the body. The susceptibility of glass to thermal fracture has been an important source of failure in service.

The thermal stress at any point in an elastic body depends on the difference in temperature between that point and the average.[1] In an infinite slab the stress is given by

$$\sigma_x = 0$$

$$\sigma_y = \sigma_z = \frac{E\alpha}{1-\mu} (T_a - T) \qquad (9)$$

where E is Young's modulus, α is the linear coefficient of expansion, μ is Poisson's ratio, T_a is the average temperature and T is the temperature at the point of interest.

When a glass plate undergoes a sudden temperature reduction by contact with a cool liquid the surface temperature drop almost instantaneously due to its high heat transfer rate. The interior bulk of the solid does not change temperature until some later time. It therefore provides a restraint against the free contraction of the surface layer. This restraint produces tensile stresses in the surface layer. Conversely the interior undergoes slight compression in order to remain in stress equilibrium as illustrated

in Figure 15a.[2] This high rate of surface heat transfer might occur in a glass building panel that is subjected to direct sun followed closely by rain. (It should be noted that most building glass thermal fractures occur during the radiant heat cycle, as shown in Fibure 15b.) If the surface temperature of the glass drops 35°C (95°F), then for soda-lime-silicate glass with $E = 10.6 \times 10^6$ psi, $\alpha = 9.2 \times 10^{-6}$ in/in.°C, $\mu = 0.21$, the maximum surface tensile stress produced would be 4300 psi according to equation (9). This stress alone would generally not be expected to produce fracture; but in conjunction with stress concentrations and applied loads a critical fracture stress might result.

When the surface temperature changes at a constant rate, the surface stress becomes dependent on the rate of temperature change, the surface heat transfer coefficient, the thermal conductivity, as well as the parameters in equation (9). A constant rate of surface temperature change produces a parabolic stress distribution through the plate thickness as illustrated in Figure 15c.

Thus far this discussion has addressed through-the-thickness temperature gradients only. Far more important with respect to the thermal fracture of glass building panels is the in-plane variation in temperature. Stresses that arise when a plate is heated uniformly through the thickness are termed membrane thermal stresses. A glass plate in a building application has its edges recessed and therefore removed from the source of radiant heat. This configuration creates a central hot spot in the exposed region of the plate. The maximum value of the stress in an

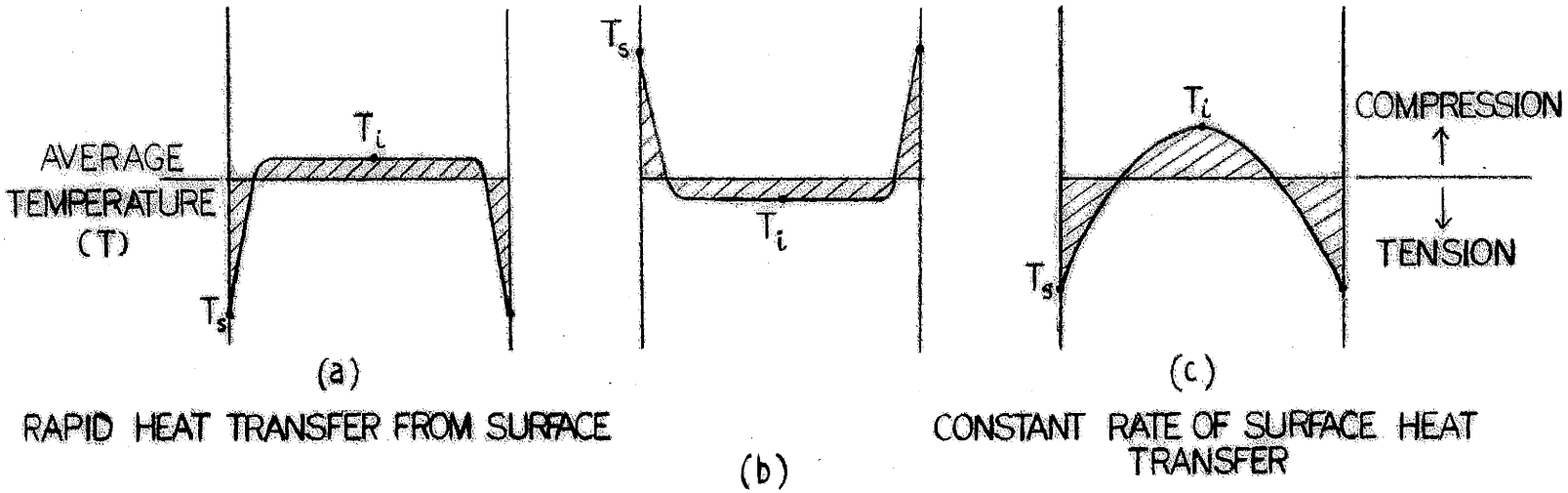

FIGURE 15: TEMPERATURE AND THERMAL STRESS DISTRIBUTIONS

infinite plate with a square hot spot is[3]:

$$\sigma_{xx} = \sigma_{yy} = 0.55\ E\alpha T \qquad (10)$$

where T is the temperature of the hot spot in a plate of zero temperature.

A finite plate centrally heated will develop tensile stresses along the edges as shown in Figure 16. Large glass plates generally fracture from the edges due to these tensile stresses. The greater the temperature difference between the central heated region and the edge, the larger the tension and the greater the likelihood of fracture. For this reason the recessed or cold edge configuration of building glass can be quite dangerous.

Thermal stresses capable of initiating fracture may arise in a uniformly heated glass body if the glass structure is not homogeneous. Stresses concentrate at the boundaries of local discontinuities such as hard second phase particle inclusions. The thermal stresses develop due to changes in expansion coefficients or elastic moduli across the particle boundaries. (It should be noted that quality annealed glass will not fracture thermally due to these local impurities.)

B. Experimental Procedure

Thermal fracture analysis was conducted on annealed soda-lime-silicate glass on the test apparatus diagramed in Figures 17 and 18. Aluminum plates 1/8" thick were clamped to the 6" x 6" x 3/16" glass samples so that a 1/2" wide perimeter of the glass was recessed from the heat source. A thin compressible foam pad was placed continuously between the aluminum and glass plates. The outside surface of the aluminum plates were coated

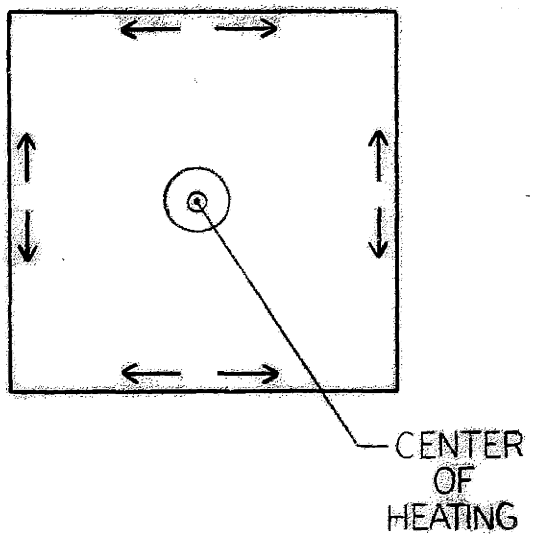

FIGURE 16: APPROXIMATE STRESS STATE OF A CENTRALLY HEATED PLATE

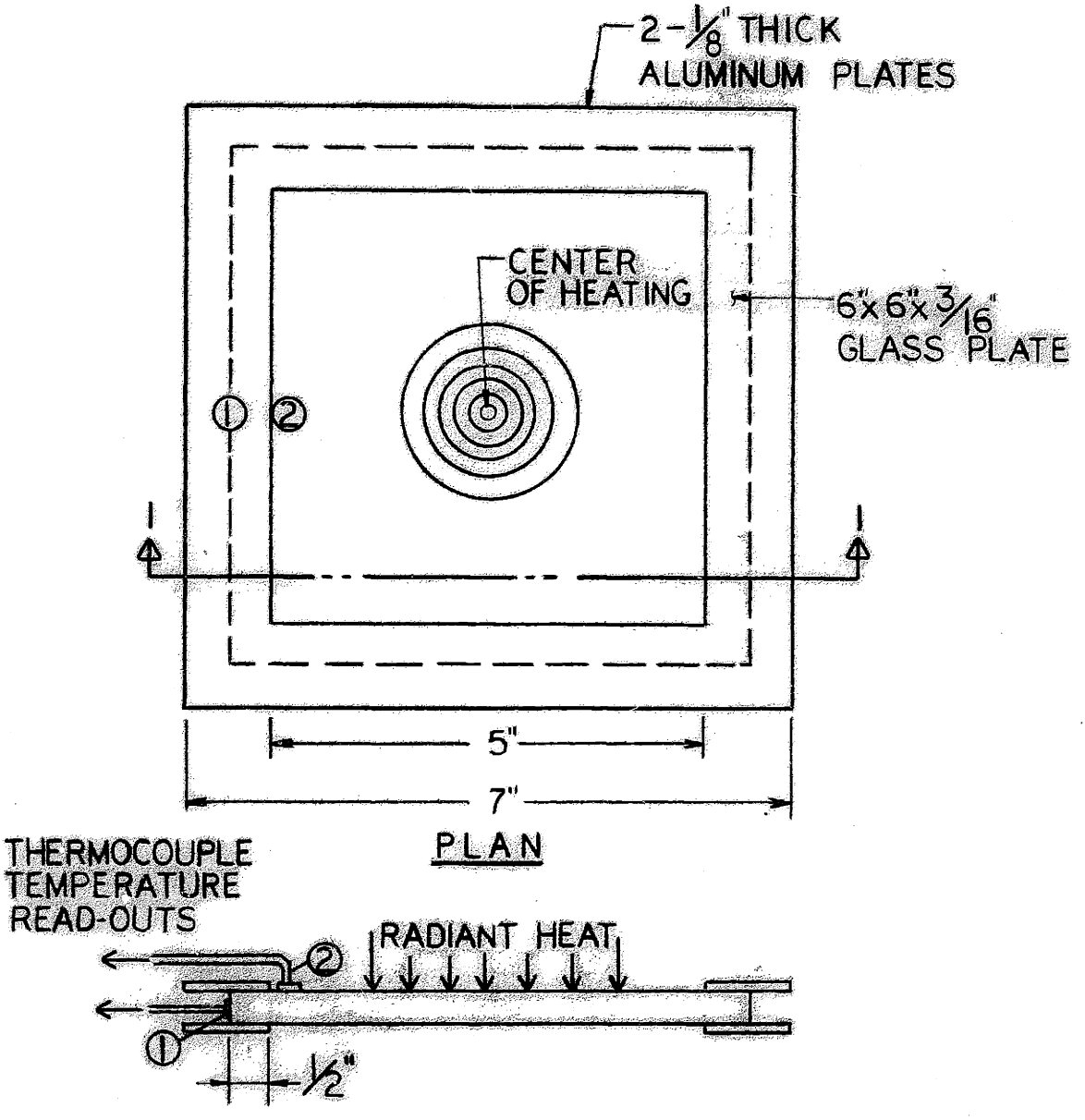

FIGURE 17: THERMAL TEST APPARATUS

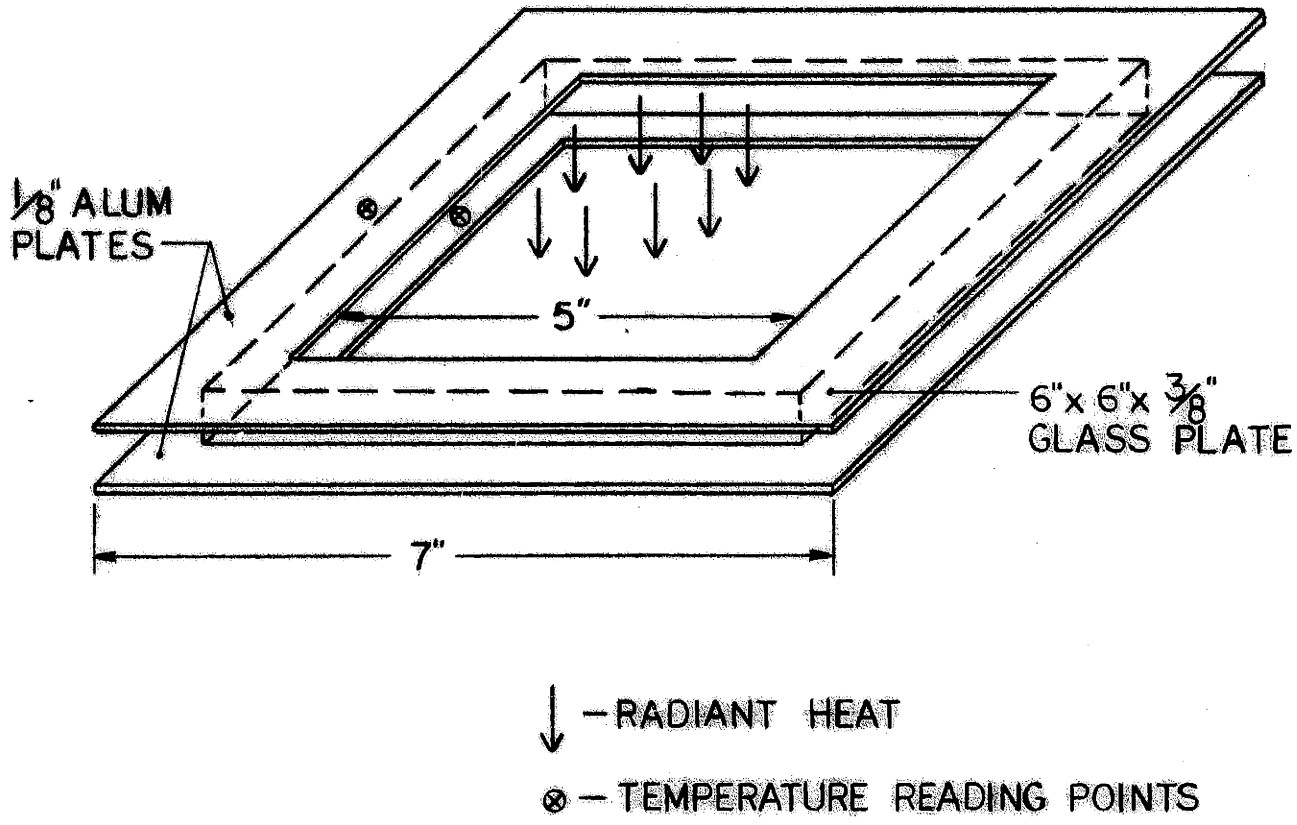

FIGURE 18: THERMAL TEST APPARATUS

with foam padding to insulate them from the infrared heat lamp. The aluminum-glass "mullion" apparatus was secured with 4 c-clamps and mounted horizontally for the test. The edge conditions of the samples tested varied from clean to severely damaged.

A number of tests were conducted to determine the temperature difference across the recessed edge sufficient to cause fracture, $\Delta T_{f(1-2)}$, the stress at fracture, σ_f as determined by the size of the fracture surface mirror, and the fracture surface morphology as a function of ΔT_f, σ_f, and clamping pressure.

Heat was supplied to the glass plates by a single 250 watt infrared heat lamp, placed a few inches above the test apparatus. The temperatures at points 1 and 2, located at the edge of the glass and just inside the aluminum mullion respectively, were recorded by direct read-out thermocouples.

C. Experimental Results and Discussion

1. Cold Edge Effect

In the first test series the mullion was clamped at the corners to eliminate direct pressure near the origin of fracture. The data are recorded on the graph shown in Figure 19. A linear relationship between σ_f and ΔT_f is indicated, although it is somewhat altered from the theoretical prediction. The departure from the theoretical is not surprising since the ΔT used in equation (9) represents the difference in temperature between the point and the average body temperature, whereas the ΔT_f measured was merely the temperature difference across the recessed edge. In addition, some inaccuracy due to the calculation of σ_f from the

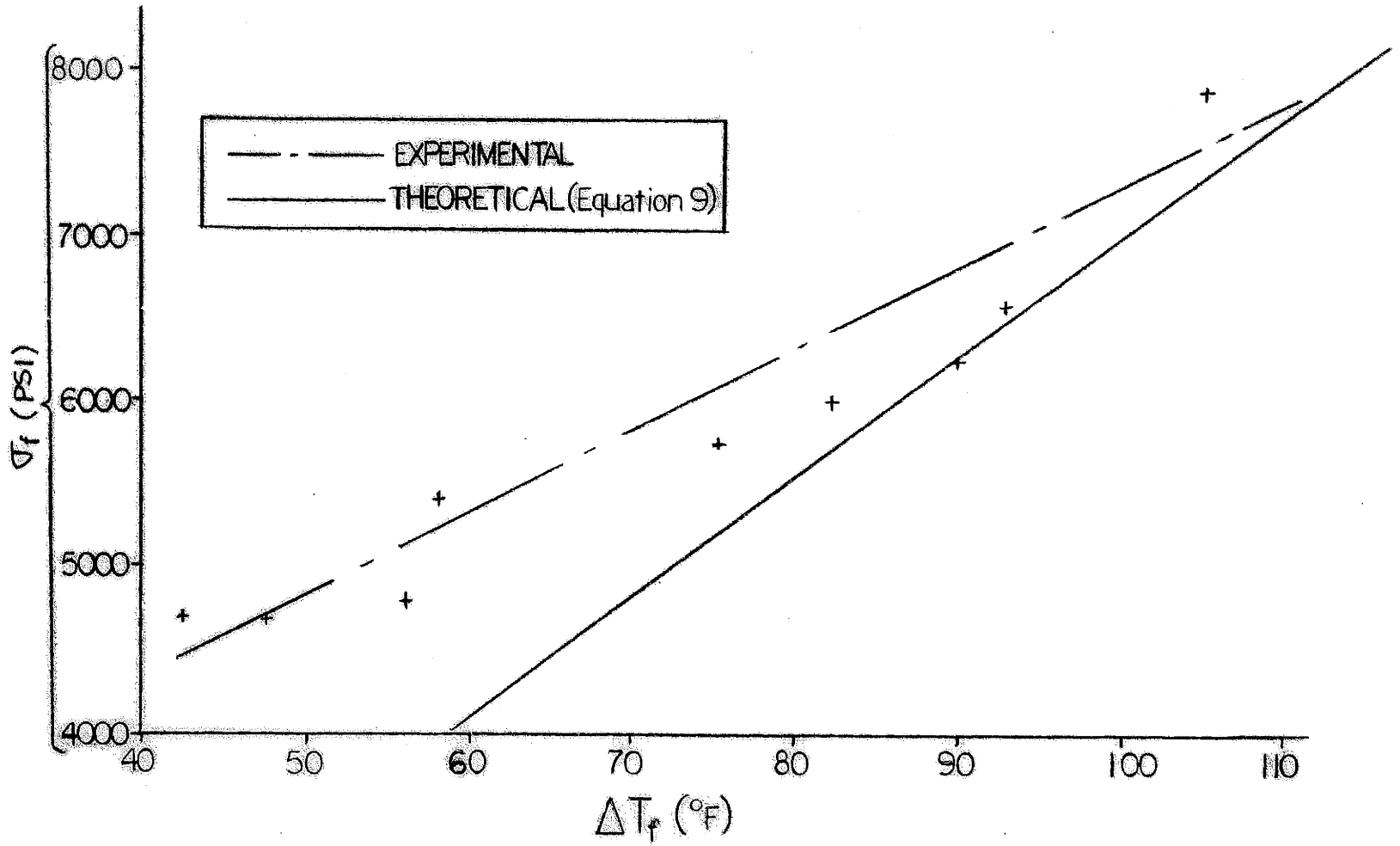

FIGURE 19: σ_f VS. ΔT_f FOR ANNEALED GLASS

size of the fracture mirror is unavoidable. The low energy fractures are not shown on the graph since no fracture mirrors existed for the estimate of σ_f. The lowest ΔT, measured across the 1/2" recessed edge, that was sufficient to cause fracture, was 42°F. Temperature differences of this magnitude are easily attainable in a building, depending on the heat transfer characteristics of the glazing and the construction detail.[4]

2. Crack Branching and Orientation

The degree of primary crack branching (i.e., number of crack paths initiated near the origin, for instance there are 5 primary cracks in Photo 69 Appendix) in thermal fractures was found to increase generally as σ_f increased. Figure 20 illustrates this approximate correlation. Fractures initiated at low stress levels produced no branching of the crack front.

The direction of thermal fracture paths was extremely varied, although all samples were heated in a similar manner. Photos 21-23 show the variety of crack patterns in plates that had no mechanical stresses superimposed on them. Initially, the crack proceded perpendicular to the tensile stresses at the edge. Shortly after emerging from the recessed edge the cracks in most of the samples began to deflect radially about the center of heat application as shown in Photo 21. At this point the crack path became wholly unpredictable. In some cases, the fracture course changed radically and the crack turned back on itself and proceded directly into the central heated zone as shown by the fractures in Photo 22. The reason for the crack path's tendency to redirect its propagation into the central heated region is not, as yet, understood. It is the opinion of this researcher that the alteration in path is the result of a major

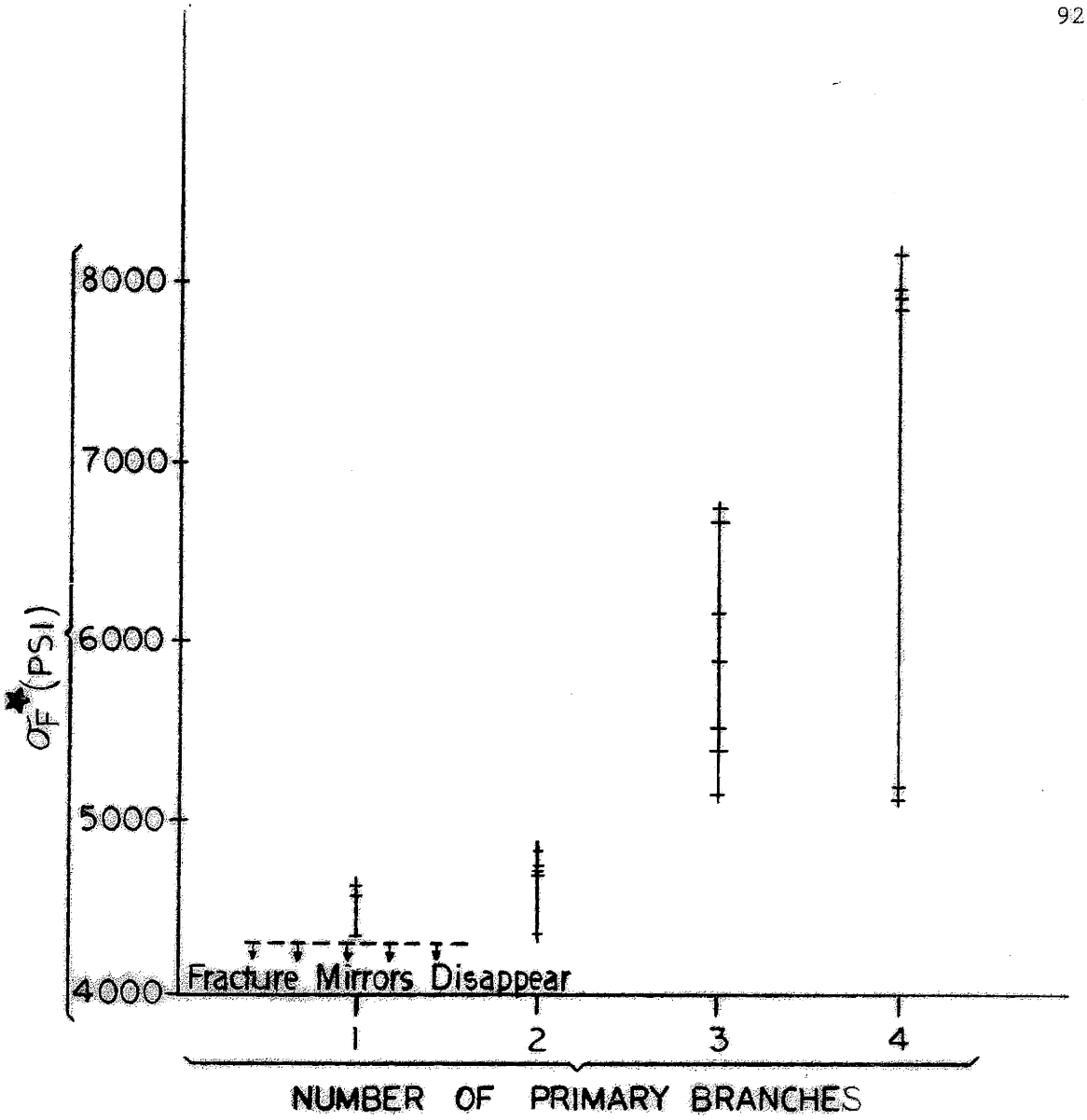

* σ_F IS ESTIMATED FROM MIRROR SIZE

FIGURE 20 : σ_f VS. NUMBER OF CRACK BRANCHES IN THERMAL FRACTURE OF ANNEALED GLASS

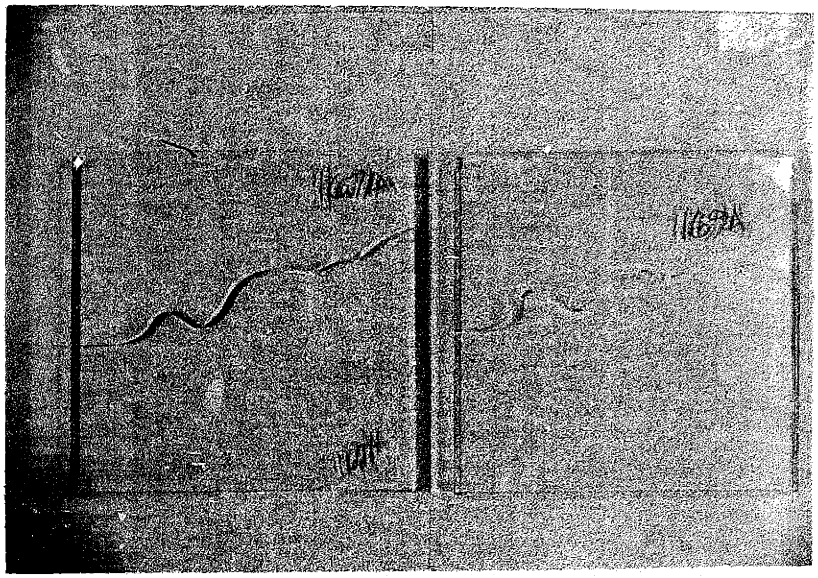

Photos 21 & 22 - Thermal Crack Patterns

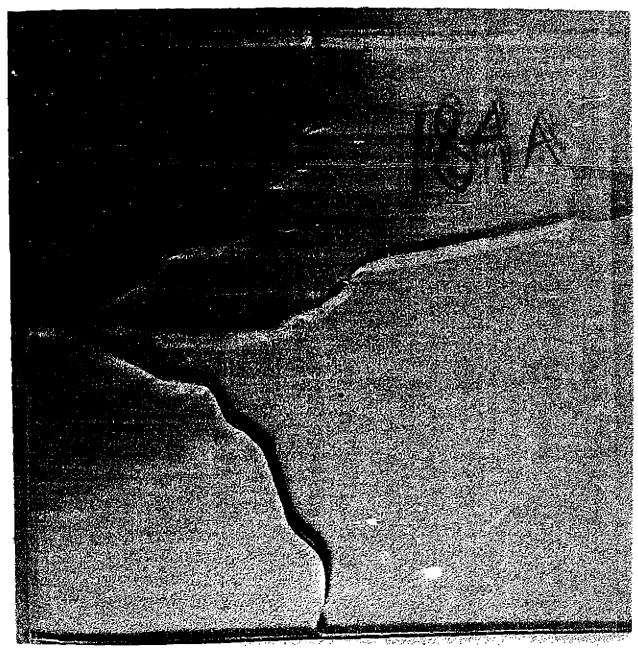

Photo 23 - Thermal Crack Pattern

internal thermal stress redistribution in response to the partial separation occurring in the plate. In some fractures, cracks both skirted the central high heat zone, and propagated through it, as shown by Photo 23.

3. Fracture Surface Morphology

The fracture surfaces exhibited the same general features as noted in bending failure. Unlike mechanically fractured surfaces, however, the mirrors were closed and the mist and hackled regions often occurred in uniform bands.

High energy thermal fractures (i.e., σ_f>6000 psi) often exhibited pronounced concentric mist/hackle regions as seen in Photos 24-26. These repeating patterns represent consecutive, separate releases of elastic energy. It should be noted that the onset of hackle in the consecutive bands corresponds exactly to the point of crack branching, thus confirming that the two are closely related as energy releasing mechanisms. Hackling very likely represents micro-crack branching. It is logical to assume then that crack branching is the fourth and final stage in the fracture surface progression from mirror to mist to hackle.

Photos 24-26 also confirm another interesting feature, that the elastic energy release of the propagating crack is not steady-state but undulating. This was indicated somewhat less obviously in a few bending fractures reported in Section IV. Generally it appears that at least three branches are required before the concentric markings are apparent. Photos 27 and 28 show the singular band associated with cracks that do not develop at least three branches.

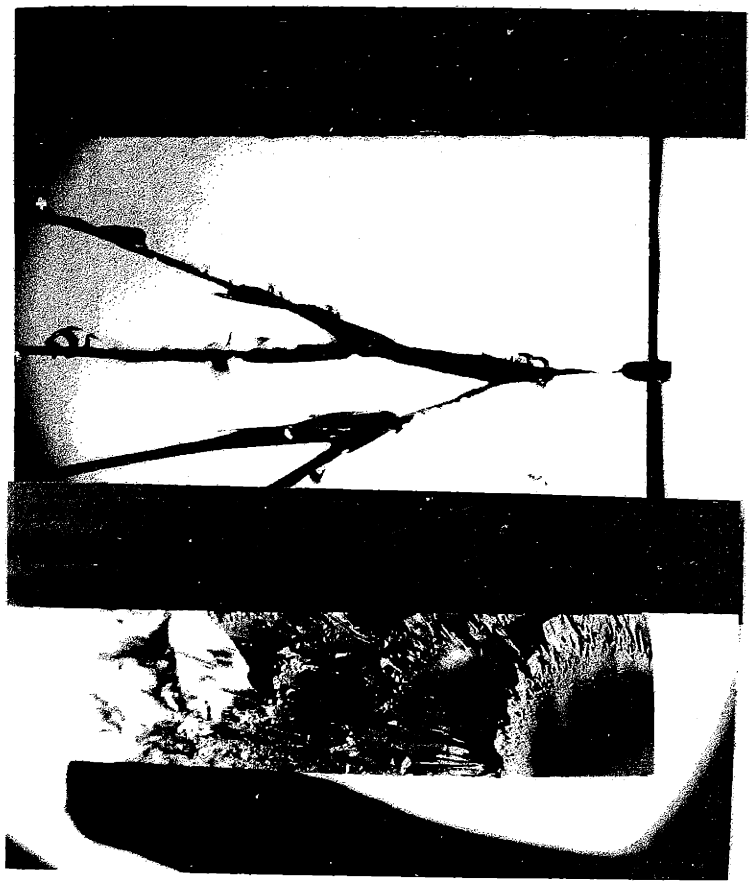

Photo 24 - Repeating Fracture Characteristics on
Thermal Fracture Surface

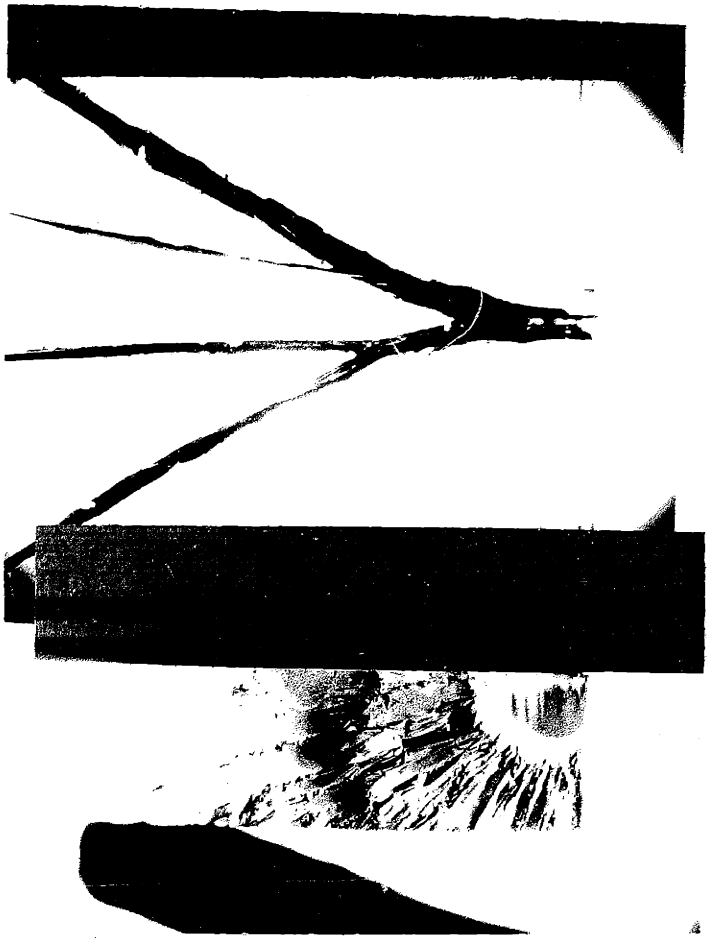

Photo 25 - Repeating Fracture Characteristics on Thermal Fracture Surface

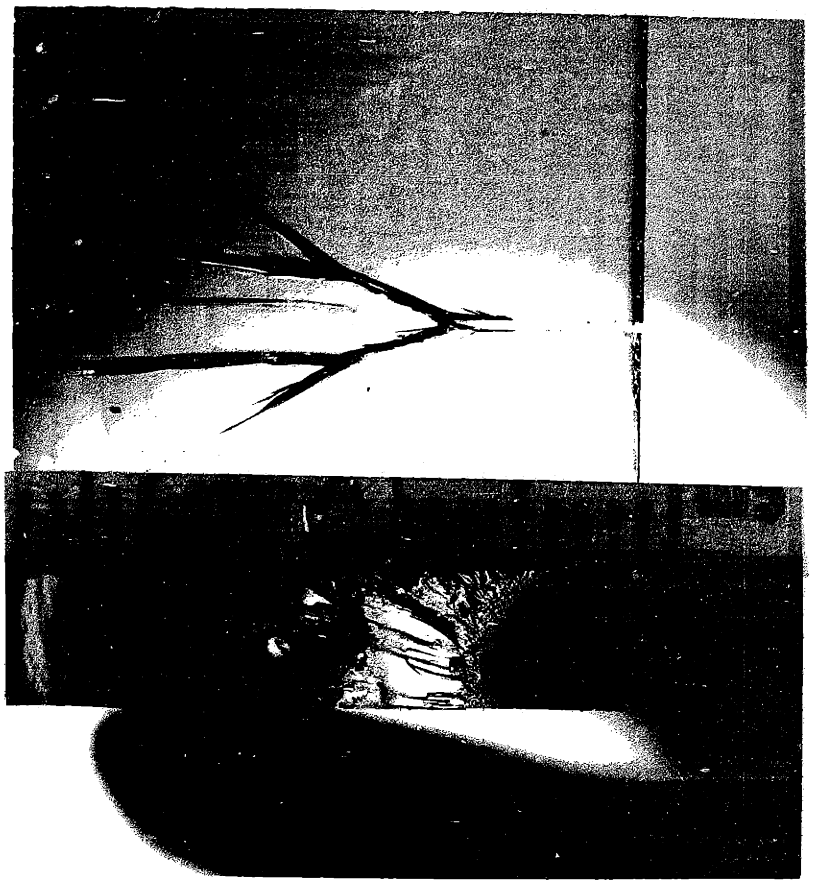

Photo 26 - Repeating Fracture Characteristics on
Thermal Fracture Surface

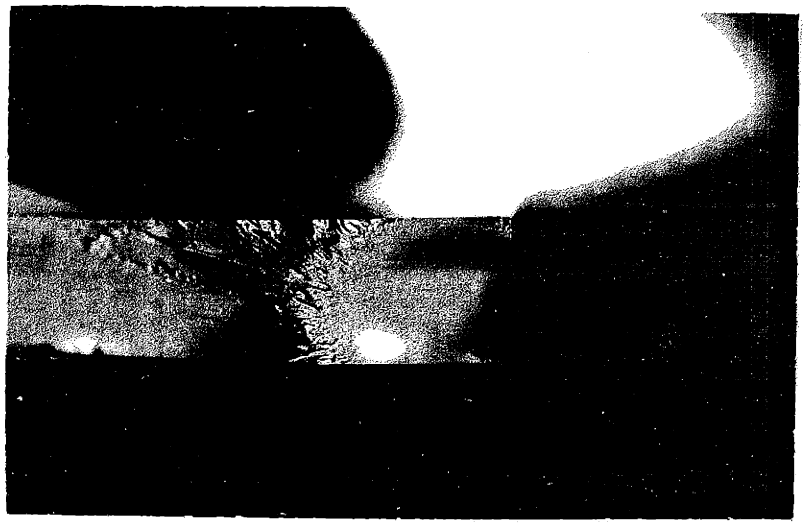

Photos 27 & 28 - Singular Characteristics on Thermal Fracture Surfaces

Regardless of the fracture energy, almost all thermal fractures show light Wallner lines near the origin and rib marks at changes in the direction of crack propagation. Other than occasional rib-marks, the fracture surface away from the fracture origin becomes extremely smooth. Here again the rib-marks represent a momentary hesitation in the crack front, or a slight change in the fracture plane due to the redistribution of stress in response to the advancing crack. Rib-marks that formed at the point of maximum crack path curvature are shown in Photo 29. (Note the symmetrical appearance that was not apparent on the fracture surfaces of mechanically fractured specimens, as shown in Photo 4.) Striations were generally absent on the fracture surfaces of thermal breaks.

A few samples were thermally fractured with additional mechanical stress supplied by a weight suspended from the center of the plate to simulate wind pressure. The fracture surface morphology was unchanged but the superimposed stresses were apparent as illustrated by the deflected crack pattern shown in Photo 30.

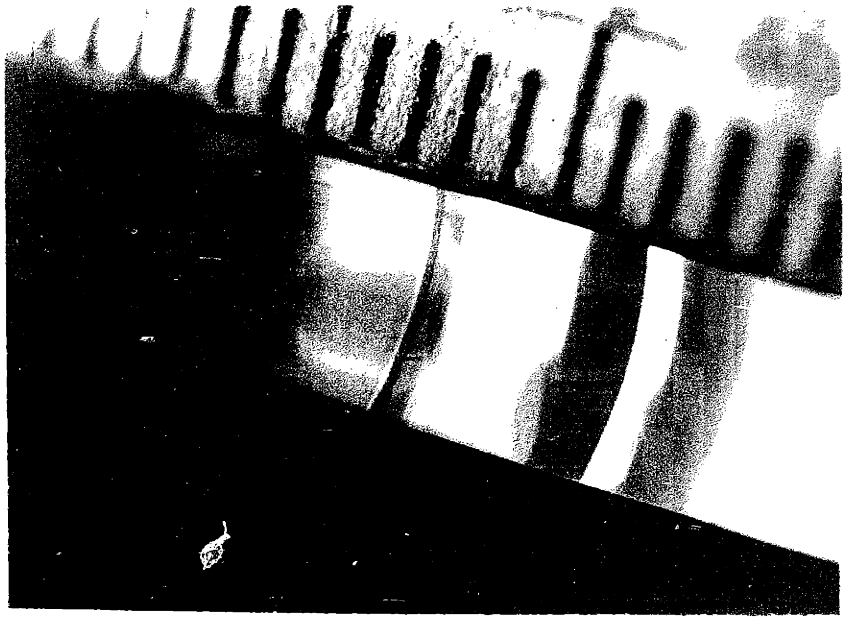

Photo 29 - Rib-Marks at Curvature of Thermal Crack Path

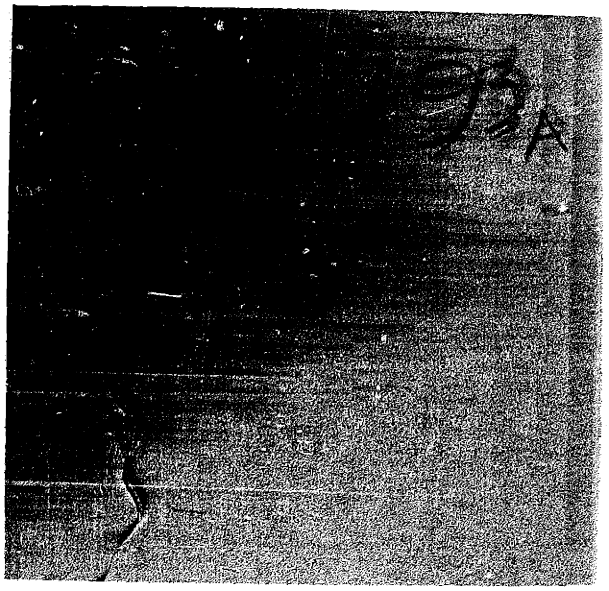

Photo 30 - Thermal Crack Pattern Deflected
by Applied Load at ⊗

VI. IMPACT FRACTURE

A. Impact Stress States

The time dependent nature of glass fracture is an important component in the overall response of glass to conditions of stress. We have already discussed in this thesis the dependencies of strength and fracture surface morphology on parameters such as load duration and loading rate. If we reduce the duration of a load and apply it at a high rate, then we enter the realm of impact. The response of materials to impact loads can be vastly different from their response to static or quasi-static loading conditions. Kolsky[1] has shown that theoretically even viscous liquids will fracture in a brittle manner when loading rates are sufficiently high (e.g., a stress build-up time of 10^{-11} seconds will fracture water). Kolsky has also shown that the strength of glass for loading times of a few microseconds is twice that for loading times of a few seconds. [Note: The high impact strength of glass is also related to static fatigue considerations as were discussed in Section IV.]

Analysis of the response of commercial plate glass to impact loading is an extremely complex task, complicated by many independent parameters such as the size of the plate, the type of edge restraint, dampers in the glazing system, and the velocity and physical nature of the impact object. The problem is compounded by the complexity of the stress state produced by impact. Impact fracture can result from four types of tensile stresses that arise due to impact.[23] Three are illustrated in Figure 21 and include contact stresses, flexure stresses produced on the surface opposite the point of impact, and hinge stresses produced on the surface of impact,

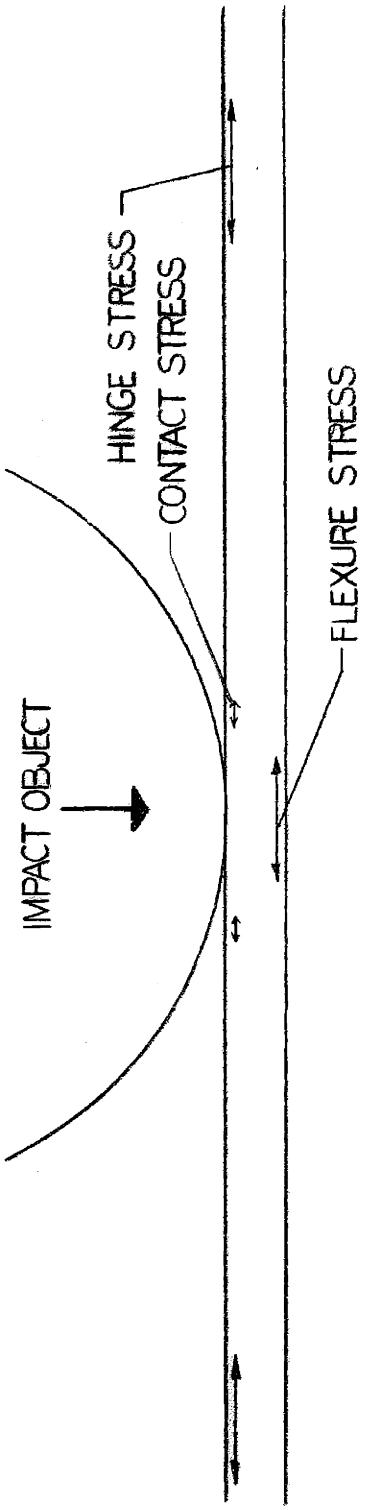

FIGURE 21: PRIMARY IMPACT STRESSES

at some distance from the impact point. A fourth type of fracture stress results from a compressive stress pulse when it is reflected at a free boundary. This type of stress is most likely developed from an explosion on one side of the glass. Fracture by reflected stress pulses is called "spalling" or "scabbing".

Contact stresses are highly dependent on the shape and hardness of the impacting object. In general, a hard spherical object in contact with a flat plate will create radial tensile stresses on the contact surface at the perimeter of the contact circle and parallel to the surface of the plate. Fracture will therefore originate at the perimeter of the contact circle and perpendicular to the surface as illustrated in Figure 22. The fracture initially propagates in a cylindrical form into the body of the glass. As the fracture nears the opposite free surface of the plate the crack front develops into the classic "cone" shown in Figure 22. If the plate is thin the cylindrical portion of the fracture is negligible. A cone of fracture may also appear on the impact surface due to pulverization of the glass at the impact point.

Flexural stresses due to impact are, like contact stresses, highly localized. A biaxial tensile stress state develops on the surface of the plate opposite the point of impact. A tensile stress perpendicular to the plate develops which is equal to approximately two-thirds the magnitude of the tensile stress parallel to the plate surface.[2] Cracks originate on the surface opposite the impacted surface and propagate back through the plate thickness toward the point of impact. Simultaneously, the fracture begins to spread radially outward from the impact point. The

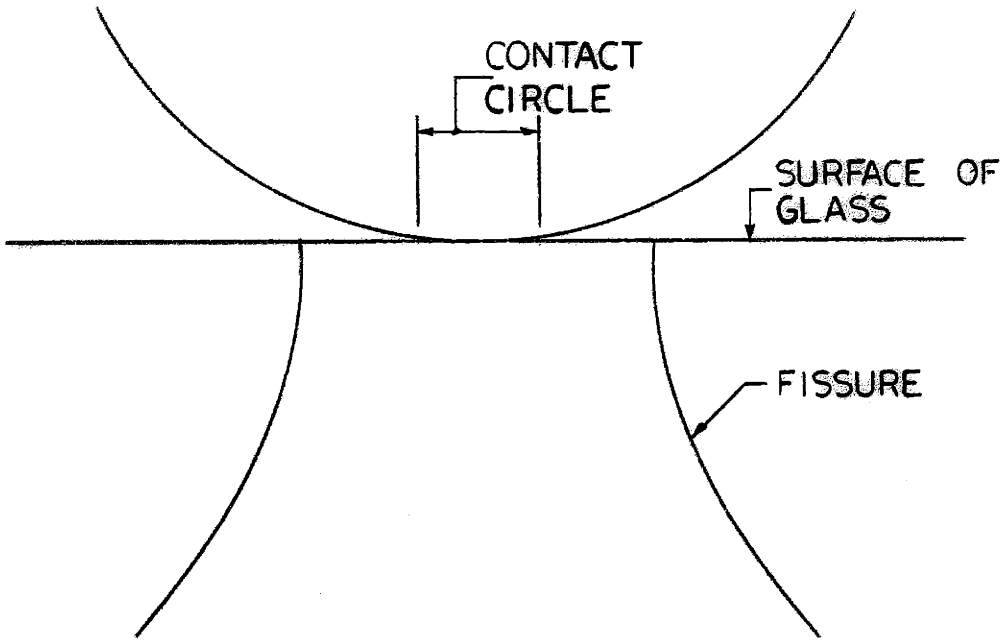

FIGURE 22: "CONE" FRACTURE DUE TO CONTACT STRESSES IN THIN PLATES

general crack pattern and fracture surface morphology for flexural and hinged impact fracture are illustrated in Figure 23.

The radial crack $\overline{AB}$ in Figure 23 was initiated by flexure stress. The location of its origin at the surface opposite the impact is indicated by the shape of the rib-marks on the fracture plane. Their concave orientation toward the point on the surface directly opposite the impact point confirms that this is the location of fracture origin. In the fracture depicted in Figure 23 the radial cracks are continuous (i.e., their propagation is uninterrupted by other crack fronts). This continuity of propagation indicates that the radial cracks are the primary fracture, and that the fracture was initiated by flexure stress.

Hinge stresses affect a relatively large volume of material compared to flexure and contact stresses. They are essentially uniaxial and reach a maximum at some distance from the point of impact. Hinge stresses caused the ring cracks shown in Figure 23. In this particular fracture sequence the ring cracks are a secondary occurrence as indicated by their discontinuous nature. Therefore, hinge stresses did not initiate this fracture. The ring crack has its origin at the surface of impact as shown by the rib-marks on the fracture plane which are concave toward the impact surface.

The orientation of rib-marks on radial and ring crack surfaces, indicate the location of the crack origin only. The rib-mark orientation is independent of the sequence of fracture initiation.

The magnitudes of the three primary impact stresses for a "moderately" hard impact were shown by Mould[2] to be as follows:

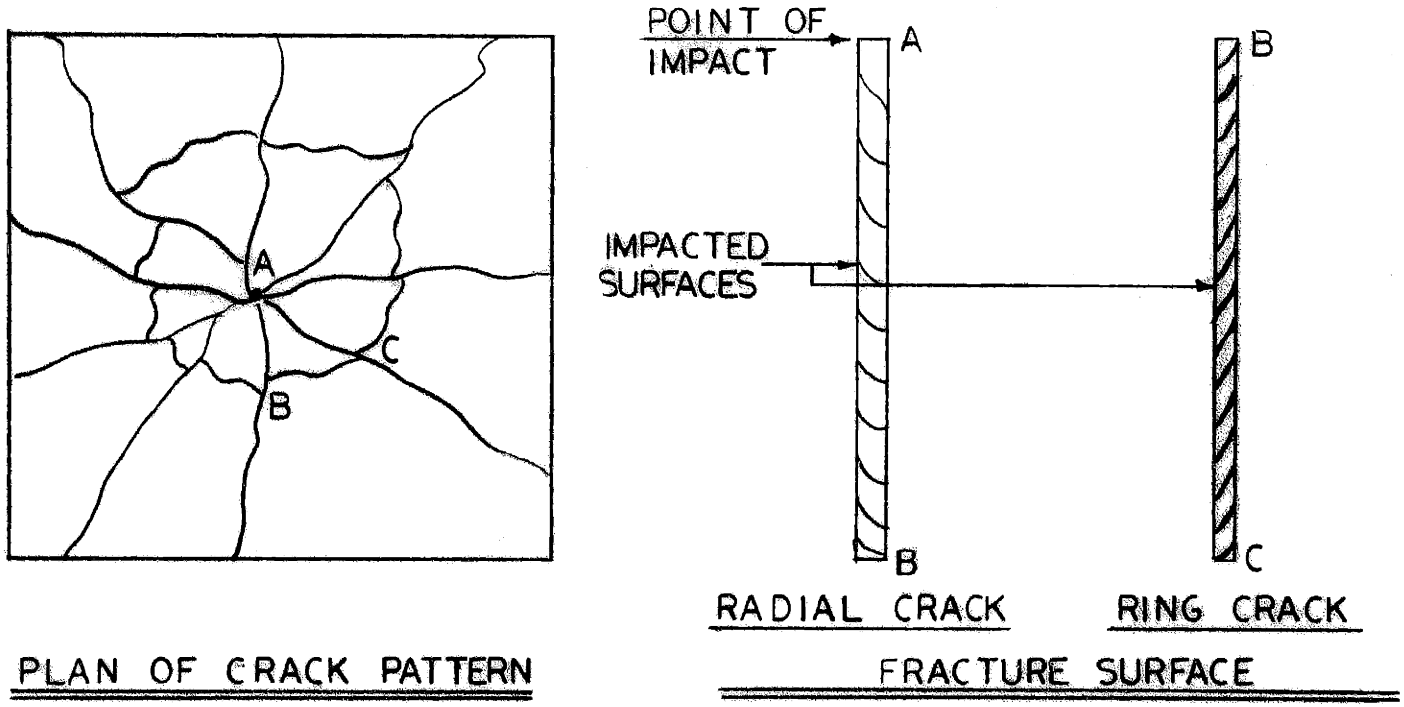

FIGURE 23: IMPACT CRACK PATTERNS

Contact Stress - 110,000 psi

Flexure Stress - 35,000 psi

Hinge Stress - 7,000 psi

These values represent the stresses developed during the impact of a filled bottle by a 1-in. diameter steel ball. The value for the contact stress may be considered a maximum since a steel ball is one of the harder common impacting objects. Mould further found that the relative values of the flexure and hinge stresses remained essentially constant regardless of variations in the velocity, mass, and hardness of the impacting object and the stiffness of the glass support. It was found that the relative value of the hinge stress increased as damping of the glass supports increased.

Although contact stresses are generally the largest stresses caused by impact, their destructive potential relative to flexure and hinge stresses is not severe. There are two reasons for this behavior. Both are related to the localized nature of the contact stress field. (The distance from the perimeter of the contact circle to the origin of fracture is generally less than or approximately equal to the diameter of the contact circle as shown in Figure 22.) First, fractures initiated by contact stresses may remain localized. A small cone shaped chip may be broken from the glass surface but the plate will remain intact. Second, contact stresses, although large, act on a very small volume of material. It is well established that the strength of a glass specimen increases as the volume of material under stress decreases. It is reasonable, therefore, that glass might withstand extremely large stresses when the stress field is highly

localized. By contrast, the hinge stresses which are the lowest in magnitude, are often the most damaging since they affect a considerable volume of glass.

A typical impact fracture sequence might proceed in the following manner.[4] At initial contact the first damage to the plate originates at a number of points lying circumferentially about the contact circle. Fractures stemming from these points form a roughly cylindrical crack which quickly flares into a cone and extends to intersect the back surface. For impacts that penetrate the glass surface a secondary cone may develop coaxial with and outside of the first. Like the primary cone, these secondary fractures originate at the impact surface. In general they flare extensively and produce spalling at the back surface. High velocity or massive impact missles may also cause the primary cone to move inward, breaking its support with the surrounding material and resulting in the erosion of material under the contact object. A crater is then formed about the area of impact.

Shortly after the primary cone develops, radial cracks form on the surface opposite the impact and spread toward the impact point. Simultaneously they begin to spread radially outward from the impact area, as discussed earlier in this section. Ring cracks develop at the impact surface usually after the radial cracks have passed. They generally originate at a radial crack, and propagate in a sweeping manner from the impact surface to the opposite face, completing separation.

As yet we have not discussed fractures produced by stress waves. This category of fracture is generally set apart from the others since it deals with loading rates many orders of magnitude greater than those

associated with "normal" impact. (The duration of load when an object strikes a glass surface is on the order of 0.001 seconds.[2] Stress waves can result in fracture for loading durations of microseconds as produced for instance by an explosive charge.) The incident impulse as supplied by a high speed impact or explosive charge is propagated through the glass from the impact point as a compressive pulse which may have a saw-tooth configuration as shown in Figure 24a. It may be assumed that the pulse passes through the plate without change in shape or intensity.[3] When the compressive pulse reaches a free surface it is reflected and its sign is changed so that it becomes tensile. The net stress level during the pulse reflection is illustrated in Figure 24b. The maximum reflected tensile stress first occurs when one-half of the pulse has reached the free surface. Fracture will be initiated when the reflected tensile stress equals the fracture stress. If the critical incident pulse is reflected from the surface, then the fracture originates on a plane parallel to that surface and a circular area is spalled out. If the critical pulse is reflected from the sides of the plate, then a section of the edge or the corner may be broken off. As the duration of the impact load--and therefore the length of the impulse stress wave--increase, the origin of fracture proceeds further into the body of the specimen.

B. Experimental Procedure

The fracture characteristics resulting from two types of impacts were investigated. In the first, impact fracture was achieved by a massive steel ball impacting at a low velocity. In the second part of the test program, a .22 caliber lead shot was impacted at a high velocity.

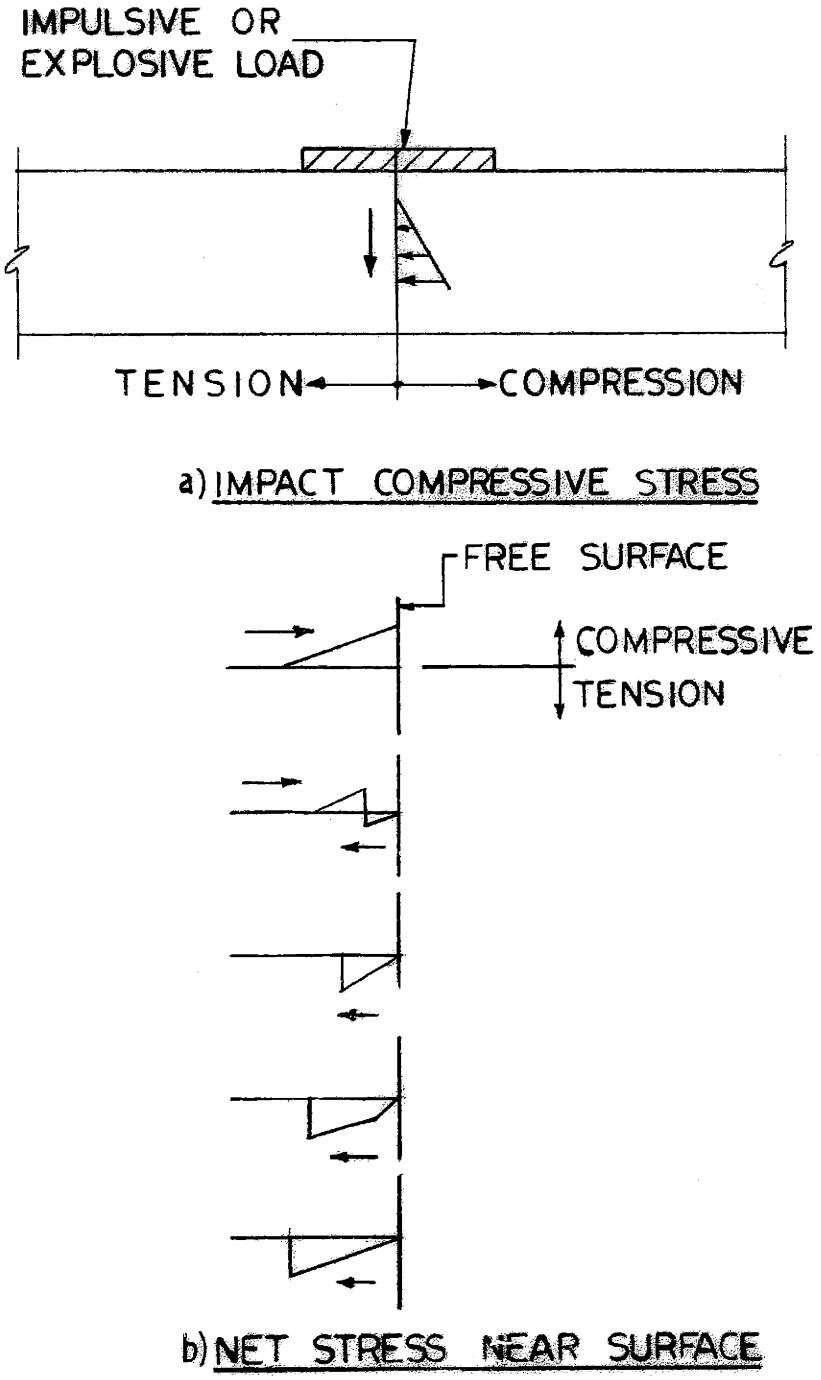

FIGURE 24 : TRANSIENT IMPULSIVE STRESSES

The high mass/low velocity fractures were studied in annealed glass only. The steel ball weighed 67 grams and was dropped from a height of 6.5 feet. The annealed plates measured 6 x 6 x 3/16 inch and were supported in the same supporting device that was used for the thermal fracture experiments (see Figure 18). The support apparatus was clamped at the midpoint of the sides of the frame by four (4) c-clamps, torqued to approximately 4 in-lbs. (Note: This torque was found by measurement in an Instron machine to correspond to a point load of approximately 60 pounds.) The impacting ball was released by breaking the circuit of an electromagnet.

The low mass/high velocity impacts were conducted on annealed, heat strengthened, and tempered plates of the same dimensions, and supported in the same apparatus as in the previous test. The .22 caliber lead pellets were fired from a CO_2 cartridge pistol at close range (approximately 4 feet).

C. Experimental Results and Discussion

1. High Mass/Low Velocity Impact. Fracture of Annealed Glass

[Note: The impact surface is the top surface in all photos.]

The plates shown in Photo 31 exhibit classic impact fracture patterns for annealed glass. The radial cracks are in general continuous and are therefore the primary fractures. The ring cracks resulting from hinge stresses are discontinuous and therefore secondary. Some radial cracks do form after the ring cracks as shown in the lower left corner of plate sample 147A. The ring pattern may form an incomplete closure as depicted in sample 148A. This type of pattern may result from the asymmetric

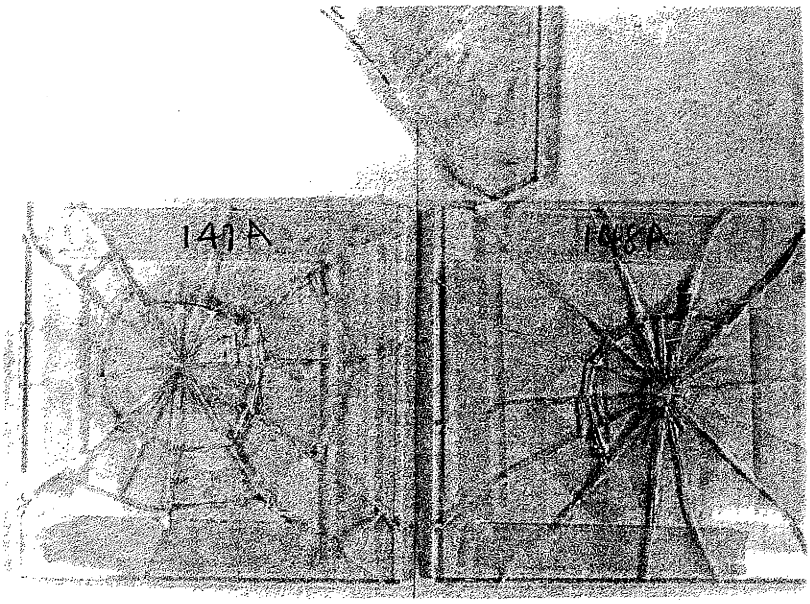

Photo 31 - Typical Impact Fracture Patterns in Annealed Glass

location of the impact point or from stresses arising due to edge clamping close to the fracture origin. Two of the three plates shown in Photo 31 had fracture cones initiated at the point of impact. The third exhibited radial cracks without cone formation. The fracture surfaces of cracks that passed through the fracture origin are shown in Photos 32 and 33. It is seen from these photos that the cone fractures show very little if any cylindrical development. The fractures appear to flare immediately after initiation for the plate thicknesses tested. The sample shown in Photo 32 had tape over the surface opposite the point of impact and so the glass separated by the cone of fracture was retained. The sample in Photo 33 had no tape applied and so the material was spalled and thrown out.

Sample 147A developed no cone of fracture. The fracture surface through the origin is shown in Photo 34. This photo illustrates radial crack initiation from the surface opposite the impact. An overview of the same surface (Photo 35) shows rib-marks, concave to the origin, beginning to appear at the extreme right side of the picture. Typical rib-marks are shown in Photo 36 for a fracture initiated on the lower surface and propagating left to right. No fracture mirrors were apparent at any fracture origins, even when examined under 60 X magnification.

A few samples were tested with the clamps removed. When this was done the origin of fracture was no longer on the axis of impact, but rather located at the edge of the plate due to bending, as shown in Photo 37.

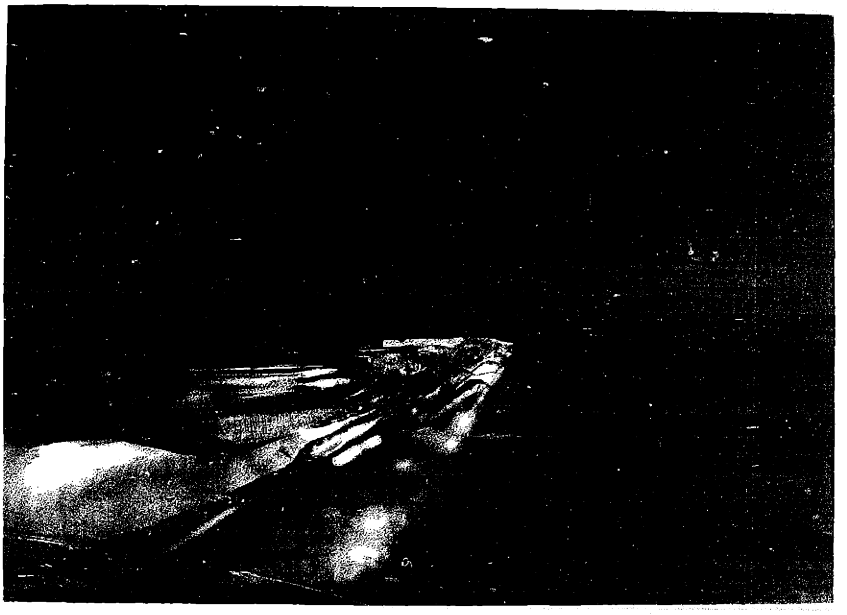

Photos 32 & 33 - Cone Fractures at the Impact Point

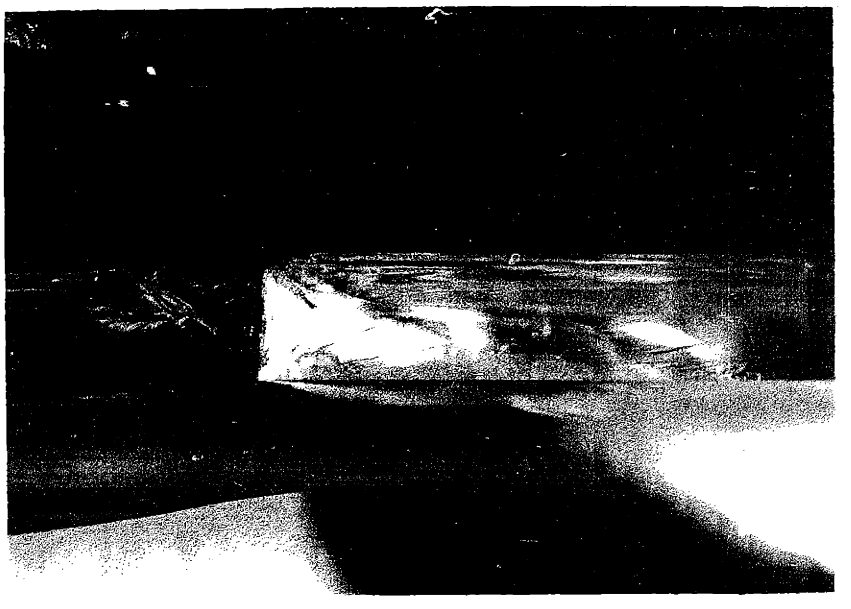

Photos 34 & 35 - Radial Crack Initiation

Photo 36 - Typical Impact Fracture Rib-Marks on Annealed Glass Fracture Surface

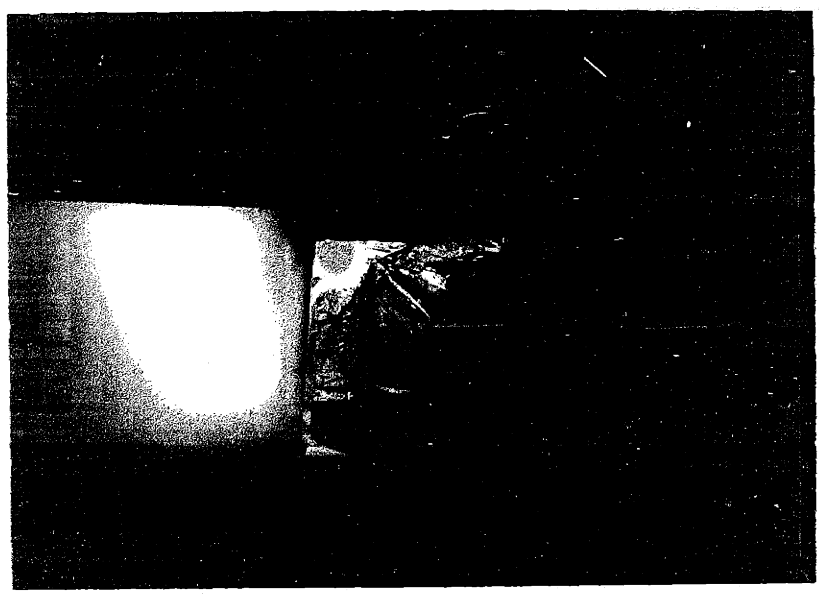

Photo 37 - Impact Fracture Patterns in Annealed Glass Plates with no Edge Support

2. Low Mass/High Velocity Impact Fracture of Annealed Glass

The low mass/high velocity impacts showed a high degree of variability in their fracture characteristics. A few plates fractured in the classic manner with primary radial cracks (see Photo 31). The plate depicted in Photo 38, however, shows by the continuity of the elliptical enclosure around the point of impact, that the ring crack is primary. It is probably the result of hinge stresses since a secondary cone developing that far from the point of impact is highly unlikely. The cracks that penetrate the interior of the ellipse are known as leader cracks. They often develop from ring fractures and propagate inward toward the point of impact.[2] The lower section of the elliptical ring crack flares broadly. Closer examination of the fracture surface in this region (Photo 39) shows bands of striations. These bands are evidence of the transient effect of stress waves as they interact and momentarily after the direction of the tensile stress field ahead of the crack tip.

3. Heat Strengthened and Tempered Glass Impact Fractures

The typical crack patterns for high velocity impact of heat strengthened and tempered plates are shown in Photos 40 and 41 respectively. Tempered plates fragmented so completely that discernible patterns were obscured. Heat strengthened plates showed radial cracks but few if any ring cracks. This is not unusual when one considers that ring cracks develop in response to relatively low hinge stresses that reach a maximum at the surface. Since heat strengthened plates are strengthened by compressive stresses at the surface, the initiation of ring cracks is suppressed. Radial cracks originate from flexure stresses of a higher

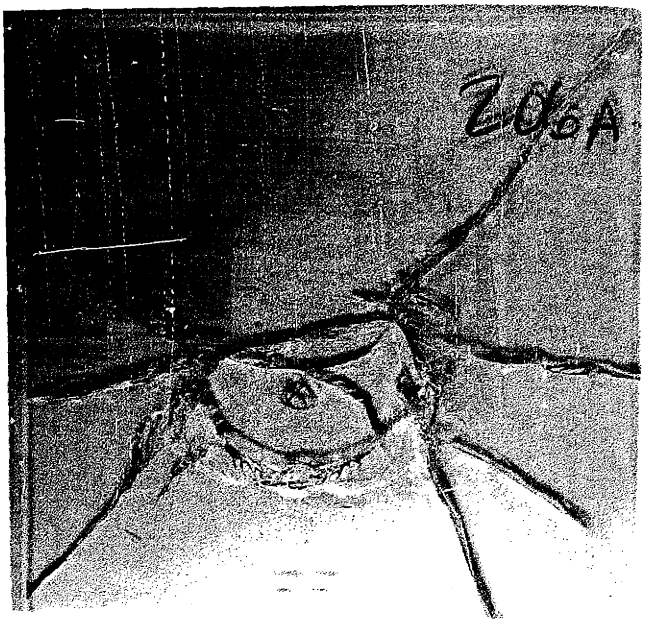

Photo 38 - Impact Fracture Pattern in Annealed Glass

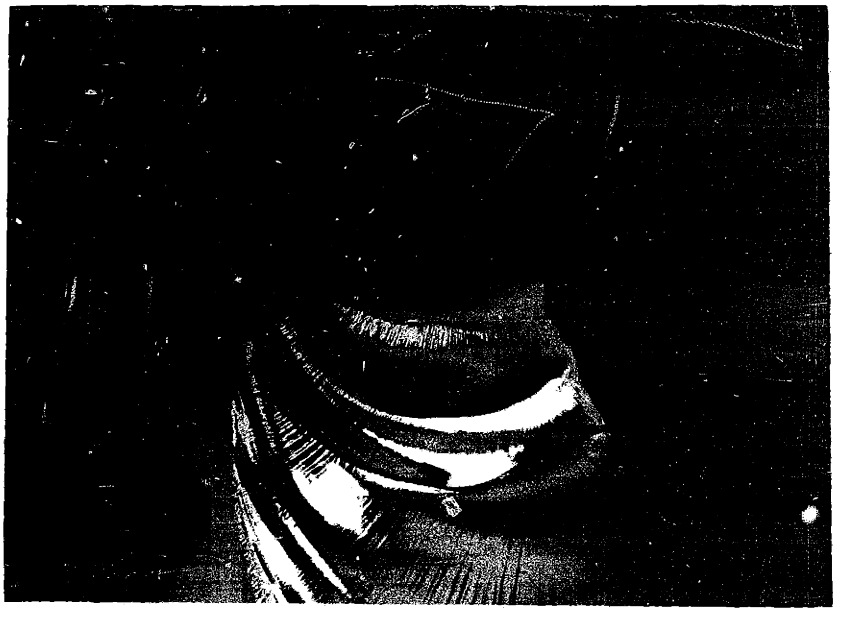

Photo 39 - Fracture Surface of Elliptical Crack Shown in Photo 38

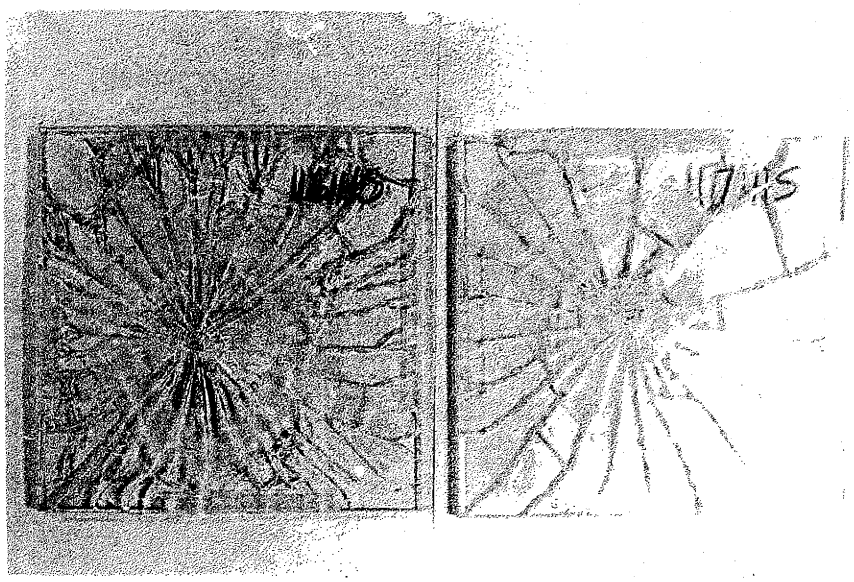

Photo 40 - Typical Impact Fracture Pattern for Heat Strengthened Glass

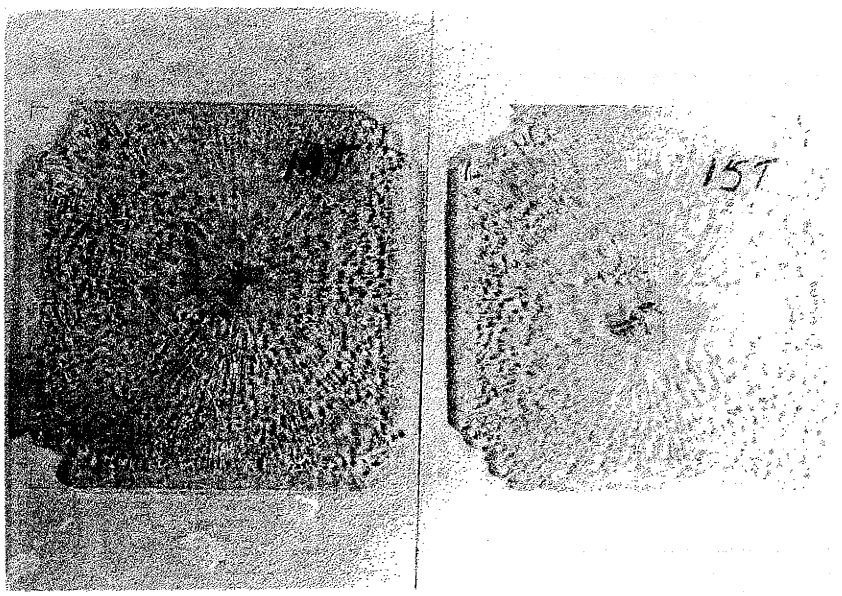

Photo 41 - Typical Impact Fracture Pattern for Tempered Glass

magnitude so their initiation is not seriously hampered. The analysis of the fracture surface at the origin of fracture in heat strengthened and tempered plates was obscured by local fragmenting of the glass and distortions due to the residual stresses present. As a rule, the fracture surface characteristics of propagating impact cracks in tempered and heat strengthened glass were identical to propagating cracks in these glasses due to other fracture modes. That is, the surface markings indicated the residual stress field. The fracture surface markings on radial cracks near the origin of fracture in heat strengthened glass was one exception to this rule. In this case the rib-marks characteristics of radial cracks in annealed glass were present. The transition from this annealed morphology to the residual was made quite near the origin (within 1/2 inch). A similar transition in fracture surface characteristics very likely occurs in tempered glass as well, but this could not be proven due to fragmenting near the origin.

VII. SUMMARY AND CONCLUSIONS

A. Mechanical Fracture

1. Annealed Glass

Mechanical loads produced by bending fractured soda-lime-silicate glass at stress levels ranging from 1000 psi to 12500 psi depending on many factors, which include loading rate, load duration, severity and distribution of flaws, and environmental conditions. A strength of 10,000 psi was a reasonable average for annealed glass without serious flaws. The strength increased by approximately 15% for each decade increment in the rate of stress application. (The range of testing was 250-25000 psi/minute.) Environmental stress corrosion weakened annealed glass by approximately 20% when the glass surface was first contacted with water, while the specimen was under stress. Static loading conditions in the presence of environmental stress corrosion and severe flaws can produce fracture at 1000 psi.

The relationship between the fracture stress and the size of the fracture surface mirror region was confirmed for annealed glass regardless of the location of the fracture origin. The calculation of the stress level at fracture by measurement of the radius of the mirror was valid whether or not the mirror was fully enclosed by bands of mist and hackle. Closure of the mirror region was found to depend on the stress gradient at the fracture origin. The stress gradient depends on the type of load application and on the geometry and orientation of the test specimen.

Typical fracture surface markings indicate fracture stress, crack front orientation, crack speed, and elastic energy release rate. The configuration of rib marks and Wallner lines was used to approximate crack speed and orientation. The approximate analysis indicated that the crack speed reached terminal velocity (about 1500 meters/second) in the outer reaches of the mirror zone and before entering the mist region. The sequential roughening of the fracture surface from mirror to mist to hackle was seen as an indication of an increasing rate of elastic energy release. The fact that the crack reached terminal velocity before extensive surface roughening occurred, casts doubt on the widely held notion that crack speed and elastic energy release rate peak simultaneously. In other words, it is often assumed that the crack progresses slowly in the mirror region, and attains terminal velocity only in the hackled region of the fracture surface; in fact this may not be the case.

The mirror/mist/hackle sequence was shown to occur in a repeating pattern in some instances. This cyclic surface roughness build-up is evidence that an instantaneous reduction in the stress ahead of propagating crack is possible even when loads are constantly applied.

Fractures at stresses below approximately 4000 psi did not release sufficient elastic energy to produce mist and hackle regions. The only characteristics apparent on these low energy fracture surfaces were rib marks, Wallner lines, and striations.

Fractures at stresses above approximately 6500 psi resulted in crack branching. The angle of branching was shown to vary linearly with the fracture stress.

Environmental stress corrosion did not apparently alter the fracture surface morphology or the correlation between fracture stress and mirror size.

Certain edge conditions produced by common trade practices (i.e., scoring and breaking by bending across the score) and considered acceptable by most glass manufacturers may in fact constitute serious weakening defects. Edges that exhibited "acceptable" shark teeth were shown to have strengths comparable to "unacceptable" edges with severe mechanical damage. ("Acceptable" shark teeth have lengths equal to or less than one-half the width of the edge.) It was also found that fractures originate at the base of the shark teeth which is synonymous with the scored line. It may be implied, therefore, that the shark teeth themselves are not serious flaws, but their occurrence is dangerous since they indicate a score line that is a serious weakening defect.

2. Tempered Glass

Fractures in unflawed (i.e., as-received) fully tempered laths were initiated at approximately 32000 psi. Fracture was produced by 4-point bending at room temperature, with a stress rate application of 2500 psi/minute. The fracture stress for flawed specimens ranged from 8400 psi to 29800 psi.

In general, the plates that fracture from the edge could not be analyzed visually since the glass at the origin was fragmented and spalled off. Fracture mirrors were apparent on the fracture surfaces of most plates that broke from surface flaws. The relationship between fracture stress and mirror size that was shown for annealed glass was found to be less reliable for tempered glass.

The approximate relationship was attributed to fluctuations in the magnitude of the residual stress acquired by different areas of the tempered plate.

3. Heat-Strengthened Glass

Heat-strengthened plates showed fracture characteristics similar to both annealed and tempered plates depending on the fracture stress and the location of the fracture origin.

Samples tested in an unflawed condition generally failed at fracture stresses between 15300-20100 psi. A relationship between fracture stress and mirror size was apparent. The fracture surface characteristics of these high energy breaks resembled those of fully tempered glass.

Flawed samples resulted in fracture at stresses between 10200 psi to 18100 psi. Fractures of surface origin showed fracture surface characteristics typical of tempered glass facture. Fractures of edge origin showed characteristics similar to those of annealed glass. This similarity was attributed to the reduction of the residual stress gradient at the edges of heat-strengthened plates. A relationship between fracture stress and mirror size was apparent for low energy fractures of surface origin. No conclusion could be determined as to the accuracy of this relationship for edge origin fractures due to the small number of samples tested.

The crack patterns associated with the low mass/high velocity impacts exhibited a more random arrangement. Ring cracks appeared as primary fractures in most samples. This implied that the hinge stress was the critical fracture initiating stress in this type of impact.

Tempered and heat-strengthened plates were fractured by low mass/high velocity impact only. Tempered plates fragmented so completely upon impact that discernible fracture patterns were obscured. Radial cracks were the predominant fracture mode in heat strengthened plates. The reason for radial crack formation despite the fact that hinge stresses were found to be critical in this type of impact, is that hinge stresses are relatively low in magnitude and occur at the surface where the residual compressive stresses can counteract their effect. Radial cracks form despite the residual stress because the flexure stress that initiates radial cracks are of considerably greater magnitude than the residual compressive stress.

B. Thermal Fracture

With respect to the cold recessed edge configuration, it was shown that the fracture stress was directly related to the temperature difference measured across the occluded glass edge. Fractures were produced at temperature differentials across the recessed edge of 42°F or more. This order of temperature differential has been shown by other researchers[V-4] to be easily obtainable in certain glazing construction details. This result emphasizes the need for heat transfer considerations in the design of window details.

The prediction of the thermal crack propagation path given a particular heating arrangement was not possible. This failure can be attributed to the present lack of understanding with respect to the thermal stress state within a finite plate during crack propagation.

The fracture surface markings characteristic of thermal fracture are similar to those associated with mechanical fracture with some notable exceptions. The fracture mirror regions produced by high-energy thermal fractures (i.e., $\sigma_f \geq 6000$ psi) were always fully enclosed by uniform mist and hackle regions. The configuration of these fracture surface markings was not similar to their appearance on mechanically fractured surfaces since a considerably less severe stress gradient usually exists with thermal loads. High-stress breaks often produced bands of repeating, concentric, mirror-to-hackle regions. In each sample that exhibited crack bifurcation it was noted that the onset of branching and the appearance of hackle occurred simultaneously. This fact is seen as support for the argument

that crack branching is merely an extension of the surface roughening device that is termed hackle.

The number of crack branches produced generally increased as the fracture stress increased. No relationship between the angle of crack branching and the fracture stress, (as was established for mechanical fracture), was apparent.

The fracture surfaces beyond the outermost hackle region were extremely smooth, marked only by occasional rib-marks at changes in the direction of crack propagation. The surfaces of low energy thermal fractures exhibited this generally featureless appearance throughout.

C. Impact Fracture

Fracture patterns developed during high mass/low velocity impacts generally exhibited primary radial cracks and secondary ring cracks. This indicated that for this type of impact situation the critical stress was the flexure stress which was formed directly below the impact object and on the surface opposite the impacted surface. The crack patterns was found to be asymmetrical due to off-center impact or due to edge clamping effects. Plates that had no rigid edge support generally fractured at the edge nearest the impact point due to bending.

Fracture mirrors were not apparent on the fracture surface except when the fracture originated at the edge of the plate due to bending. It is assumed that fracture mirrors were produced, but fragmentation of the glass in the vicinity of the origin obliterated them.

VIII. SUGGESTIONS FOR FURTHER RESEARCH

The endeavor to correlate the physical circumstances of a glass plate at the moment of fracture initiation with the fracture surface characteristics, ultimately bears on the successful determination of complex static and dynamic stress fields associated with stable and unstable crack propagation. Further insight into the configuration of the stress field ahead of a running crack might provide the necessary link to elucidate presently unexplained fracture surface morphology. For instance, what are the physics of an unstably propagating crack that allow an instantaneous reduction in the stress level ahead of the crack when the loads that initiated fracture are continuously applied? What causes the crack front to split into the characteristic striations when reacting to an undulation in the principal stress direction rather than reorienting itself as a whole as it does in the formation of rib-marks? How and why does the crack reform a singular front after splitting apart in the hackle region? What circumstances allow the formation of absolutely featureless fracture surfaces?

A considerable portion of glass panel failures in buildings come under the low stress fracture category. For this reason it would be of great interest to investigate further the mechanisms associated with low energy breaks such as environmental stress corrosion and static fatigue. How do these processes physically affect the growth of cracks that can lead to long-term failure?

The weakening effect of impurities and inhomogeneities in the glass

structure is an area that would yield fruitful research. Crystalline inclusions have often been blamed for glass fracture especially in the case of fully tempered glass. What is the form and magnitude of the stress concentration at various particle inclusions and discontinuities under applied, residual, and thermal loads?

The nature of thermal loads and their contribution to glass fracture is an area that requires additional work, especially in light of the results of this paper which show how critical even relatively low thermal gradients can be. A clarification of various thermal stress states would provide useful information to improve our understanding of common fracture surface markings and their implications.

There is need to determine the relationship of fracture stress to the rate of heat application, and to the rate of edge heat transfer. How efficient are various glazing construction details in implimenting the required heat transfer? How does tinted or frosted glass change the thermal design problem?

REFERENCES

II

[1] A. A. Griffith, Proc. of Int. Congr. Appl. Mech. [55] (1924)

[2] C. Inglis, Trans. Inst. Naval Archit. [55], 219 (1913)

[3] G. R. Irwin, Encyclopedia of Physics [6] (1958)

III

[1] S. M. Wiederhorn, J. Amer. Ceram. Soc. [52], 99 (1969)

[2] R. J. Charles, Progress in Ceramic Science, Pergamon Press, [1], 1-38 (1961)

[3] W. D. Kingery, H. K. Bowen, D. R. Uhlmann, Introduction to Ceramics (2nd ed.), John Wiley and Sons, Inc., 796 (1976)

[4] A. J. McEvily, A.S. Tetelman, Fracture of Structural Materials, John Wiley and Sons, Inc. (1967)

[5] W. B. Hillig, R. J. Charles, J. Appl. Phys. [3], 123 (1961)

[6] C. J. Phillips, American Sci. [53], 20 (1965)

[7] E. B. Shand, Ceramic Bulletin [46], 11 (1967)

[8] J. L. Glahart, F. W. Preston, J. Appl. Physics [17], 189 (1946)

[9] R. J. Charles, J. Appl. Physics [29], 1549 (1958)

[10] S. M. Wiederhorn, J. of Amer. Ceram. Soc. [50], 407 (1967)

[11] J. R. Varner, V. D. Frechette, J. Appl. Physics [42], 1983 (1971)

[12] C. Gurney, S. Pearson, Proc. Royal Soc. [A 192], 537 (1958)

[13] F.W. Preston, J. of the American Ceramic Society, 175 (1936)

[14] M. J. Kerper, T. G. Scuderi, Ceramic Bulletin [43], 9 (1964)

[15] M. J. Kerper, T. G. Scuderi, Ceramic Bulletin [44], 1] (1965)

[16] E. B. Shand, J. Amer. Ceram. Soc. [42], 10 (1959)

[17] J. J. Mecholsky, R. W. Rice, S. W. Freeman, J. Amer. Ceram. Soc. [57], 10 (1974)

[18] L. Orr, Materials Research and Standards, [Jan.], 23 (1972)

[19] D. G. Holloway, The Physical Properties of Glass, Wykeham Publications Ltd., 177 (1973)

[20] H. Kolsky, D. Radar, in Fracture, edited by H. Leibowitz, Academic Press [I], 553 (1968)

[21] R. H. Doremus, Glass Science, John Wiley and Sons, Inc., Chap. 15, 16 (1973)

[22] H. Schardin, in Fracture, edited by B. L. Averbach, D. K. Felback, G. T. Hahn, D. A. Thomas, Technology Press and John Wiley and Sons Inc. (1959)

[23] E. M. Yoffe, Phil. Mag. [42], 739 (1951)

IV

[1] L. Orr, Materials Research and Standards, [Jan.], 23 (1972)

[2] H. Kolsky, D. Radar, in Fracture, edited by H. Leibowitz, Academic Press [I], 553 (1968)

[3] W. B. Hillig, R. J. Charles, High Strength Materials, John Wiley and Sons, Iec. (1965)

[4] M. J. Kerper, T. G. Scuderi, Ceramic Bulletin [44],12 (1965)

V

[1] R. H. Doremus, Glass Science, John Wiley & Sons Inc., N.Y. Chap. 5 and 16 (1973)

[2] Kingery, H. K. Bowen, D. R. Uhlmann, Introduction to Ceramics (2nd ed.), John Wiley and Sons, Inc., 796 (1976)

[3] D. J. Johns, Thermal Stress Analysis, Pergamon Press, N.Y., 34 (1965)

[4] L. Orr, "Engineering Properties of Glass", pp. 51-62

VI

[1] H. Kolsky, D. Radar, in Fracture, edited by H. Leibowitz, Academic Press [I], 553 (1968)

[2] R. E. Mould, J. Amer. Ceram. Soc. [35], 9 (1952)

[3] W. Johnson, Impact Strength of Materials, Edward Arnold, Ltd., N.Y. (1972)

[4] C. F. Cline, V. D. Frechette, Ceramic Bulletin, [49], 11 (1970)

APPENDIX PHOTOGRAPHS

Photo	Mechanical Fracture - Annealed Glass
42	Featureless Fracture Surface; σ_f = 2730 psi
43	σ_f = 9500 psi
44	Fracture from Surface Score; σ_f = 8500 psi
45	$\dot{\sigma}$ = 250 psi/min.; σ_f = 8100 psi
46	$\dot{\sigma}$ = 2500 psi/min.; σ_f = 9200 psi
47	$\dot{\sigma}$ = 25000 psi/min; σ_f = 10700 psi
48	σ_f = 3540 psi
49	σ_f = 7000 psi
50	σ_f = 12400 psi
51	Static Fatigue; t_f = ∿120 min.; σ_f = 6800 psi
52	Static Fatigue; t_f = 41 min.; σ_f = 3300 psi
53	Accelerated Environmental Stress Corrosion; σ_f = 5300 psi
54	Static Fatigue; t_f = 13 min.; σ_f = 1000 psi
55	Static Fatigue and Accelerated Stress Corrosion; t_f = 95 min.; σ_f = 1000 psi
56	No Shark Teeth; σ_f = 11150 psi
57	Shark Teeth; σ_f = 5810 psi
58	Mechanical Damage, σ_f = 5540 psi
59	Typical Crack Branching
	Mechanical Fracture - Tempered Glass
60	Surface Origin; σ_f = 20,600 psi
61	Surface Origin; σ_f = 18,750 psi
62	Surface Origin; σ_f = 13,100 psi

APPENDIX PHOTOGRAPHS (Cont'd)

Photo	
	Mechanical Fracture - Heat Strengthened Glass
63	Types of Branching in Heat Strengthened Plates
64	Surface Origin; σ_f = 16,000 psi
65	Edge Origin; σ_f = 14,150 psi
66	Typical Fracture Surface Ribs in Heat Strengthened Glass
	Thermal Fracture - Annealed Glass
67	Typical Thermal Crack Pattern
68	Typical Thermal Crack Pattern
69	Typical Thermal Crack Pattern
70	Thermal Crack Pattern Deflected by Applied Load at X
71	ΔT_f = 58°F; $\sigma_f \simeq$ 5420 psi
72	ΔT_f = 47°F
73	ΔT_f = 45°F
74	Surface Origin; σ_f = 6720 psi
75	Clamping at Edge Plus Applied Load; $\sigma_f \simeq$ 4660
76	Clamping at Edge Plus Applied Load; $\sigma_f \simeq$ 4370

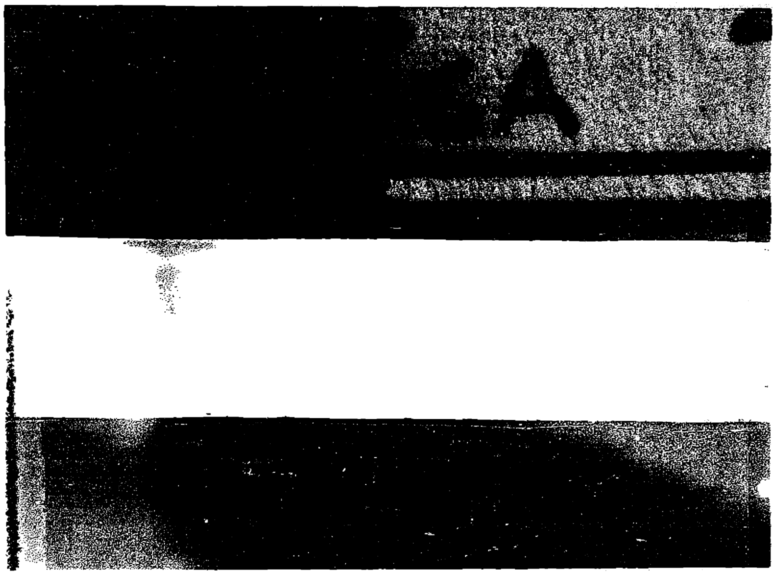

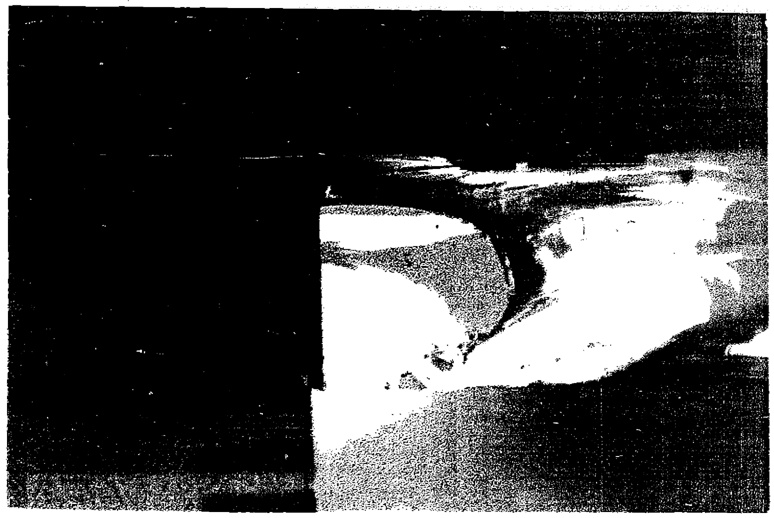

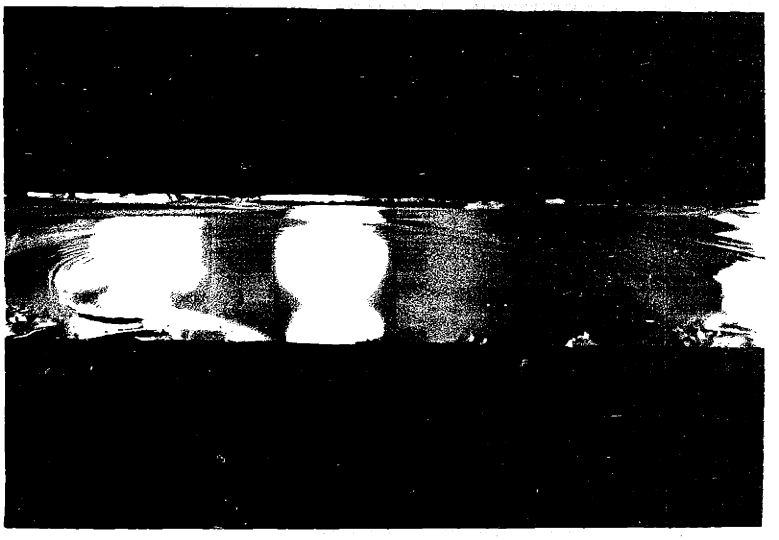

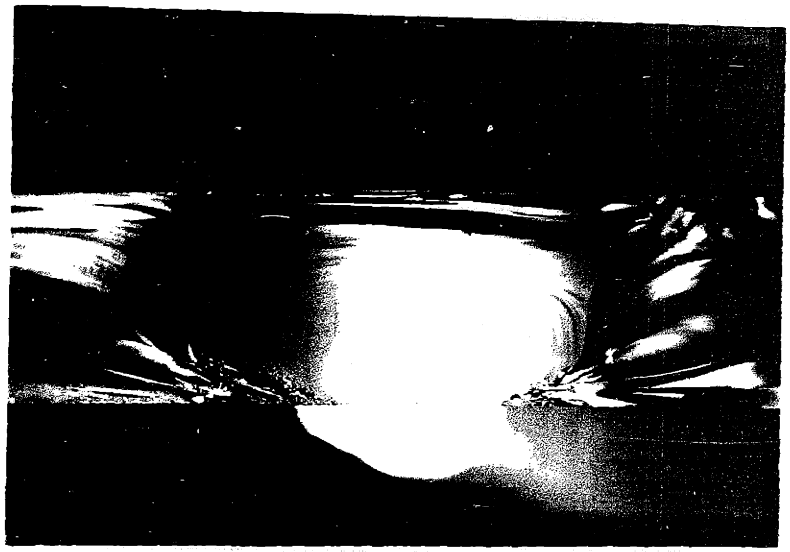


20A

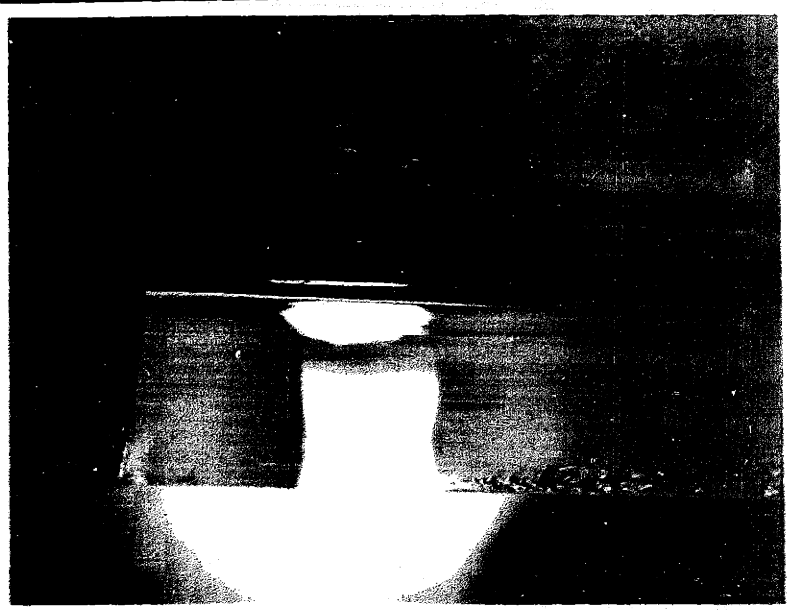

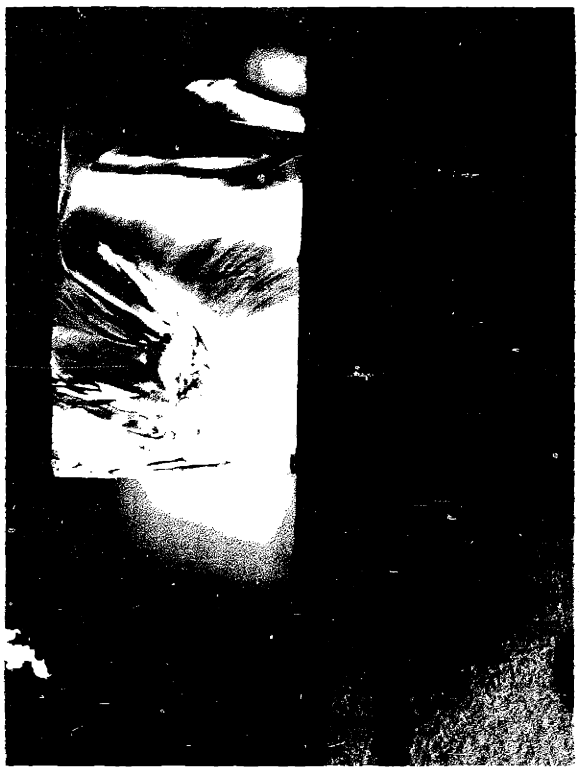

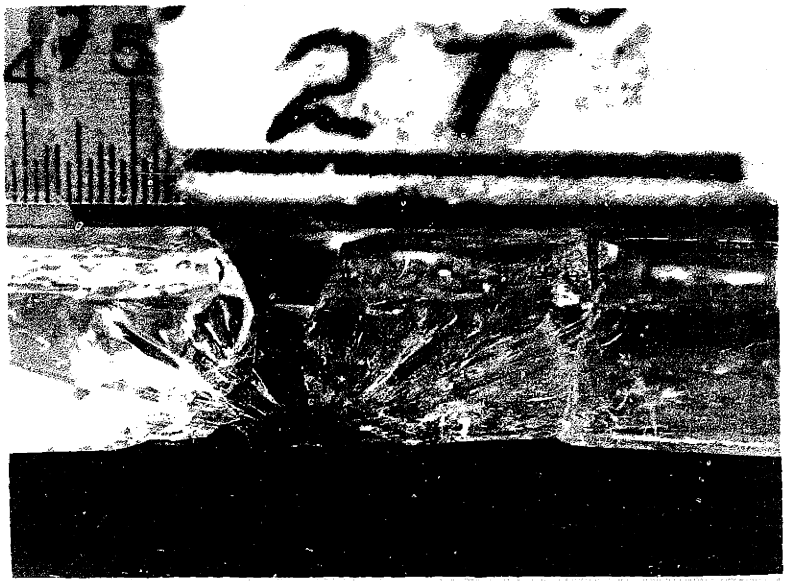
2T

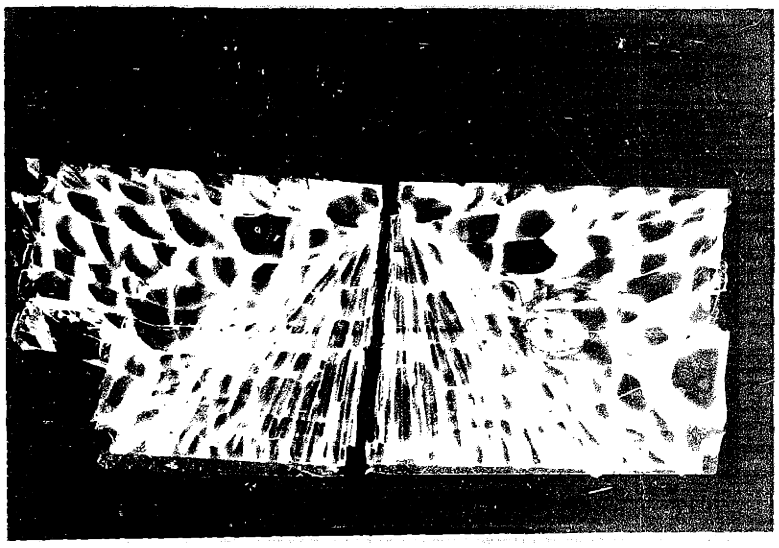

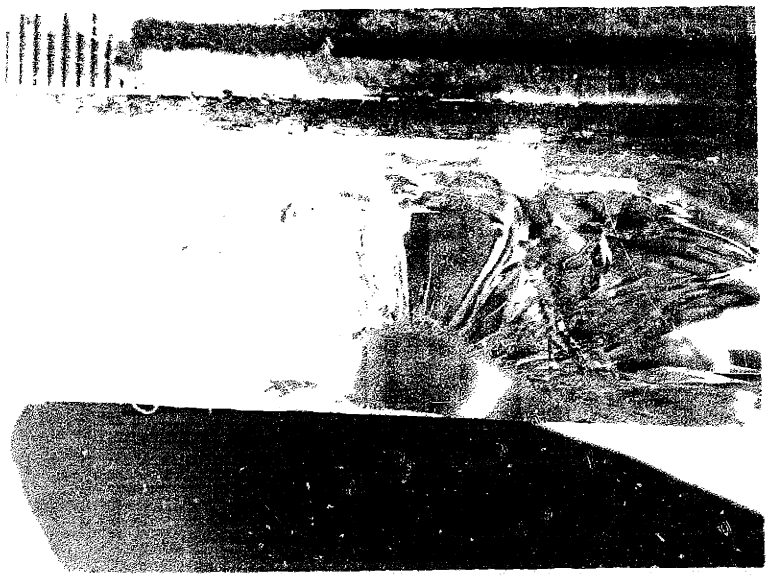

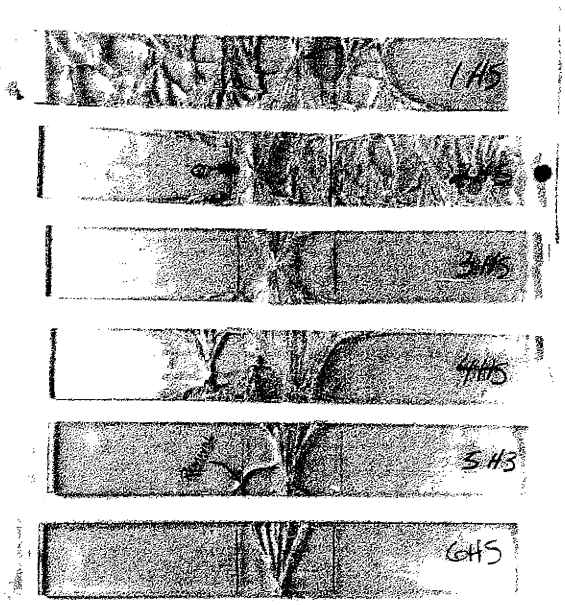
1 HS
2 HS
3 HS
4 HS
5 HS
GHS

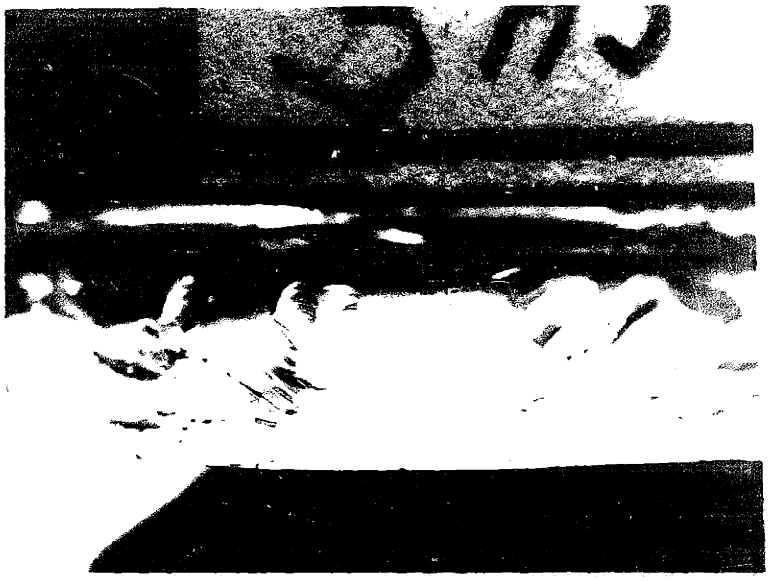


ID #5

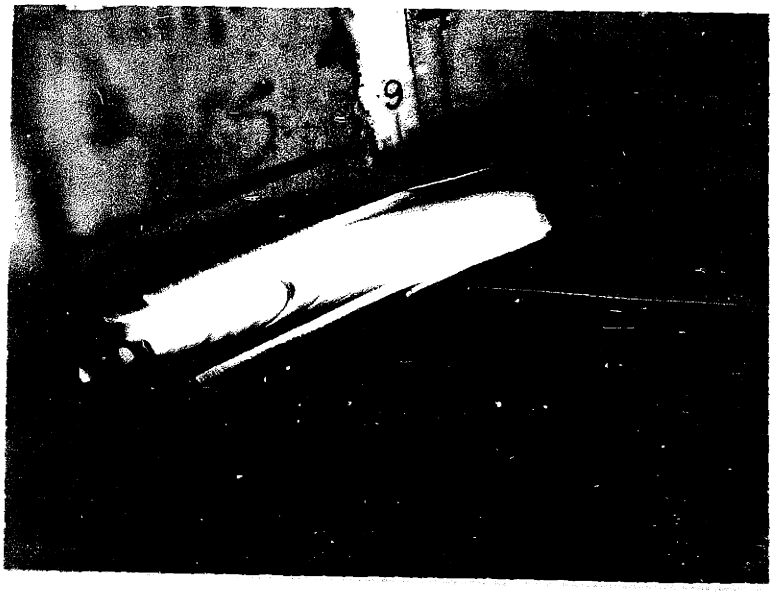

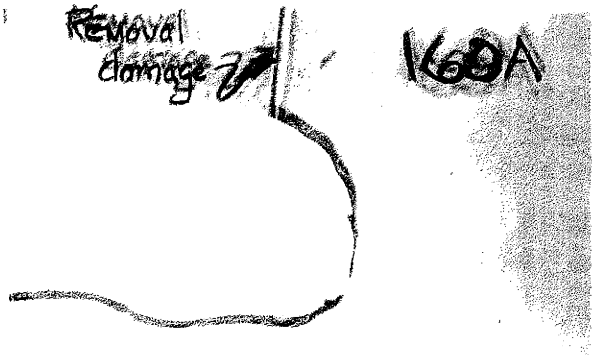
Removal
damage
160A


172A

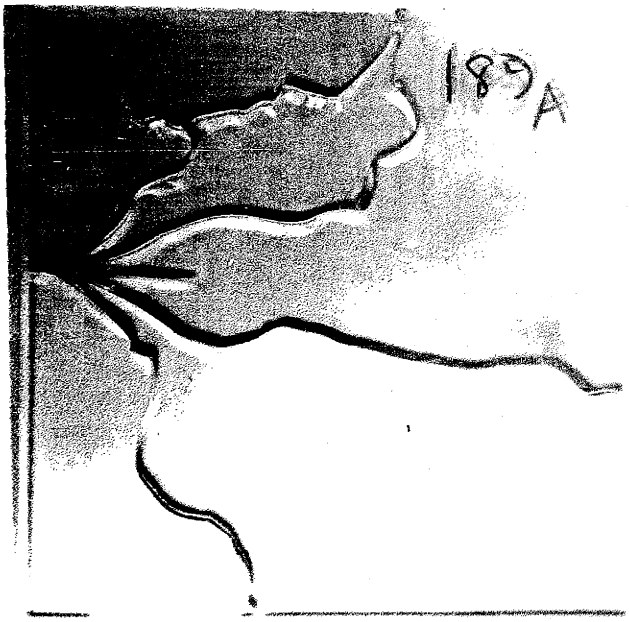
189A

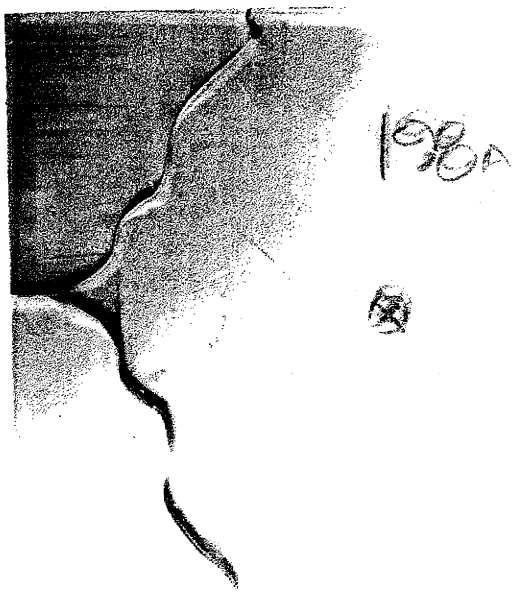

70

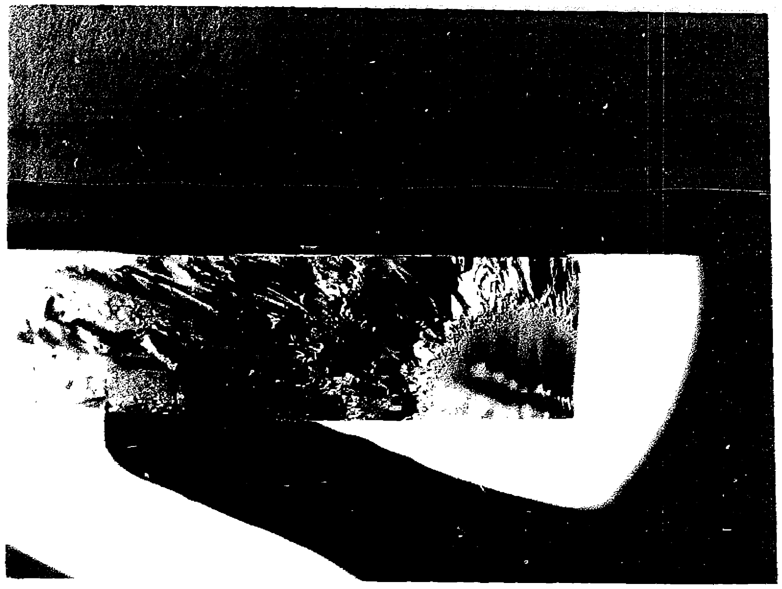

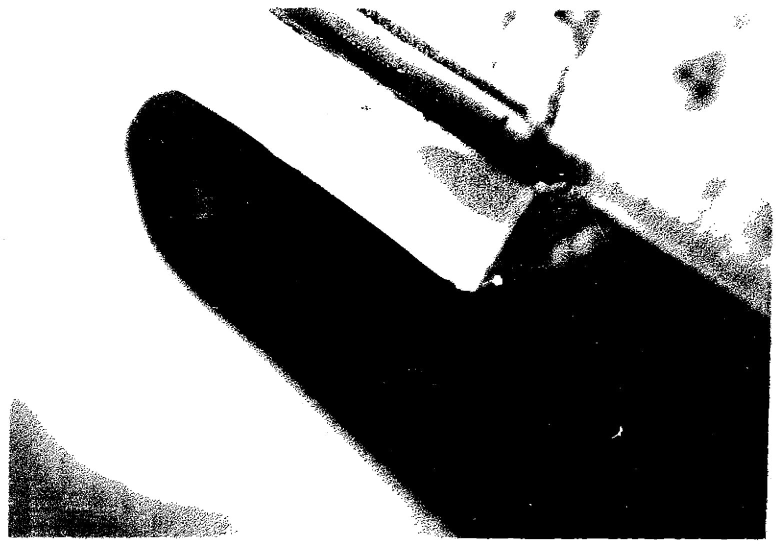

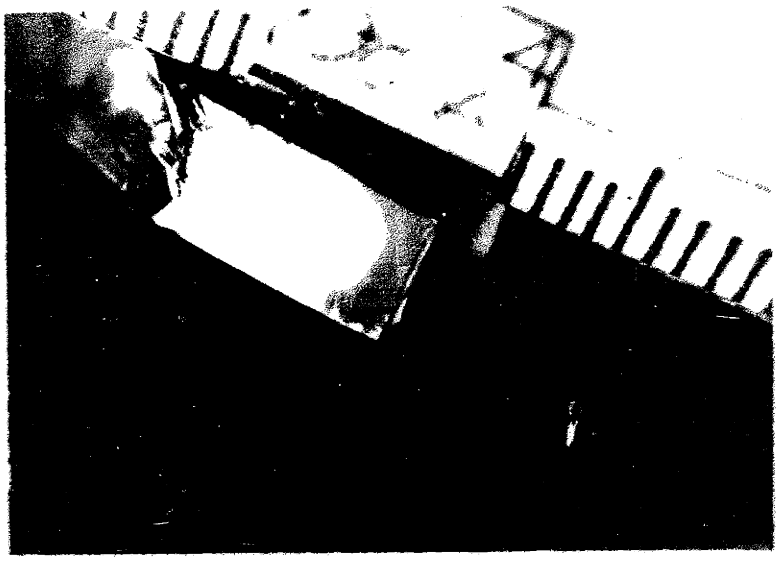

TINTED GLASS EDGE STANDARDS

ACCEPTABLE TINTED CLEAN-CUT EDGES may have:

Score if wings do not fly out.

Convolutions

Shark Teeth if penetration is not more than ½ glass thickness.

Serration Hackle only within 6 inches of corners.

Flare if not more than 1/32-inch on ¼-inch glass, and 1/16-inch on thicker glass. Flare not allowed where setting blocks contact glass.

Bevel if not more than 1/16-inch.
Flake Chips only within eight inches of corners and if not larger than ¼-inch across.

TINTED BORDERLINE EDGES may have all the defects acceptable for tinted clean-cut edges plus:

Shark Teeth if penetration does not go through glass thickness.

Serration Hackle if not deep or dense and if spalling is not present.

Flake Chips if not larger than ¼-inch across.

An illustrated poster dealing with edge standards and outlining the correct step-by-step procedure for cutting tinted glass—is available for display near cutting tables or elsewhere in glass shops. The poster 20" x 28" is available free of charge from PPG Industries. Simply write for: "Tinted Glass Poster" and address your inquiry to:

PPG Industries
Glass Advertising Department
One Gateway Center
Pittsburgh, Pa. 15222

Clean Cut Edges:

Edge 1—IDEAL

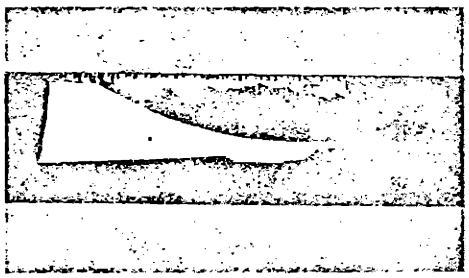

Edge 2—ACCEPTABLE—Convolutions

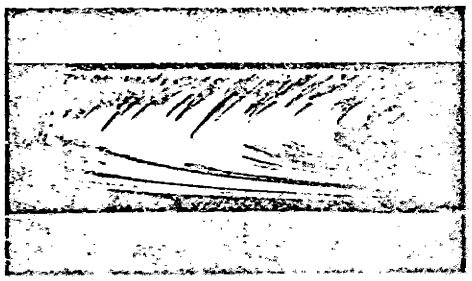

Edge 3—ACCEPTABLE—Shark Teeth